Department of State Development

RB 2015/29

What lies beneath the western Gawler Craton?

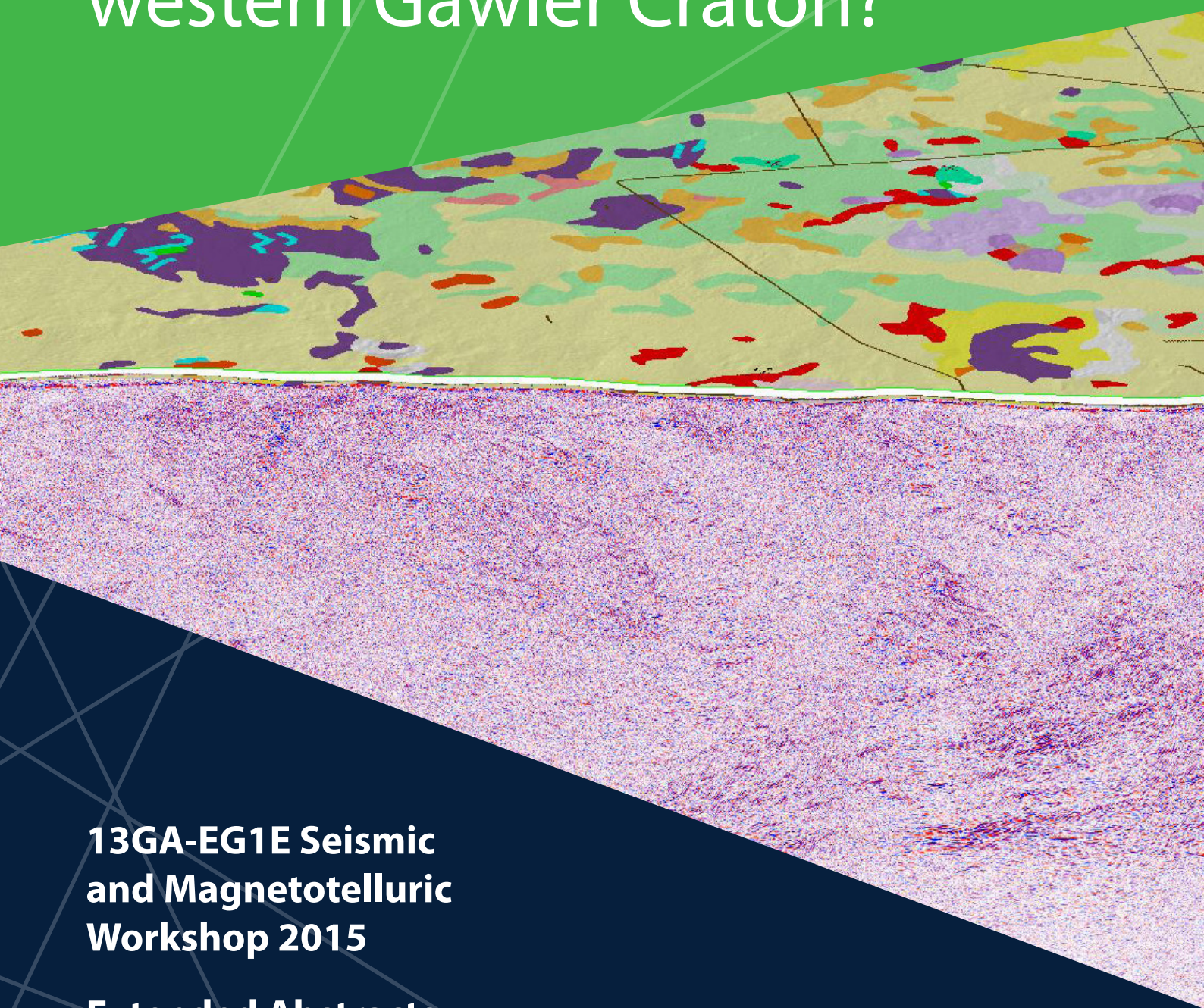

13GA-EG1E Seismic and Magnetotelluric Workshop 2015

Extended Abstracts

www.minerals.statedevelopment.sa.gov.au

SOUTH AUSTRALIA

Government of South Australia

Department of State Development

Government of South Australia
Department of State Development

Resources and Energy
Department of State Development
Level 7, 101 Grenfell Street, Adelaide
GPO Box 320, Adelaide SA 5001
Phone +61 8 8463 3000
Email Resources.CustomerServices@sa.gov.au
www.minerals.statedevelopment.sa.gov.au

South Australian Resources Information Geoserver (SARIG)
www.statedevelopment.sa.gov.au/sarig

Report Book 2015/00029

South Australian Resources Information Geoserver (SARIG) SARIG provides up-to-date views of mineral, petroleum and geothermal tenements and other geoscientific data. You can search, view and download information relating to minerals and mining in South Australia including tenement details, mines and mineral deposits, geological and geophysical data, publications and reports (including company reports).
www.statedevelopment.sa.gov.au/sarig

Preferred way to cite this publication.
(a) For reference to an individual contribution:

Reid, A. J., and Dutch, R. A., 2015, Lithostratigraphy, structure and metamorphic architecture of a reworked Paleoproterozoic continental rift in the western Gawler Craton in Dutch, R. A., Pawley, M. J., and Wise, T. W., eds., What lies beneath the western Gawler Craton? 13GA-EG1E Seismic and Magnetotelluric Workshop 2015, Report Book 2015/00029. Department of State Development, South Australia, Adelaide.

(b) For reference to the publication:

Dutch, R. A., Pawley, M. J., and Wise, T. W., 2015, What lies beneath the western Gawler Craton? 13GA-EG1E Seismic and Magnetotelluric Workshop 2015, Report Book 2015/00029. Department of State Development, South Australia, Adelaide.

Front cover. Western Gawler Craton 1:2,000,000 scale surface geology over 13GA-EG1 seismic section.

26/11/2015-204703

What lies beneath the western Gawler Craton?

13GA-EG1E Seismic and Magnetotelluric Workshop 2015

Extended Abstracts

Edited by R.A. Dutch, M.J. Pawley and T.W. Wise

Adelaide

Preliminary edition

PACE
PLAN for ACCELERATING EXPLORATION

GEOLOGICAL SURVEY SOUTH AUSTRALIA

AuScope

Australian Government
Geoscience Australia

EXPLORATION INCENTIVE SCHEME

Geological Survey of Western Australia

www.statedevelopment.sa.gov.au/sarig
www.minerals.statedevelopment.sa.gov.au

SOUTH AUSTRALIA

Government of South Australia
Department of State Development

Foreword

The compilation of written and associated oral presentations within *"What lies beneath the western Gawler Craton? 13GA-EG1E Seismic and Magnetotelluric Workshop 2015"* is an important step in building our geological understanding of one of the greatest geological frontiers on the Australian continent. Little is known about the bedrock geology underlying the Nullarbor Plain and its eastern margins, largely because drill hole sections and samples are sparse across the region, but also because in parts, such as the far west of South Australia, the regional geophysical coverage has previously been derived from early programs with widely spaced data acquisition. The geological knowledge from this region is critical for not only understanding the geological evolution of South Australia, but a large part of the geological reconstruction of the Australian continent. This publication marks some of the first steps in addressing this lack of data and knowledge and thereby provides critical foundations for new insights and understanding of our country.

The region bridges some of the most highly endowed mineral provinces of the Earth, with the Gawler Craton in the east and the Yilgarn Craton to the west. Surprisingly, however, there is largely unknown potential for the region to host new mineral provinces, although already it appears to offer promise for Neoarchean gold, magmatic Ni-Cu sulphides, magnetite iron ore and the sedimentary cover having potential for hosting further mineral sands deposits and uranium. The region also hosts components of larger gas and oil systems, such as associated with the Officer Basin, as well being part of the hinterland for the offshore oil and gas potential within the area of the Great Australian Bight. As we begin to look through and within the widespread cover that has so far provided a major impediment for the discovery of Earth resources we now look to take the opportunity to realise the potential for this large part of South Australia.

This compilation is largely derived from the momentum achieved by results from the Eucla – Gawler Seismic Survey (13GA – EG1), and for this volume specifically its eastern end. This survey represents the longest single east-west transect of deep seismic reflection data acquisition in Australia, and it would not have been possible without the collaboration between Geoscience Australia, AuScope, the Geological Survey of Western Australia and the Geological Survey of South Australia (through its *PACE Frontiers* initiative). The seismic survey was also accompanied by a magnetotellurics survey , and has since provided the foundations for further magnetotelluric data acquisition as part of the AusLAMP program and a new airborne magnetic and radiometric geophysical survey in the far west of South Australia. Each of these ongoing data acquisition programs represent new and essential pieces of the 'puzzle' for revealing the geology and resource potential of this region.

I would like to thank the efforts and leadership of Rian Dutch, Mark Pawley and Tom Wise in compiling this volume, as well as the outstanding contributions from each of the authors that have come from a diverse range of organisations. The registered participants of the workshop will also make valuable contributions, as well as future readers of this report that are hopefully part of building upon the legacy of this current state of data acquisition and understanding. The development of a more detailed geological understanding of this part of the Australian crust is long overdue, and we can now look forward to evolving our insights with this first major step!

Dr Steven Hill
South Australian Chief Government Geologist
Director, Geological Survey of South Australia

Contents

Complete set of abstracts, seismic data and Plate 1 can be downloaded from **www.minerals.statedevelopment.sa.gov.au**

13GA–EG1 Eucla-Gawler Seismic Survey – Acquisition and processing of the western Gawler Craton section

J. Holzschuh
Resources Division, Geoscience Australia

1 Introduction

Geoscience Australia in collaboration with the Geological Survey of Western Australia (Royalties for Regions Exploration Incentive Scheme), the Geological Survey of South Australia (*PACE Frontiers*) and AuScope funded the Eucla-Gawler 2D deep seismic survey 13GA-EG1. The seismic survey acquisition and processing were managed and processed by Geoscience Australia. Geokinetics Australasia Ltd were contracted to collect the Eucla-Gawler 2D deep seismic reflection survey from November 2013 to February 2014. Deep seismic reflection data and gravity readings were acquired along the 834 km seismic line. Magnetotelluric (MT) data (Thiel et al., 2015, this volume) were also acquired along the seismic line after the completion of the seismic survey. The main objectives of the project were to acquire deep crustal seismic data to:

1. Image the crustal architecture of the geology underlying the Eucla Basin and its relationship to the Gawler Craton to the east and the Yilgarn Craton to the west;
2. Establish the subsurface extent of the Eucla Basin and look for large structural zones that may have provided fluid pathways for mineralisation.

2 Seismic acquisition

The 2D land Vibroseis reflection seismic survey acquisition commenced on 28 November 2013, from Haig, WA and continued east along roads and tracks parallel to the Trans Australian Railway ending at Tarcoola, SA, on 7 February 2014. The location of the line is shown in Figure 1. Acquisition parameters for the survey are shown in Table 1. The seismic data were collected with a spread of 600 live channels over 12 km with the source array located at the centre of the spread. The maximum offset receiver groups were 6 km from the source.

The seismic data were recorded using a Sercel 428XL recording system in SEG-D demultiplexed format. The recording system cross-correlated each of the 3 recorded sweeps for each VP with its respective reference sweep and stacked the cross-correlated sweeps, creating a single 20 s record for each VP. An average survey production rate of 150 VPs or 12 km per day was achieved.

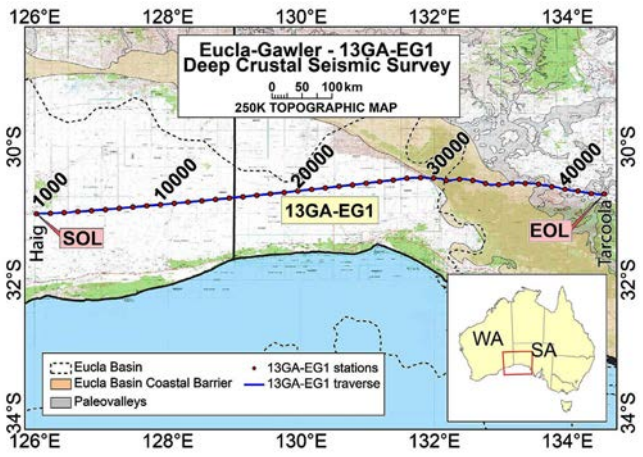

Figure 1 *Seismic line location with station numbers. Eucla Basin outline from FrOG Tech P/L, 2005. Start of line (SOL) and end of line (EOL) are shown. The palaeovalleys are from the regional palaeovalley map (Bell et al., 2012).*

Table 1 *Acquisition parameters used for the Eucla-Gawler L203 seismic survey.*

Line	13GA–EG1
Source type	3-4 AHV-IV Vibroseis Trucks
Source array	12 m pad-to-pad, 7.5 m move up
Sweep length	3 x 12 s
Sweep frequency	6–64 Hz, 10–96 Hz, 8–80 Hz
Vibration Point (VP) interval	80 m
Receiver group	6 x 10 Hz vertical geophones @ 3.3 m spacing
Group interval	20 m
Number of recorded channels	600
Fold (nominal)	75
Record length	20 s @ 2 ms
Stations	1000 – 42704, 834 km
Elevation ranges	92.6 m to 244.5 m AHD

3 Seismic reflection processing

Seismic processing for the eastern 360 km of the seismic line has been completed, from stations 24019 to 42704. The reflection seismic data for the Eucla-Gawler survey was processed by the Seismic and Magnetotelluric Acquisition and Processing Section of the Resources Division of Geoscience Australia, using the Paradigm Echos processing software on a Red Hat Enterprise Linux HP Proliant DL585G7 server. The basic processing sequence applied to the data is shown in Table 2. A reduced processing stream was used in the field to produce field stacks to QC and monitor data quality while the survey was in progress. Field QC was performed by Geokinetics geophysicists and

initially supervised by Geoscience Australia geophysicists in the field. As the line was essentially a 2D transect, it was processed using algorithms that are based on assumed 2D geometry. This 2D assumption has implications for processing and for the interpretation of the resulting processed data, which is explained in the description of the key processing steps.

Table 2 *Seismic reflection processing sequence for line 13GA–EG1.*

- Crooked line geometry definition (CDP interval 20 m, nominal fold 150)
- SEG-D to Disco format conversion, resample to 4 ms
- Quality control displays
- Inner trace edits
- Common midpoint sort
- Gain recovery (spherical divergence)
- Spectral equalisation over 8 to 92 Hz (1000 ms AGC gate)
- Application of floating datum residual refraction statics
- Velocity analysis
- Application of automatic residual statics
- Normal moveout (NMO) correction and 15 percent stretch mute
- Band pass filter
- Offset regularisation and dip moveout (DMO) correction
- Common midpoint stack
- Omega-x migration
- Signal coherency enhancement (digistack 0.5 and fkpower)
- Application of mean datum statics, datum 250 m, replacement velocity varies.
- Trace amplitude scaling for display

3.1 Crooked line geometry definition

The seismic line followed along roads and tracks that are parallel to the Trans-Australian Railway and hence was not straight. To process crooked line data using the Common Depth Point (CDP) method, it is necessary to bin the data into common midpoint gathers based on a calculated CDP line. The CDP line represents a curve of best fit through the source-receiver midpoints which optimises the fold of the data (Fig. 2). Each trace (source-receiver pair) is allocated to the nearest CDP bin to its midpoint. The CDP bins were defined to be 20 metres along the line, and 1200 m wide across the line. The effect of the bin size and midpoint scatter within the bin is most critical at shallow depths. Where the line has sharp bends, there is likely to be smearing and poor resolution of shallow data. The effect of bends on deeper data can also be significant, depending of the relative directions of the seismic line and the dip of the structures to be imaged.

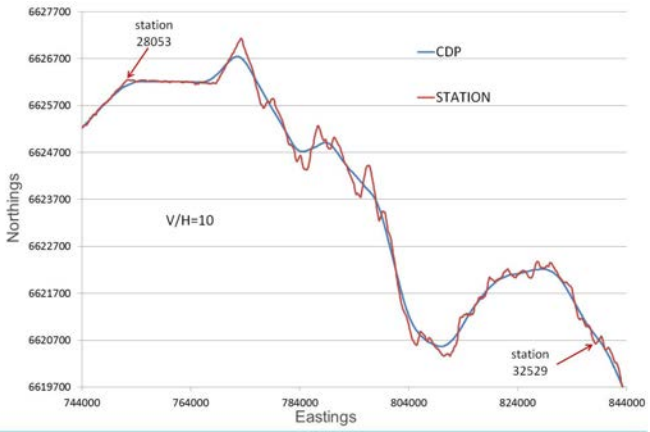

Figure 2 *Smoothed CDP line showing acute bends in station line, coordinates Map Grid Australia (MGA) GDA94 MGA ZONE 52. Image has been stretched vertically ten times to highlight difference in lines.*

The CDP line was processed as if it was straight, ignoring the effects of changing azimuth along the line. This simplification of the processing to a 2D geometry right at the start of the processing sequence is reasonable for large sections of the line which are relatively straight, however, it is not possible to correctly migrate, and therefore correctly image, reflections at significant bends in the line.

3.2 Refraction statics

Variations in surface elevation, weathering layer depth and weathering layer velocity can produce significant time delays in land seismic data. Variations over a short distance relative to the spread length can degrade the stack, as the reflections do not align across the traces to be stacked. Variations over distances longer than a spread length will not significantly affect the stack quality, but can introduce spurious long wavelength structure on the stacked reflections. Static corrections are applied in the processing stream in order to remove these effects. Static corrections for the Eucla-Gawler reflection seismic processing were calculated based on picking first break refracted arrivals from shot records and creating a near surface refractor model of the weathering layer. The refraction statics were applied in two stages using a floating datum. An intermediate step of automatic residual statics produced fine tuning of the corrections. The final statics were calculated relative to a datum of 250 m (AHD). Variation in refraction first arrivals along the line are shown in Figure 3.

Once the first breaks for the line have been picked and edited and the number of layers to be modelled is selected, the refractor model can be calculated. Usually, a one or two layer model can provide a suitable solution to the modelling of the weathering. For the Eucla-Gawler line, single layer models were tested to represent the weathering and these models varied across the seismic line. The numerous refractor models created and tested are shown in Figure 4.

Over the Eucla section no refraction statics were applied from stations 24019-27468 as the refraction statics diminished reflections. The first breaks in this region were difficult to pick with polarity reversals and high amplitude background noise. The refraction models possibly had "hidden layer problems" due to fast limestone at the surface overlaying slower sediments. Refraction requires layers to increase in velocity with depth. If a buried layer is overlain by a faster layer no critical refraction will occur along the boundary interface and refraction will not detect the slow layer.

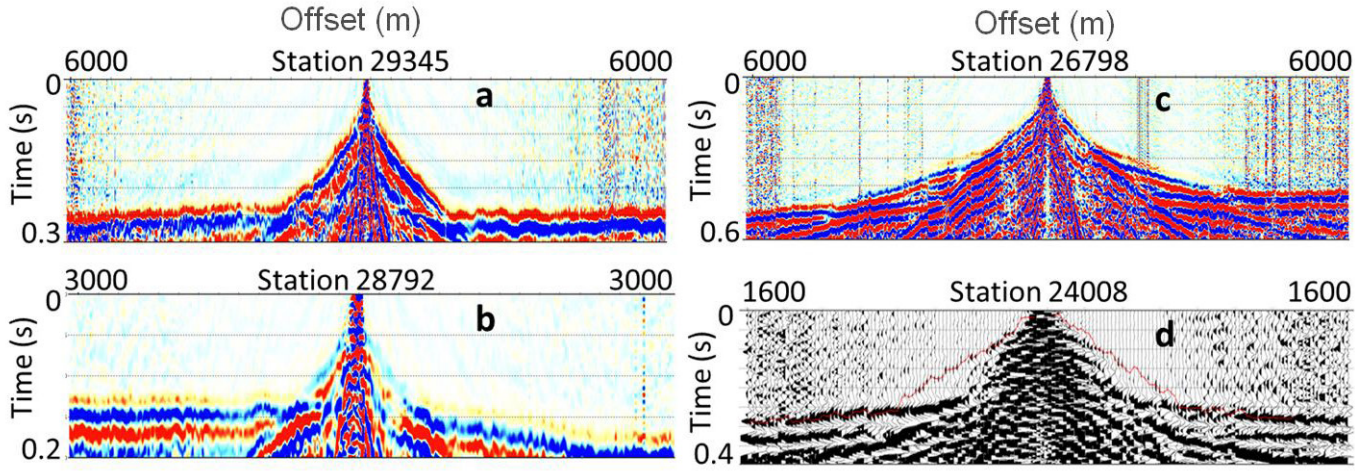

Figure 3 *Variations in first arrivals over the limestone section of the data, all refractors have been corrected to 6000 m/s, i.e. 6000 m/s layers are horizontal.* ***(a)*** *shows first arrivals as positive polarity (red) for slow and fast layer,* ***(b)*** *shows first arrivals as negative polarity (blue) for slow layer.* ***(c)*** *shows changing velocities and multiple layers.* ***(d)*** *shows the difficulty in picking first breaks (thin red line), with noise and possible reflection hyperbolas in the data.*

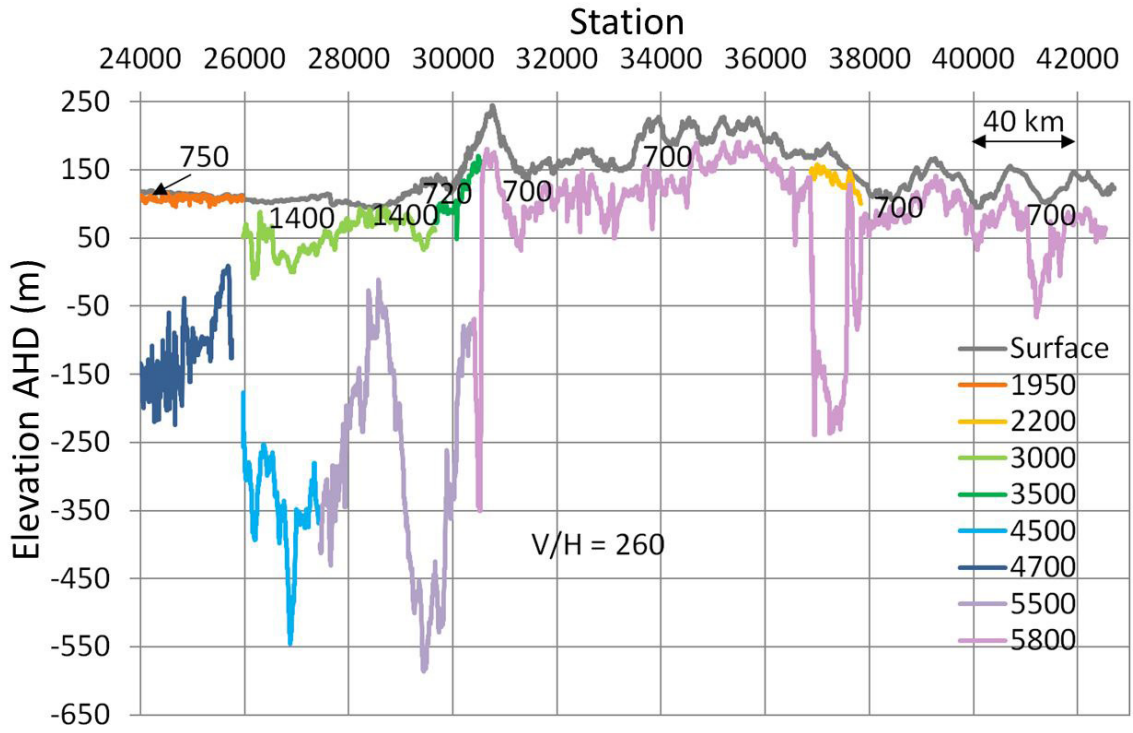

Figure 4 *Refraction models for the seismic line 13GA-EG1E. Values are approximate average refractor velocities in m/s. The eastern end of the Eucla limestone is near station 30000, where the slow 700 m/s sand overlaying fast 5800 m/s bedrock begins.*

The replacement velocity for the final static shift used was 5500 m/s (stations 27469-30428). Over the Gawler section the replacement velocity used was 5800 m/s (stations 30429-42704 EOL).

The refraction statics applied over data that had very slow sand dunes (average 700 m/s) over fast bedrock (5800 m/s) had a significant effect on the data and led to a major improvement (stations 30429-42704 EOL); many reflections could not be imaged without applying refraction statics. The large velocity contrast of the weathering to the bedrock as well as the large changes in sand thickness is causing adjacent traces to be out of alignment prior to statics correction. Figure 5b shows the effects of refraction statics in this region, used to correctly image the geometry of the near surface features as well as enhancing reflections deeper in the section (to 6 s TWT).

In Figure 4, between stations 36000 and 38000 a faster layer, 2200 m/s, was found within the basin structure, and is indicative of a water table. This matches the regional palaeovalley map (Bell et al., 2012; see Fig. 1), showing palaeovalleys in the region of stations 36000 to 38000.

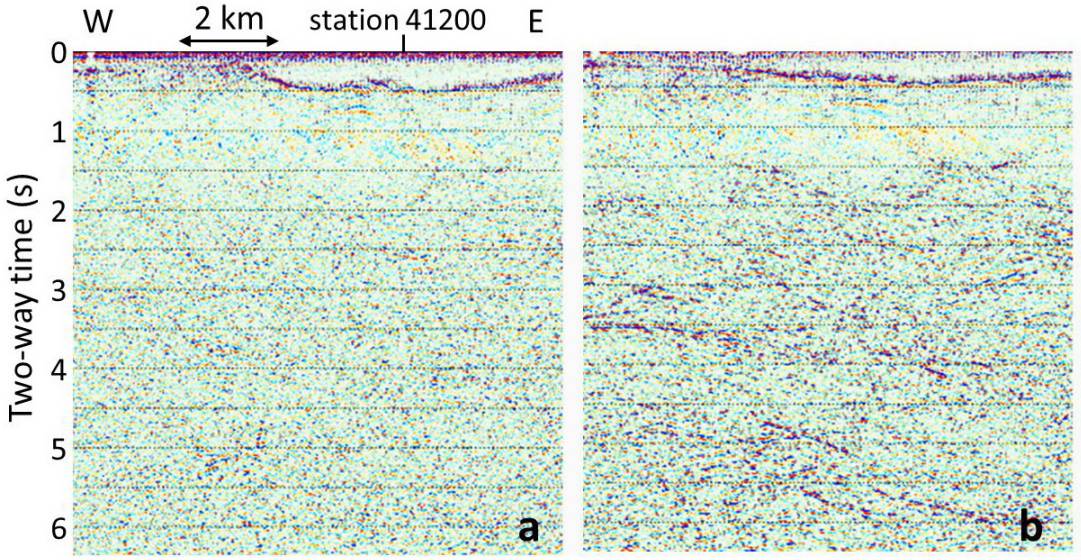

Figure 5 ***(a)*** *Has no refraction statics applied.* ***(b)*** *Has refraction statics applied, with greatly improved reflections and the shape of the base of sand weathering corrected.*

3.3 Spectral equalisation

Spectral equalisation is a process used to sharpen the reflection wavelet and suppress low frequency energy, primarily ground roll energy, which is surface wave energy that is generated by the vibrators. The frequency spectrum of the data is flattened over a specified frequency range and within a specified time gate. The high energy, low frequency ground roll is thereby reduced relative to the higher frequency energy of the reflections. The resulting data has better resolution, particularly in the shallow (0 – 2 s) section. The selection of appropriate frequency range and time gate is based on selective testing and spectral analysis of the data.

3.4 Normal moveout correction

Normal moveout (NMO) correction removes time variations across CDP gathers by adjusting for the time delays caused by increasing offset between source and receivers across the gather. The NMO correction is applied as a stacking velocity which best aligns the reflections in the CDP gather. Constant velocity stacks were used to define the stacking velocity field, producing a velocity field varying in time and space (along the line) which maximises the stack response of the data.

When applying NMO correction, far offset data will be stretched and an artificial increase in wavelength appears. This is relatively large for horizontal reflections with low stacking velocities. The data that are over-stretched are muted, a process called stretch mute. For the eastern part of 13GA-EG1 a 15 percent stretch mute with 6000 m/s velocity was used.

3.5 Dip moveout correction

Dip moveout (DMO) correction, also known as partial prestack migration, adjusts the NMO correction for the increase in stacking velocity as structural dip increases, and has the effect of correcting the NMO to account for different dips occurring along the line. The process effectively moves reflection energy between traces within and between CDP gathers based on apparent dip of the reflections, and creates a new set of DMO-corrected CDP gathers. After DMO, intersecting dipping and flat reflections will correctly stack with the same stacking velocity (Fig. 6). DMO is a very computer intensive processing step.

Figure 7 shows the final migrated seismic line with the post DMO stacking velocity spectrum beneath it, velocities picked from 0 s to 6 s. As maximum offsets for the seismic data are 6 km, there is not a significant hyperbolic moveout for reflections in the CDP gather below 6 s. Accordingly stacking velocities are extrapolated from 6 s to 20 s as they are the only good velocity approximation for later times in the section and changing them, i.e. increasing the velocities as expected, will not change the reflection image.

Some of the DMO stacking velocities are displayed on the final 8 s seismic plots and TIF file images (Fig. 8). These velocities were applied to stack the data before the mean refraction statics were applied, i.e. velocities were applied prior to moving the data to its final datum. The mean refraction statics shift is plotted as a profile above the seismic data. As an example, the velocity box for CDP 43100 shows that the velocity 3300 m/s was applied at time 198 ms. The mean static at CDP 43100 of -25 ms was applied for the final datum corrected image, i.e. -25 ms was added to the trace data. So, on this datum corrected image at CDP 43100 the 3300 m/s velocity was applied at 173 ms (198 + -25 = 173) on the stack.

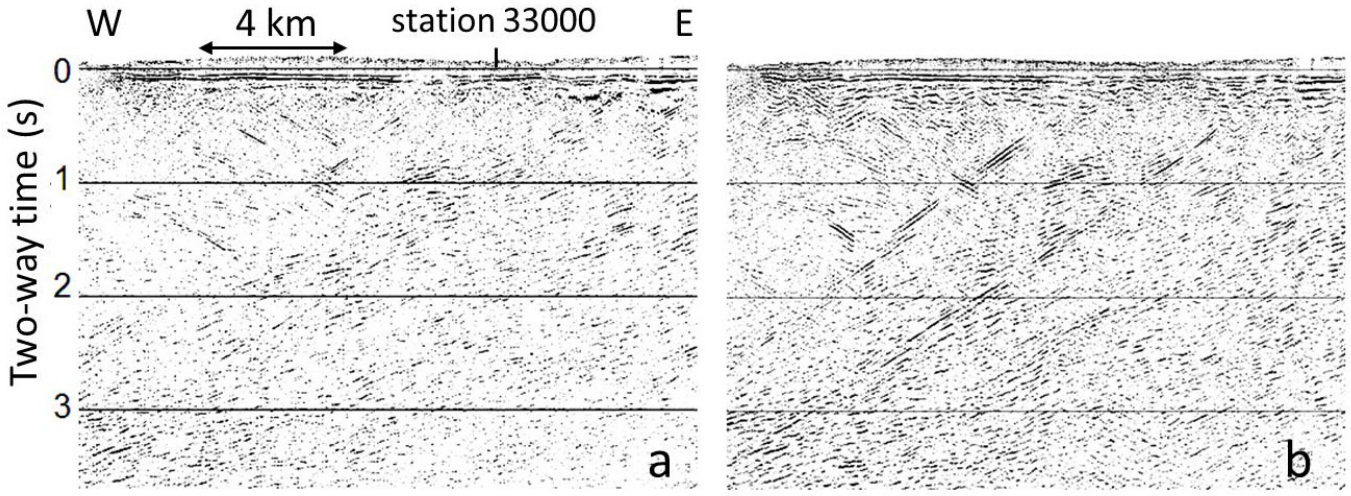

Figure 6 ***(a)*** *Normal moveout (NMO) corrected stack; and* ***(b)*** *DMO corrected stack enhancing dipping reflections that will migrate up to the near surface. Stacks shifted to datum AHD 250 m.*

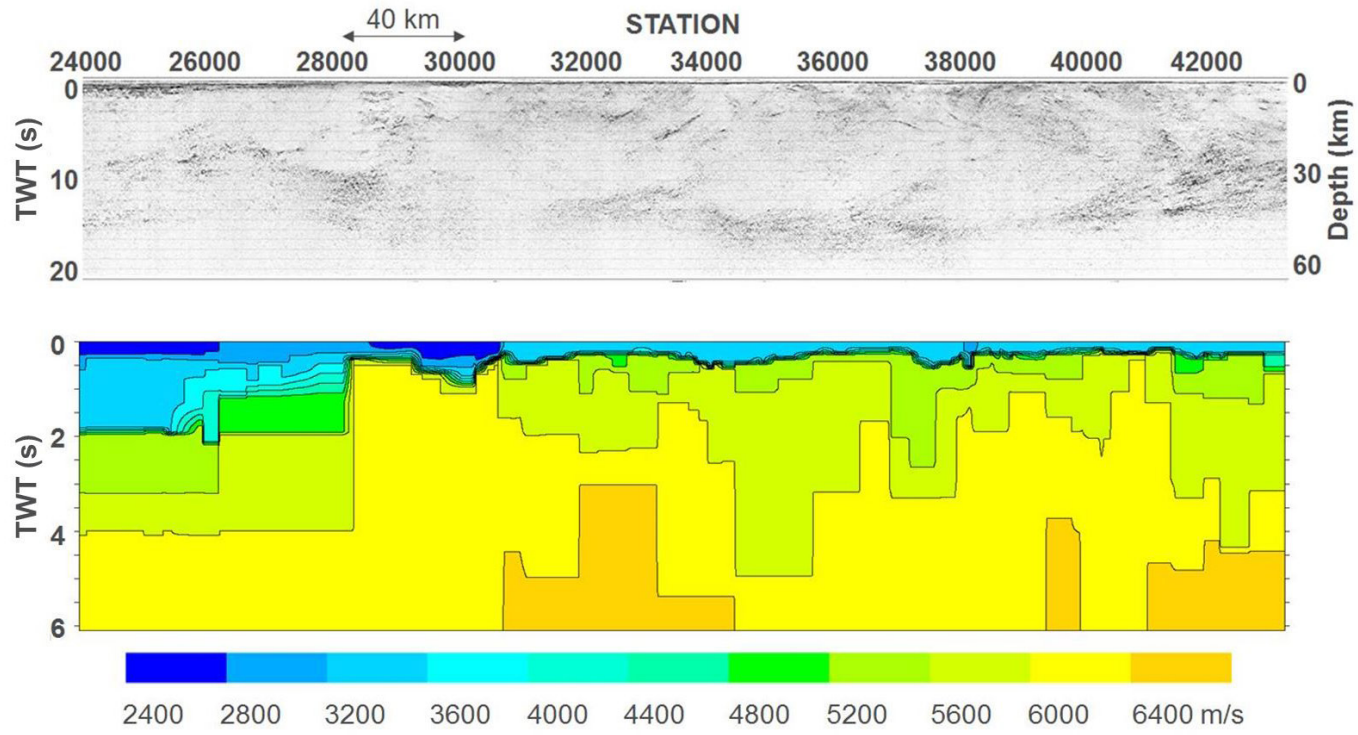

Figure 7 *The final migrated seismic line with the post DMO stacking velocity spectrum beneath it. Velocities were picked from 0 to 6 s. The time axes represent the travel time from the surface to the reflector and back which is called the Two-Way Time (TWT). The vertical scale of the upper image is equal to the horizontal scale with depths approximated assuming an average crustal velocity of 6 km s-1, so 1 s TWT is 3 km depth.*

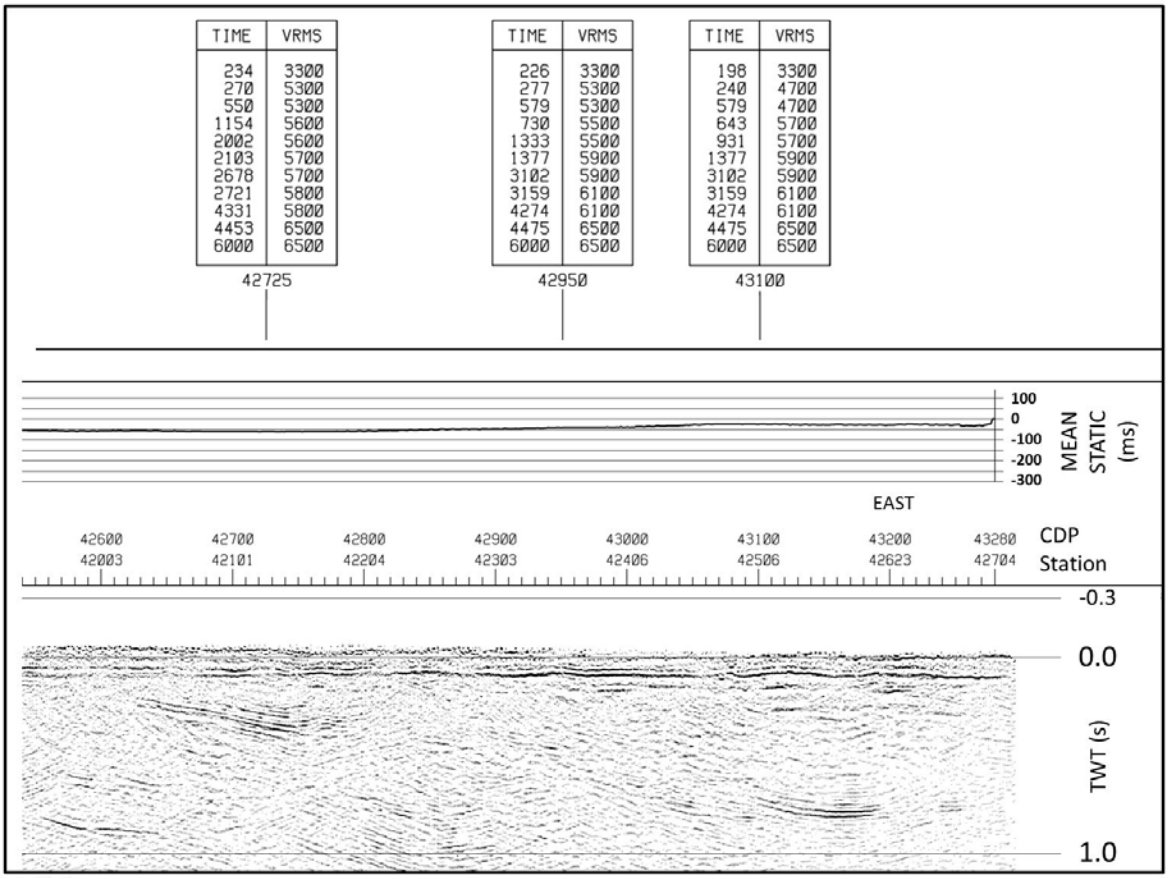

Figure 8 *A sample of post DMO stacking velocities are displayed in the boxes above the seismic section. The mean static shows how much the final data image has been shifted to move the data to the correct datum, i.e. 0 s = 250 m AHD.*

3.6 Common midpoint stack

Common midpoint stack is simply the summing of traces in a CDP gather to produce a single trace at the CDP location. The traces in the gather are aligned by the NMO and DMO processes to sum optimally. Stacking the data improves the signal to noise ratio of the data by √n, where n is the number of traces summed (the fold). A nominal fold of 150 resulted from the acquisition geometry for the Eucla-Gawler survey when using 20 m CDP bins.

3.7 Post-stack time migration

Migration is the final processing step and moves dipping reflections to their most likely lateral positions. Reflections that appear as dipping on the stack section will be moved up dip and shortened after migration. Diffraction hyperbolas resulting from discontinuities, such as terminations of reflectors at faults, and which are visible on the stack section, should collapse to a small region after migration. However, areas of poor signal to noise ratio, sharp bends and boundaries of high amplitude and low amplitude (strong and weak) reflections in the line can produce artefacts in the data which will not migrate successfully.

The main parameters to be selected when performing migration are the velocity field and dip ranges to process. The velocity field used is usually a percentage of the stacking velocity. Different migration velocities were tested and the optimum migration velocities were selected for different sections along the seismic line.

The final migrated time section should have dipping reflections in the correct spatial location. The Omega-X (frequency-space) migration algorithm used to process the Eucla data is a finite difference approximation to the monochromatic wave equation, as described in Yilmaz (2001). The effect of migration on the stacked data is illustrated in Figure 9 which shows stack and migrated images of part of the Gawler Craton. The lower image (migration) shows how the migration process collapses diffraction energy and moves dipping reflectors up dip to the correct location.

3.8 Signal enhancement

Coherency filters were applied to the data to enhance reflections for the final display images.

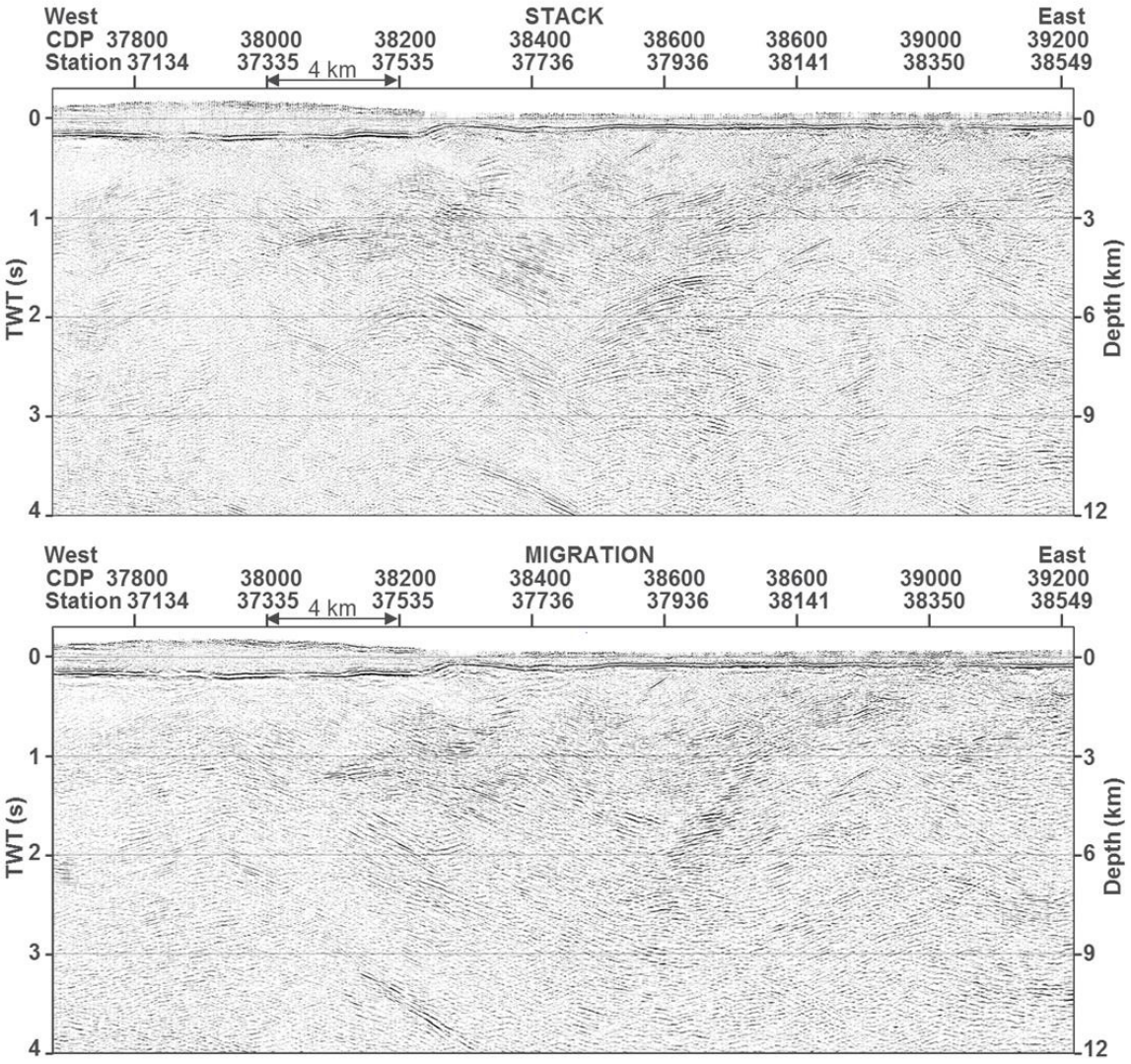

Figure 9 *Final stacked (upper) and migrated (lower) sections for part of the Eucla-Gawler seismic line. The vertical scale is equal to the horizontal scale with depths approximated assuming an average crustal velocity of 6000 m s-1.*

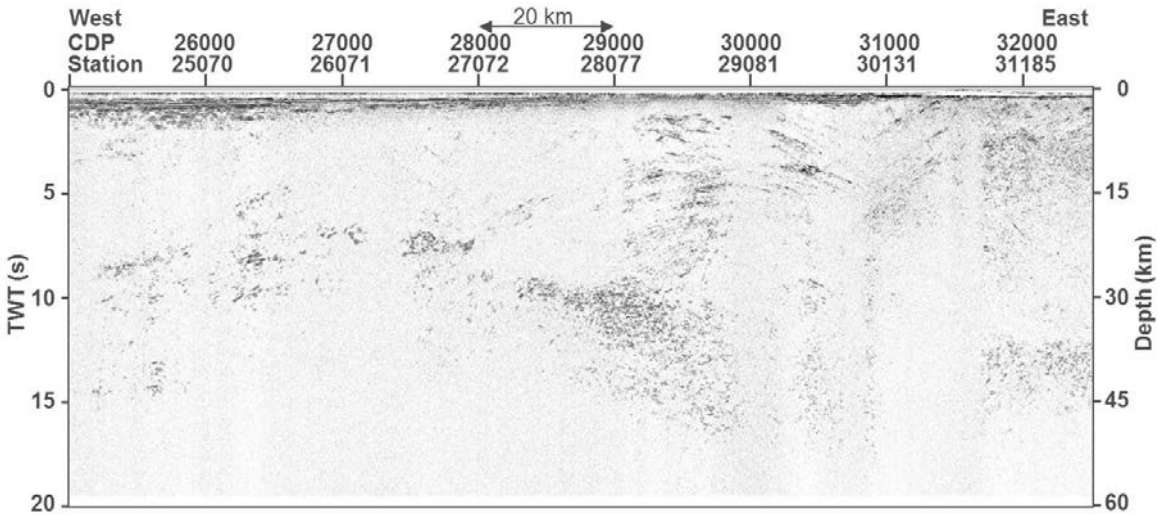

Figure 10 *DMO stack L203 13GA-EG1. Diminished reflections occur under areas with thick sand dunes (CDPs 31200 to 32200) or Eucla limestone (CDPs 25000 to 29000) at the near surface. Station numbers locate this on Figure 1. The vertical scale is equal to the horizontal scale with depths approximated assuming an average crustal velocity of 6000 m s-1.*

3.9 Regions of low reflectivity

In some regions, the data appeared to have low amplitude and incoherent reflectivity and this has some correlation with thick weathering or sedimentary layering at the surface, suggesting source energy and/or reflected energy penetration problems at the near surface (Fig. 10). Diminished reflections occur under areas with thick sand dunes (CDPs 31200 to 32200) or Eucla limestone (CDPs 25000 to 29000) at the near surface. Thick sand will attenuate source and reflected energy and is also seen in Figure 9 with reflection amplitudes lower under the thick weathering layer, left of CDP 38200. Fast dense limestone at the surface overlaying slower less dense sediments can also cause some reflected energy from depth to reflect back down due to the large negative reflection coefficient.

In order to better image the lower crust in the regions with low reflectivity the data were binned at 100 m CDP spacing to increase the nominal fold from 150 to 750, compared with the 20 m CDP spaced data. The data were resampled to 8 ms to reduce data size and speed up processing, with a Nyquist (maximum) frequency of 62.5 Hz. No spectral equalisation was applied to ensure maximum data amplitude was preserved. No DMO was applied to speed up the processing. Migration was applied to the NMO corrected stack. Figure 11b shows the improved imaging of the lower crust and Moho with the high fold data as compared to the lower fold data (Fig. 11a).The lower fold data has improved imaging of the middle/upper crust, as it had DMO and post DMO velocities applied prior to migration.

Stacking the data with larger CDP spacing (binning) increases the fold and is a fast way to improve and check lower crust reflectivity. The Fresnel Zone is the horizontal dimension of seismic resolution and increases with an increase in depth and increase in velocity but decreases with higher frequencies (Yilmaz, 2001). For example, at 10 s time on the 8 ms resampled seismic data, using the maximum frequency of 62.5 Hz and stacking velocity of 6000 m/s, the Fresnel Zone is 2400 m. Further increasing the CDP spacing up to this 2400 m Fresnel Zone could be used for imaging data at times 10 s and later with similar horizontal resolution and substantially increasing the fold of the data, hence improving the signal to noise ratio and producing enhanced seismic reflectivity.

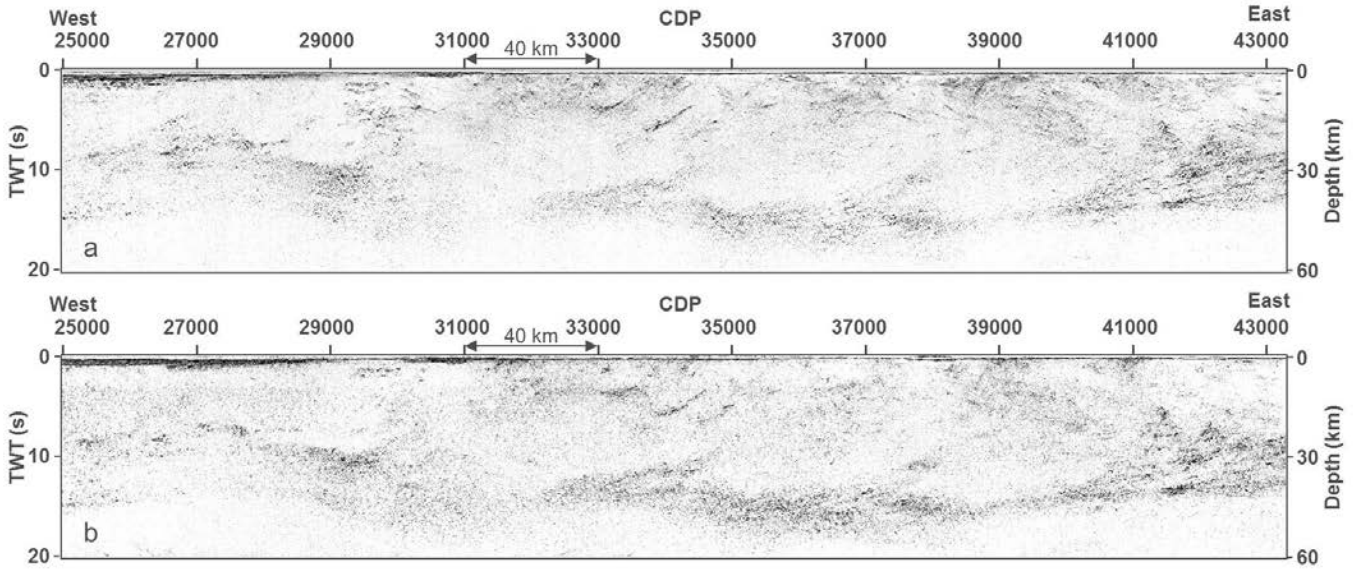

Figure 11 *Top image (a) is a migrated DMO stack with 20 m CDP spacing and 150 nominal fold. The lower image (b) is a migrated NMO stack with 100 m CDP spacing and nominal fold of 750, no spectral equalisation or DMO was applied. The higher fold image (b) has improved imaging in the lower crust. The upper image (a) has improved imaging in the upper crust as it had DMO and post DMO velocities applied. The vertical scale is equal to the horizontal scale with depths approximated assuming an average crustal velocity of 6000 m s-1.*

4 Conclusions

834 km of 150 fold deep seismic reflection data were acquired from Haig, WA and continued east along a road/track parallel to the Trans Australian Railway ending at Tarcoola, SA. The traverse spanned parts of the Eucla Basin and Gawler Craton. Here the seismic processing for eastern part of the line, which covers the Gawler craton, is described. For most of the seismic line, the seismic data provide images of the full depth of the crust through this region. The processed data provide valuable information on the nature of the major crustal structures and sedimentary layering in this area, and are of a quality that meets the scientific objectives of the project.

Acknowledgements

This document is modified from Costelloe and Holzschuh (2010). Land access was organised by the Geological Survey of Western Australia and the Geological Survey of South Australia. Project management by Tristan Kemp, data processing was done by Josef Holzschuh. Figures 1, 3, 4, 5 and 6, and their descriptions are taken from Holzschuh (2015).

References

Bell, J. G., Kilgour, P.L, English., P. M., Woodgate, M. F., Lewis, S. J. and Wischusen, J.D.H. (compilers), 2012, WASANT Palaeovalley Map - Distribution of Palaeovalleys in Arid and Semi-arid WA-SA-NT. (First Edition), scale: 1:4 500 000. Geoscience Australia Thematic Map (Geocat No 73980) – hard copy and digital data publication: http://www.ga.gov.au/cedda/maps/96.

Costelloe, R., and Holzschuh, J., 2010, 2008 Gawler Craton-Officer Basin-Musgrave Province-Amadeus Basin (GOMA) seismic survey, 08GA-OM1: acquisition and processing, in Korsch, R. J., and Kositcin, N,, eds., GOMA (Gawler Craton–Officer Basin–Musgrave Province–Amadeus Basin) Seismic and MT Workshop 2010. Geoscience Australia Record 2010/39, 1–6.

FrOG Tech P/L, 2005, OZ SEEBASE™ Study. Public Domain Report to Shell Development Australia (www.frogtech.com.au/products/oz-seebase).

Holzschuh, J., 2015, Extracting near surface information from complex regional seismic data with thick limestone and sand dunes at the near surface. Extended Abstract; 2015 SEG Near-Surface Asia Pacific Conference, Hawaii. Society of Exploration Geophysicists, Tulsa, Oklahoma.

Thiel, S., Duan, J., and Wise, T. W., 2015, Crustal resistivity structure of the western Gawler Craton and margins derived from the 13GA-EG1E magnetotelluric profile, in Dutch, R. A., Pawley, M. J., and Wise, T. W., eds., What lies beneath the western Gawler Craton? 13GA-EG1E Seismic and Magnetotelluric Workshop 2015, Report Book 2015/00029. Department of State Development, South Australia, Adelaide.

Yilmaz, Ö., 2001, Seismic Data Analysis: Processing, Inversion, and Interpretation of Seismic Data. Society of Exploration Geophysicists, Tulsa, Oklahoma.

FURTHER INFORMATION

J. Holzschuh
Josef.Holzschuh@ga.gov.au
Resources Division, Geoscience Australia,
GPO Box 378, Canberra, ACT 2601

Lithostratigraphy, structure and metamorphic architecture of a reworked Paleoproterozoic continental rift in the western Gawler Craton

Anthony Reid and Rian Dutch
Geological Survey of South Australia, Department of State Development

1 Introduction

While the western Gawler Craton is generally poorly exposed at the surface, geophysical imagery and drillhole intersections show that it is a structurally and lithologically complex region containing an array of different lithological and stratigraphic packages, each with their own associated mineral potential (Figs 1, 2; Daly et al., 1995; Daly et al., 1998). In particular, the region is host to Neoarchean gold deposits (Poustie et al., 2002; Birt and Reid, 2007), has potential for magmatic Ni-Cu sulphides associated with mafic and ultramafic rocks and also for magnetite iron ore resources (e.g. Gawler Iron Project, Iron Road Ltd; ASX release 10/04/2013; www.ironroadlimited.com.au). The cover sequences themselves also preserve their own energy and mineral potential, with potential for gas and oil reserves within the Neoproterozoic to Devonian rocks of the Officer Basin (Morton and Drexel, 1997), mineral sands within Eocene paleoplacer deposits of the Eucla Basin (Hou et al., 2011) and paleochannel-hosted roll front uranium potential within the Paleogene drainage network of the region (e.g. Hou and Alley, 2003). Understanding the geological evolution and crustal architecture of this region has implications for our understanding of the formation and location of these diverse styles of mineralisation.

The purpose of this paper is to review the geological evolution of the western Gawler Craton region with a focus on the macro-scale stratigraphy, various magmatic events, and the nature of the orogenic events that have affected the region as a basis for interpretation of the deep crustal seismic section (13GA-EG1E) across this region. We also provide a brief outline of the major cover sequences that blanket the region; the Officer Basin and the Eucla Basin. The east-west deep crustal seismic reflection line (13GA-EG1E) provides a cross section of the crust through this region and traverses a region of great structural complexity. The dominant structural trend of the Gawler Craton in this region trends towards ~030°, which means that the east-west oriented seismic section runs approximately orthogonal to the strike. We therefore gain an image of the geometry of this region and can now provide some constraints on the structural architecture.

2 Major lithostratigraphic subdivisions of the western Gawler Craton

The major lithostratigraphic units have been described as occurring within several geological domains: the Gawler Range Volcanics Domain, Nuyts Domain, Wilgena Domain, Fowler Domain, Christie Domain and Nawa Domain (Fig. 2; Table 1). A detailed description of the domains of the Gawler Craton was given by Ferris et al. (2002) and further reviews have been provided by Fraser and Reid (2007) and Kositcin (2010).

Here we provide a brief review of the geology of the major lithostratigraphic units of the region, with reference to the geological domains within which these units occur. In stratigraphic order these units begin with the Neoarchean to early Paleoproterozoic Mulgathing Complex, which is preserved within both the Wilgena and Christie domains. Following this, the younger lithostratigraphic units begin with the Paleoproterozoic metasedimentary basins that are preserved within the Fowler and Nawa domains. This is followed by a description of the predominantly magmatic events that occurred within the western Gawler Craton in the Paleoproterozoic to early Mesoproterozoic, now preserved across many of the domains, but especially so within the Nuyts and Gawler Range Volcanics domains.

The region has been subject to a number of significant deformation and metamorphic events, which can be grouped into the Sleafordian, Kimban, Kararan, and Coorabie orogenies, and also includes solid state deformation associated with the St Peter Suite in the Nuyts Domain (Table 2).

Figure 3 provides a schematic stratigraphic column for the western Gawler Craton which summarises the broad geological evolution of the region.

2.1 Mulgathing Complex: basin evolution and associated igneous events

The Mulgathing Complex occupies the region around Tarcoola and extends north and westwards to the Karari Shear Zone (Fig. 1). Isotopically similar gneisses of equivalent age occur to the north of the Karari Shear Zone, which suggests that the metamorphic rocks of the Nawa Domain are underlain by a Mulgathing Complex basement (Reid et al., 2014b). The Mulgathing Complex hosts the Challenger gold mine and is a region with exploration activity largely focussed on gold

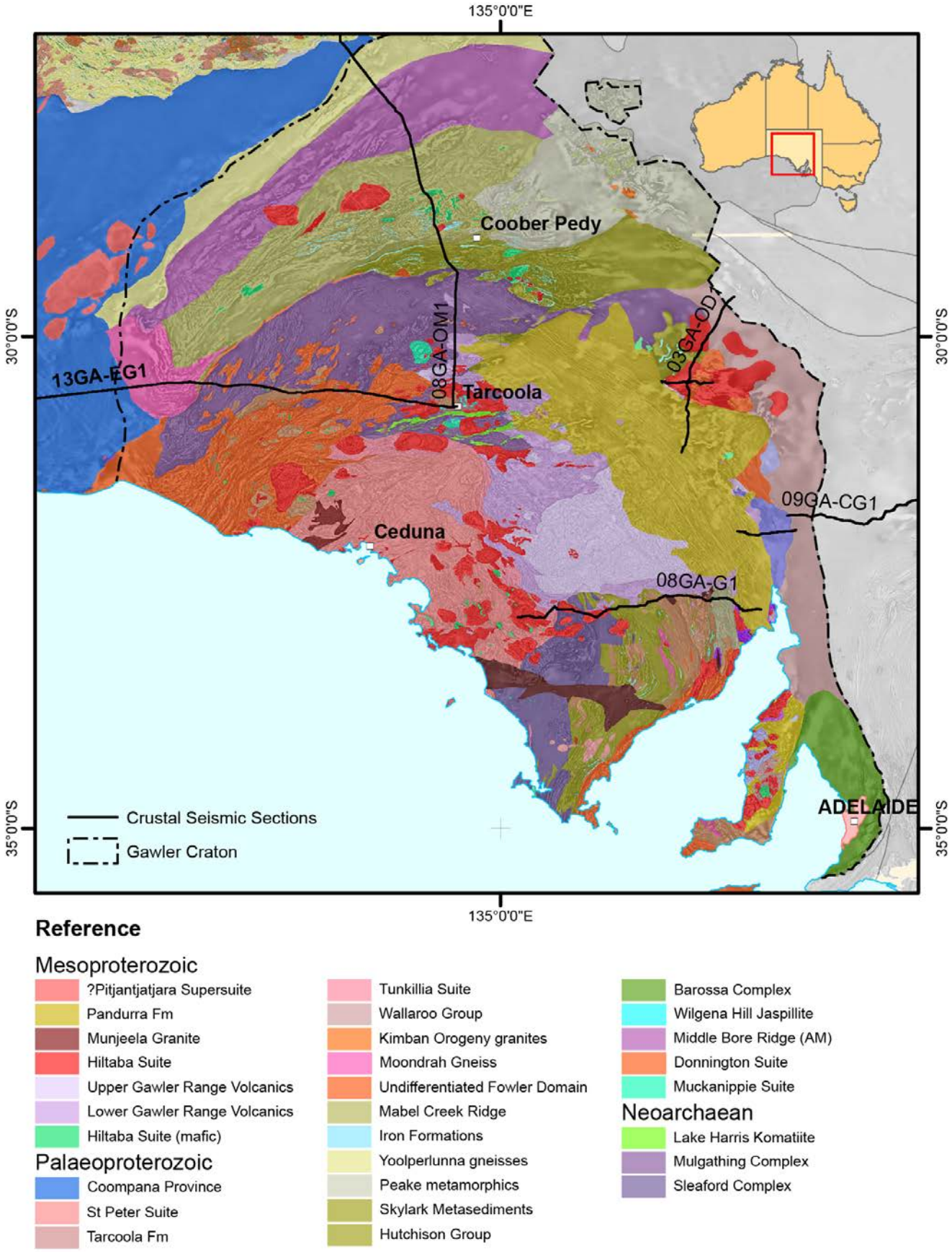

Figure 1 *Interpreted crystalline basement geology of the western Gawler Craton. Also shown is the location of the deep crustal seismic line 13GA_EG1.*

mineralisation, mafic-ultramafic-related Ni-Cu sulphides associated with komatiitic flows within the Harris Greenstone Domain and magnetite iron ore within metamorphosed iron formation (Daly and van der Stelt, 1992; Daly et al., 1998; Birt and Reid, 2007; Reid and Daly, 2009).

The Mulgathing Complex preserves evidence for volcano-sedimentary basin development from *c.* 2555 – 2480 Ma, terminated by orogenesis from *c.* 2465 – 2410 Ma (Reid et al., 2014b). Mafic and ultramafic rocks extruded as typical Al-depleted Archean komatiites and komatiitic basalt are present within the Harris Greenstone Domain at *c.* 2520 Ma

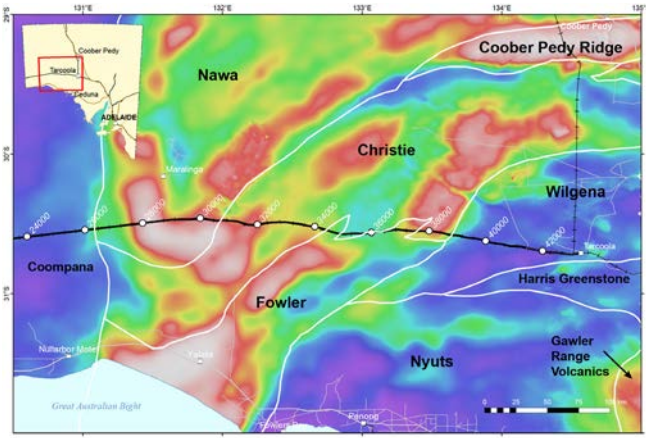

Figure 2 *Geological domains of the western Gawler Craton superimposed on a regional Bouguer gravity image. Data from Department of State Development.*

(Hoatson et al., 2005; Swain et al., 2005). The Harris Greenstone Domain also contains sequences of metamorphosed clastic and chemical sediments, including iron formations and carbonate rocks (Daly and Fanning, 1993). The metasedimentary units of the Mulgathing Complex are collectively termed the Christie Gneiss, which includes a range of lithologies including meta-carbonate, magnetite-rich iron formation and clastic metasedimentary rocks. The various lithologies of the Christie Gneiss were deposited from *c.* 2520 Ma to younger than *c.* 2485 Ma (Swain et al., 2005; McFarlane et al., 2007; Reid et al., 2014b). The metasedimentary Christie Gneiss is intercalated with felsic metavolcanic and volcaniclastic rocks, collectively termed the Kenella Gneiss (Daly and Fanning, 1993), deposited between *c.* 2535 – 2500 Ma (Swain et al., 2005; Fanning et al., 2007; Reid et al., 2014b). Rocks of the Christie Gneiss and Kenella Gneiss were intruded by mafic and felsic intrusives between *c.* 2530 – 2505 Ma (e.g. Glenloth Granite and Mobella Tonalite; Reid et al., 2014b). All of these rocks were subjected to metamorphism and deformation during the *c.* 2465 – 2410 Ma Sleafordian Orogeny (Daly and Fanning, 1993; McFarlane, 2006; Reid et al., 2014b).

Peak metamorphic conditions during the Sleafordian Orogeny reached granulite facies in the Mulgathing Complex. Available P-T estimates suggest temperatures >750 °C and pressures >5 kbar (Teasdale, 1997; Tomkins and Mavrogenes, 2002; McGee et al., 2010).This high temperature-low to moderate pressure event produced isoclinal to tight folds within the gneisses and was associated with partial melting and syn-tectonic magmatism.

Table 1 *First order lithostratigraphic units of the western Gawler Craton and their relationship to geological domains of the region.*

Lithostratigraphic unit	Age range (Ma)	Unit type	Domains in which this unit is present
Mulgathing Complex	2555 – 2420	Deformed during Sleafordian Orogeny, subsequently acted as basement to other units; multiply deformed	Principally within Wilgena and Christie domains, but also present as isolated enclaves within Fowler Domain, and as the basement to all other domains
Metasedimentary rocks of the Fowler Domain	c. 1760 – 1700	Volcano-sedimentary basin intruded by syn- and post-tectonic intrusives; multiply deformed	Fowler Domain
Metasedimentary rocks of the Nawa Domain	c. 1790 - 1720	Volcano-sedimentary basin intruded by syn- and post-tectonic intrusives; multiply deformed; e.g. Moondrah Gneiss	Nawa Domain
Tunkillia Suite	1690 – 1670	Widespread predominantly felsic intrusive; late syn- to post Kimban Orogeny	Fowler, Christie, Wilgena and Nyuts domains
Tarcoola Formation	c. 1650	Volcano-sedimentary basin	Wilgena Domain
St Peter Suite	c. 1620 – 1605	Magmatic suite; isotopically juvenile	Nyuts Domain
Gawler Range Volcanics	c. 1595 - 1575	Volcanic succession; subdivided into Lower and Upper units	Gawler Range Volcanics, Wilgena and Christie domains
Hiltaba Suite	c. 1585	Predominantly A-type intrusives	Gawler Range Volcanics, Fowler and Wilgena domains

Table 2 *Deformation and metamorphic events (orogenies) of the western Gawler Craton and their relationship to geological domains of the region.*

Event	Age range (Ma)	Metamorphic style	Associated magmatism	Domains affected
Sleafordian Orogeny	2465 – 2410	Moderate pressure-high temperature	Abundant; felsic and mafic	Principally Wilgena and Christie domains, but evident in Fowler and Nawa domains
Kimban Orogeny	c. 1730 – 1690	Moderate pressure-high temperature	Abundant; felsic and mafic	Fowler and Nawa domains; zones of local reworking (shear zones) in Christie and Wilgena domain
Deformation associated with St Peter Suite	c. 1620 – 1610	Moderate heat flow	Abundant; felsic and mafic	Nyuts Domain; solid state deformation fabrics within the St Peter Suite; syn-emplacement
Kararan Orogeny	c. 1600 – 1560	Moderate to low pressure-high temperature	Abundant; felsic and mafic	Fowler, Nawa, Coober Pedy Ridge domains; localised deformation within the Christie and Nyuts domains
Coorabie Orogeny	c. 1470 – 1450	Moderate heat flow	Minor; felsic	Fowler and Nawa domains

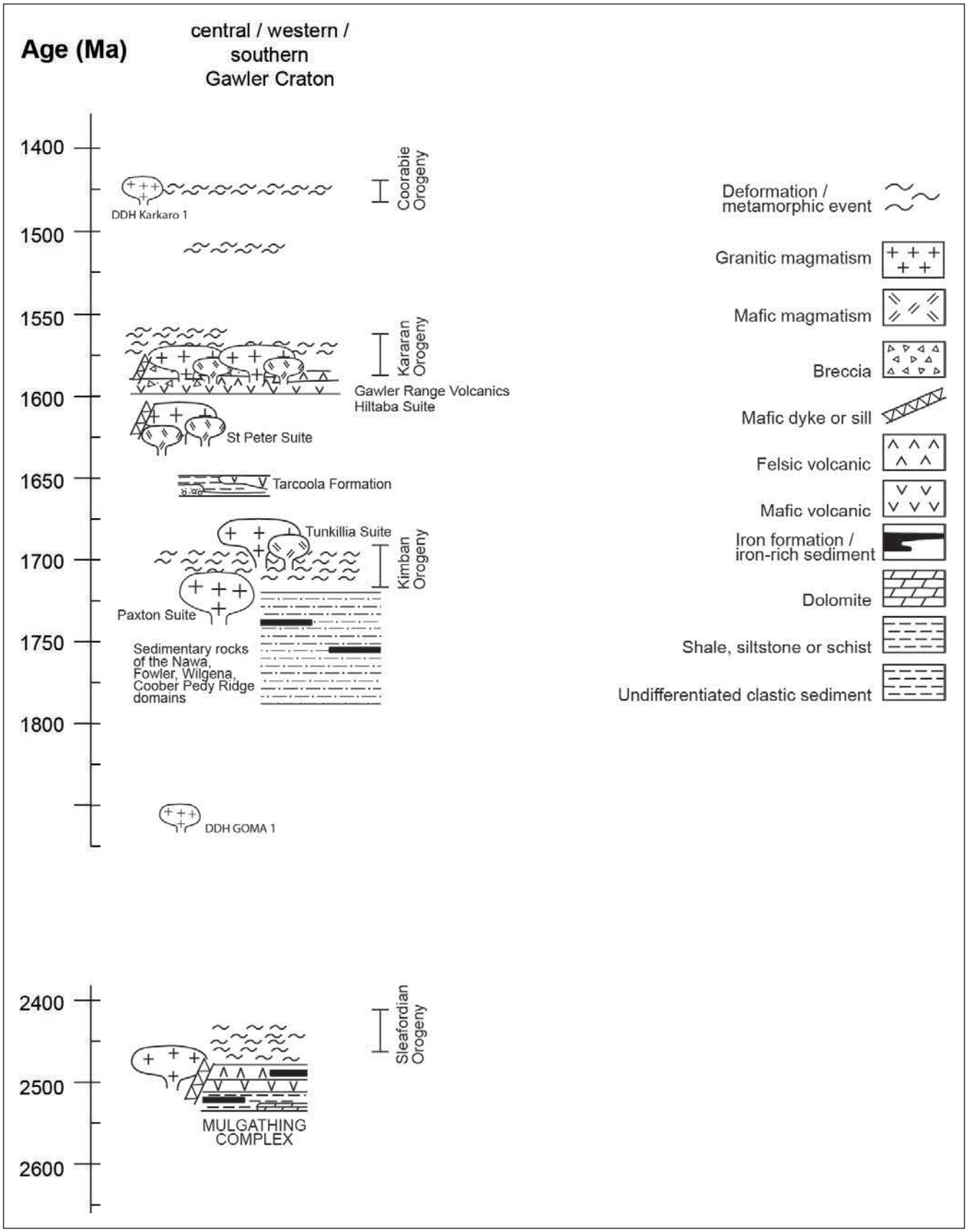

Figure 3 *Schematic stratigraphic column for the geology of the western Gawler Craton, including the Nawa Domain.*

2.2 Paleoproterozoic rifting: metasedimentary and meta-igneous rocks of the Fowler Domain and Nawa Domain

The Mulgathing Complex forms the basement to Paleoproterozoic sedimentary rocks preserved within the Fowler and Nawa domains. Volumetrically minor sedimentary rocks of possibly similar age are also present in the Wilgena Domain north of Tarcoola in the form of the Labyrinth Formation (*c.* 1715 Ma) and underlying Eba Formation (Howard et al., 2011a).

The Fowler Domain is a region of metamorphic rocks with relatively high magnetic intensity, comprising voluminous, dense, Palaeoproterozoic mafic and granitic intrusions together with interleaved metasedimentary rocks revealed in exploration drilling. The Fowler Domain is bounded by the Tallacootra and Coorabie shear zones and is dissected by a series of complex, anastomosing shear zones (Fig. 4). These shear zones divide the Fowler Domain into the Colona, Barton, Central and Nundroo blocks, which are regions of similar magnetic character with some significant lithological distinctions (Table 3; Daly and Martin, 1989; Daly et al., 1994; Teasdale, 1997; Constable et al., 2005). Geochronology and structural analysis of the shear zones of the Fowler Domain shows they were active during a number events including the Kimban Orogeny, Kararan Orogeny and Coorabie Orogeny (discussed below; Stewart et al., 2009).

The Fowler Domain contains a variety of metasedimentary lithologies including sillimanite–garnet–feldspar–quartz gneiss and banded iron formation. Detrital zircon data from metasedimentary rocks of the Fowler Domain indicate the sedimentary rocks are dominated by *c.* 1750 Ma zircon, contain older detrital components ranging in age up to 3130 Ma, and preserve maximum depositional ages of between 1760 and 1700 Ma (Fig. 5; Howard et al., 2011c). Metasedimentary rocks are moderately evolved in terms of their bulk Sm-Nd isotopic composition ($\varepsilon Nd_{1700\ Ma}$ = -4.3 to -3,4) and a greater range of Hf isotopic composition of individual detrital zircons, which suggest that, on average, the sedimentary protoliths in the Fowler Domain derived from a comparatively evolved but age-restricted source region (Howard et al., 2011c).

Igneous intrusions within the Fowler Domain include metamorphosed calc-alkaline cumulus gabbrodiorite and tonalite together with gabbro and altered chromite-bearing olivine-rich ultramafics (Daly et al., 1994; Morris et al., 1994). The Fowler Domain also contains abundant felsic intrusives, which are most evident in the northern portion of the domain (Barton Block), where the intrusions form curvilinear to elongate bodies of high magnetic intensity that stand out against the relatively low magnetic intensity of the surrounding Mulgathing Complex gneisses (Fig. 4). These intrusive rocks include equivalents of both the *c.* 1680 Ma Tunkillia Suite and *c.* 1595 – 1575 Ma Hiltaba Suite (Teasdale, 1997; Fanning et al., 2007). Daly et al. (1998) suggest that the mafic rocks could have been sills intruded into the sedimentary basin into which the clastic sediments were deposited. We note that the timing of sedimentation and magmatism in the Fowler Domain overlaps the timing of formation of the early phases of the Willyama Supergroup in the Curnamona Province.

The Nawa Domain occurs to the west and north of the Karari Shear Zone, has virtually no surface exposure, and only a handful of drill holes have been drilled into crystalline basement. Data from those basement-intersecting drill holes suggest however, that the Nawa Domain preserves evidence for Paleoproterozoic sedimentation and intrusive activity similar in age and composition to the Fowler Domain. The predominant rock types of the Nawa Domain are meta-sedimentary and

Table 3 *Summary of lithological associations and timing relationships of shear zone-bounded blocks within the Fowler Domain.*

Block	Lithological summary	Key drill holes
Nundroo Block	Dominated by intermediate to mafic lithologies including diorite, cumulate gabbro, tonalite and amphibolite; interlayered with metapelitic gneiss comprising garnet-sillimanite-biotite-K-feldspar-plagioclase-quartz-(magnetite).	Nundroo DDH 1-3; NDR series
	Overprinted by localised, high strain, relatively low grade mylonite and ultramylonite zones.	
	Coarse grained pegmatite cross-cuts mylonite.	
	Mafic lithologies are interpreted to have intruded into metasedimentary protoliths.	
Central	Dominated by felsic intrusive rocks; minor mafic material. Two generations of granite: medium grained, equigranular, weakly foliated granitoids of the Tunkillia Suite and a more biotite-rich phase of granites, possibly part of the Hiltaba Suite.	BAC and NDR series; NDR 13 intercepts foliated granite of the Hiltaba Suite
Barton	Rock types include: metasedimentary rocks biotite±sillimanite±garnet-Kfeldspar-magnetite gneiss and schist with maximum depositional ages from c. 1740 – 1720 Ma; and a range of mafic and ultramafic rocks including olivine-chromite bearing peridotite, two pyroxene metagabbro, to hornblende-garnet±biotite amphibolite. The mafic rocks are interpreted to be intrusive into the metasedimetary succession.	BAC and TAL holes, including TAL1 which has metamorphosed iron formation
	Also present are abundant felsic to intermediate, medium-coarse grained, variably deformed Tunkillia Suite granitoids. Mylonitic lithologies also abundant, ranging from augen gneiss to ultramylonite; may be overprinted by biotite-epidote, indicating K-rich metasomatism.	
Colona	Rock types include strongly magnetic, intermediate-mafic intrusive igneous rocks; granodiorite, tonalite and gabbro; where dated, gabbro was emplaced at c. 1740 Ma; deformed and metamorphosed during the Kimban Orogeny at c. 1718 Ma. Exrtensive mylonite formation resulted in hydrous mineral assemblages within mafic rocks (biotite-hornblende-epidote). These lithologies are cross-cut by late stage fine to medium grained undeformed granite.	COL series; including COL 43D which intersects metagabbro

meta-igneous rocks formed between *c.* 1775 – 1690 Ma (Payne et al., 2006; Fanning et al., 2007; Howard et al., 2011b). Metasedimentary rocks include quartz-rich clastic sediment and iron-rich sediment that is represented by magnetite-rich gneiss such as the Moondrah Gneiss of the south-western Nawa Domain in drill hole Ooldea DDH 2 (Fig. 1; Daly et al., 1998). The metasedimentary rocks of the Nawa Domain show virtually identical zircon provenance to similar aged rocks in the Fowler Domain (Fig. 5), being dominated by *c.* 1750 Ma zircon and having relatively few older provenance populations (Payne et al., 2006). The metasedimentary rocks have moderately evolved $eNd_{1750\ Ma}$ values between -5 and -3.8, indicating derivation from a provenance region less evolved than an average of the Archean portion of the Gawler Craton (Payne et al., 2006). Lu-Hf isotopic data from individual zircons from metasedimentary rocks of the Nawa Domain show a greater εHf range, from -7 to +5, but with mean εHf values around -1 (Armit et al., 2010). Meta-igneous rocks of the Nawa Domain include *c.* 1775 – 1750 Ma felsic rocks, which are also isotopically less evolved than an average of Archean basement of the Gawler Craton (eNd_{2500Ma} +3.8 to -3.7), suggesting that they formed via mixing of mantle-derived melts with a felsic lower crust (Howard et al., 2011b). These metasedimentary and meta-igenous rocks are interpreted to overlie or intrude an older basement (Daly et al., 1998), which comprises *c.* 1920 Ma and *c.* 2460 Ma orthogneiss (Fanning et al., 2007; Howard et al., 2011b; Reid et al., 2014a).

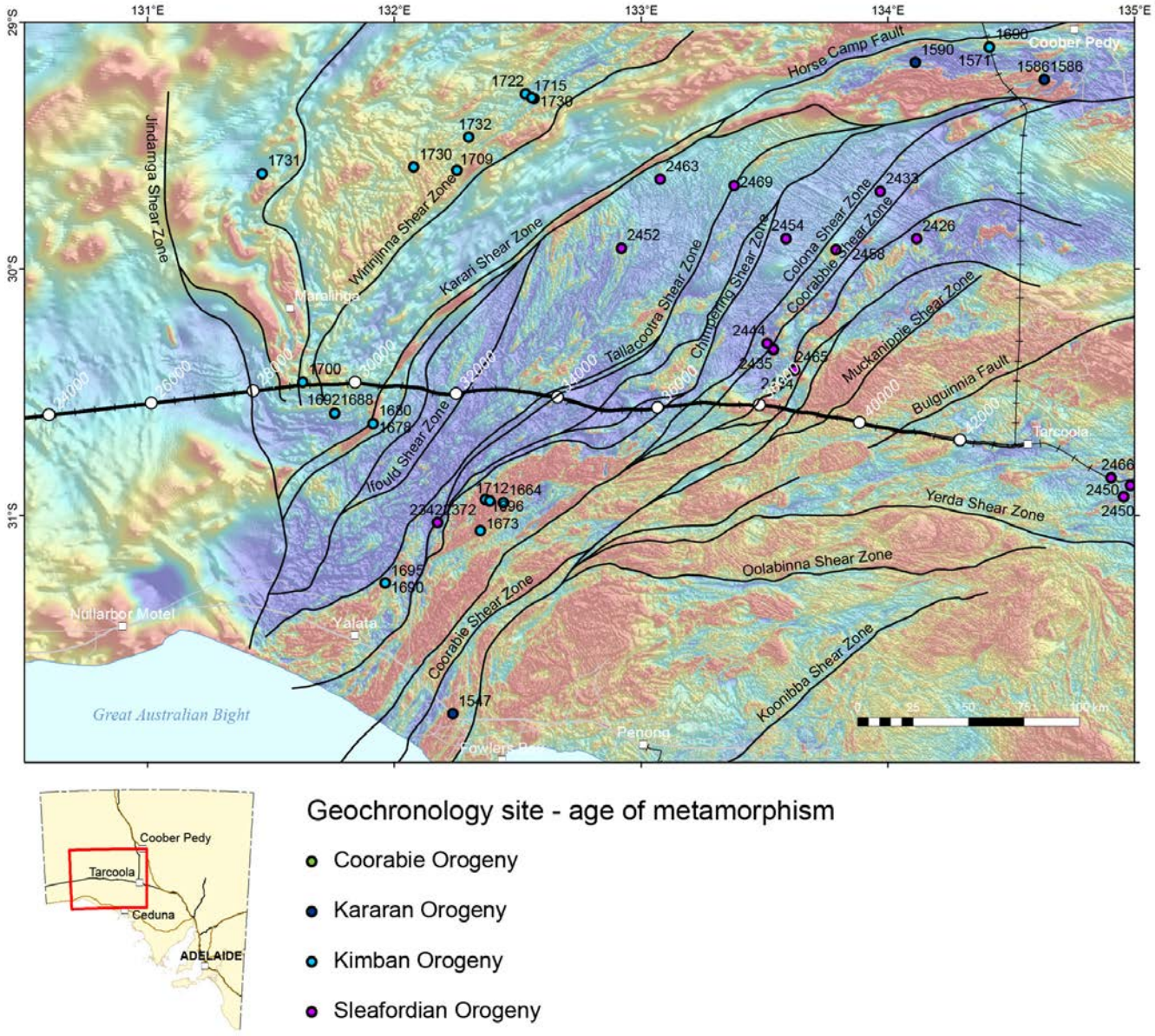

Figure 4 *Major structures of the western Gawler Craton including the location of the Fowler Domain superimposed on a regional reduced to pole total magnetic intensity image. Data from Department of State Development. Also shown are monazite or zircon U-Pb ages for metamorphism in Ma for geochronology sample sites across the region. Data points are subdivided into corresponding orogenic events. These data derived from studies including Teasdale (1997); Tomkins (2002); Tomkins et al. (2004); Payne et al. (2006); Fanning et al. (2007); Hand et al. (2007); Payne et al. (2008); Dutch and Hand (2009); Cutts et al. (2011); Howard et al. (2011b); Howard et al. (2011c); Fraser et al. (2012); Cutts et al. (2013); Reid et al. (2014a); Reid et al. (2014b).*

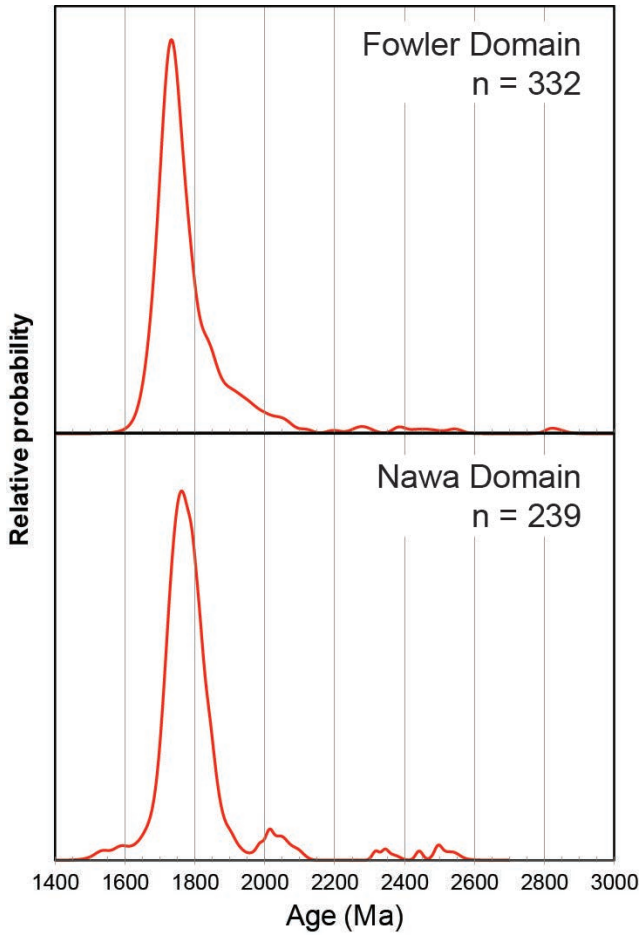

Figure 5 *Probability density distribution for detrital zircon U-Pb ages from samples across the western Gawler Craton. A) Data from the Fowler Domain of Howard et al. (2011c), comprising 8 samples and 332 individual zircon analyses. B) Data from the Nawa Domain of Payne et al. (2006), comprising 3 samples and 239 individual zircon analyses. Note $^{207}Pb/^{206}Pb$ ages plotted; not filtered for discordance.*

Geophysical data reveal that rocks of the Nawa Domain are deformed by a series of north-east trending structures that are predominantly north-dipping (Korsch et al., 2010; Baines et al., 2011). At least some of the north-dipping structures likely formed during development of the Paleoproterozoic basin, with these basin-bounding structures being reactivated during the Kimban and Kararan orogenic events (Daly et al., 1998; Payne et al., 2008; Betts et al., 2010; Fraser et al., 2012; Cutts et al., 2013), and again during the reworking associated with shear zone reactivation at *c.* 1450 Ma (Fraser and Lyons, 2006).

The Coober Pedy Ridge Domain is also present in the northern Gawler Craton and is located between the Karari Shear Zone and the Horse Camp Fault (Fig. 1) and represents a pop-up structure formed during deformation on these crustal scale shear zones (Korsch et al., 2010). The Coober Pedy Ridge Domain comprises metasedimentary and meta-igneous rocks with virtually identical characteristics to similar rocks of the Nawa and Fowler domains (Daly et al., 1998), being dominantly clastic sediments formed at *c.* 1750 Ma and intruded by *c.* 1730 Ma mafic and felsic igneous rocks (Fanning et al., 2007). Deformation and high to ultra-high temperature metamorphism within the Coober Pedy Ridge occurred at *c.* 1590 Ma and is associated with Hiltaba Suite-aged intrusions (Fanning et al., 2007; Payne et al., 2008; Cutts et al., 2011).

2.3 Kimban Orogeny: major crustal reworking event

The Fowler and Nawa domains were reworked during the Kimban Orogeny as evidenced by *c.* 1710 – 1680 Ma metamorphic ages from ortho- and paragneisses of the region (Payne et al., 2008; Howard et al., 2011c; Cutts et al., 2013). Metamorphic conditions during this event are broadly medium temperature and moderate pressure and this event is associated with emplacement of mafic and felsic intrusions (Fanning et al., 2007; Hand et al., 2007). A detailed structural study of the western Gawler Craton by Stewart et al. (2009) showed that the Kimban Orogeny was associated with north-south orientated pure shear, associated flattening and with relatively minor and partitioned simple shear across the region. Reactivation of structures during the Kimban Orogeny may also have occured across the Christie Domain, with numerous shear zones, including the Tallacootra and Coorabie shear zones, deforming Mulgathing Complex gneisses (Fig. 2). These structures are also spatially associated with the boundaries of interpreted Tunkillia Suite granites (Fig. 2).

The Tunkillia Suite is a *c.* 1690 – 1670 Ma predominantly felsic igneous suite formed by melting of a moderately juvenile protolith combined with minor assimilation of Archean crust, most likely formed in a 'post-orogenic' setting (Payne et al., 2010b). The Tunkillia Suite is present between shear zones such as the Yerda and Oolabinna (Fig. 4), and also occurs throughout the Fowler Domain in regions that underwent strong Kimban-aged deformation, which suggests that magma flow was facilitated by late stages of deformation during the Kimban Orogeny.

2.4 Tarcoola Formation: post-Kimban Orogeny sedimentation

The Tarcoola Formation is a fault-bound package of clastic sediment and minor mafic volcanic rocks occurring in the central Gawler Craton, with an estimated thickness of >2000 m (Daly, 1993). The formation has a number of distinct units that grade upwards from a basal conglomerate, into quartzite, mafic and local felsic tuff, and carbonaceous shales. A felsic tuff within the Tarcoola Formation gave an age of *c.* 1656 Ma (Daly et al., 1998), indicating the rock package was deposited subsequent to the Kimban orogeny. The Tarcoola Formation is interpreted to have been deposited within a series of graben or half graben structures (Daly, 1993) and is therefore a late Paleoproterozoic cover sequence that overlies the Mulgathing Complex in the central Gawler Craton. The Tarcoola Formation has been deformed by broad open folds at lower greenschist facies. Quartz veining is associated with the folding and local thrusting and is host to the bonanza gold mineralisation of the Tarcoola

goldfield (Daly et al., 1990). This mineralisation event occurred at *c.* 1585 Ma and is part of the mineralisation within the Central Gawler Gold Province (Daly et al., 1990; Budd and Fraser, 2004; Budd and Skirrow, 2007).

2.5 Magmatism within the Nuyts Domain: the St Peter Suite

The Nuyts Domain is a semi-circular region dominated by magmatic rocks and bound on the east by the Yarlbrinda Shear Zone and on the west by the Coorabie Shear Zone (Fig. 1). The magmatic rocks within this domain include three suites: the Nuyts Volcanics, the St Peter Suite and the Munjeela Suite. The Nuyts Volcanics are a volumetrically minor series of *c.* 1630 Ma felsic porphyritic volcanics which occur on islands of the Nuyts Archipelago (Rankin et al., 1990; Rankin and Flint, 1991), but little is known of their geochemical evolution.

The St Peter Suite makes up the bulk of the magmatic rocks of the Nuyts Domain and comprises a relatively juvenile magmatic suite that represents an addition of mantle material into the crust of the Gawler Craton at *c.* 1620 – 1605 Ma. The St Peter Suite comprises mafic and felsic magmas that are generally enriched in large ion lithophile elements (e.g. Rb, K, Ba) and depleted in Ta, Nb and Ti, and is isotopically juvenile with respect to the typical Archean-Paleoproterozoic crust of the Gawler Craton (Flint et al., 1990; Swain et al., 2008). These features have led some authors to propose that the St Peter Suite may have formed in response to subduction zone processes in a late Paleoproterozoic magmatic arc (Ferris et al., 2002; Swain et al., 2008).

The St Peter Suite preserves evidence for deformation associated with its emplacement, and includes some mafic rock types including gabbro and pyroxenite, which may have potential for Ni-Cu sulphides (Flint et al., 1990). If the St Peter Suite did form within a subduction zone setting, the elevated H_2O contents expected of subduction-related magmas together with the mingling and mixing of mafic and felsic magmas could result in a fertile region for other styles of mineralisation in particular porphyry Cu-Au systems potentially analogous to magmatic arc settings of the Pacific Rim.

The *c.* 1585 Ma Munjeela Suite comprises peraluminous, muscovite-biotite±garnet±tourmaline-bearing S-type granites coeval with the Gawler Range Volcanics–Hiltaba Suite magmatic event (Payne et al., 2010a). These granites are therefore likely to have been generated through melting of a sedimentary precursor. Munjeela Suite granites contain rare metasedimentary enclaves, detrital zircons from which have provided a maximum depositional age of *c.* 1625 Ma (Payne, 2008), indicating that there was a sedimentary succession in this region that may have been broadly coeval with the formation of the Nuyts Volcanics and, potentially, with the early phases of the St Peter Suite. No field relationships between these units have been observed.

2.6 High temperature early Mesoproterozoic magmatism: Gawler Range Volcanics and Hiltaba Suite

The Gawler Range Volcanics erupted at *c.* 1590 and form a broadly circular mass of lava flows that range from basalt to rhyolite in composition in the central Gawler Craton. The Gawler Range Volcanics are subdivided into a lower and upper package (Fanning et al., 1988; Blissett et al., 1993; Daly et al., 1998; Allen et al., 2003; Allen et al., 2008). The lower Gawler Range Volcanics shows the greatest lithological diversity, with fissure-like eruptions of basalt, basaltic andesite and rhyolite present. The lower Gawler Range Volcanics is also rarely interlayered with coarse clastic sediment of variable thickness. Subsequently, the region of the central Gawler Craton was covered by a series of extensive felsic lava flows of the upper Gawler Range Volcanics, which extend across the region and in to the central-western Curnamona Province (Benagerie Volcanic Suite), making the preserved remnants of this volcanic event cover an estimated >100 000 km^2 (Wade et al., 2012). Associated with the Gawler Range Volcanics, emplacement of mostly high level granitic bodies occurred across the Gawler Craton, including the western Gawler Craton. This intrusive magmatic event appears to have outlasted the extrusive volcanism (or at least the preserved volcanic edifice) with magmatism continuing from *c.* 1595 Ma to as young as *c.* 1575 Ma (Hand et al., 2007). While this early Mesoproterozoic magmatic event is most concentrated in the central Gawler Craton, evidence for magmatism of this age is also present in the Fowler Domain, suggesting this magmatothermal event affected much of the crust of the western Gawler Craton.

In the western extent of the Gawler Range Volcanics Domain and in the region around Tarcoola, magmatism was associated with fluid flow, sericite-chlorite alteration and in places Au-dominated mineralisation. The Tunkillia 223 deposit has contained resources of 558 000 ounces of gold and 1.48 million ounces of silver (WPG Resources, ASX Release 04/02/2015, http://www.wpgresources.com.au/) and the various deposits of the Tarcoola gold field accounts for historical production of around 2300 kg Au, at an average grade of 37.5 g/t Au, including about 1779 kg at an average grade of 42.8 g/t Au from the Tarcoola Blocks mine (Daly et al., 1990). In addition, a total (measured, indicated, and inferred) resource of 1.545 million metric tons (Mt) at 1.8 g/t Au for a total of 2781 kg Au has been outlined historically at the Perseverance, Last Resource, and Wondergraph deposits (Hughes, 1998), with more recent work reporting total proven plus probable resource of 900 Mt at a grade of 2.6 g/t Au containing 74 000 oz Au (WPG Resources, Annual Report, 23/10/2015, http://www.wpgresources.com.au/). This mineralisation formed in response to the deformation and fluid flow associated with the Gawler Range Volcanics-Hiltaba Suite magmatic event and are considered to be part of an early Mesoproterzoic mineral province, the Central Gawler Gold Province (Drown, 2003; Ferris and Schwarz, 2003; Budd and Fraser, 2004; Budd and Skirrow, 2007).

2.7 Mesoproterozoic deformation and metamorphism

Both synchronous with and subsequent to eruption of the Gawler Range Volcanics and emplacement of Hiltaba Suite plutons, the Gawler Craton underwent variable degrees of partitioned strain and associated metamorphism. In the northern Gawler Craton, regions such as the Nawa Domain and Coober Pedy Ridge were metamorphosed to granulite facies at *c.* 1580 – 1560 Ma (Daly et al., 1998; Fanning et al., 2007; Cutts et al., 2011). In the Fowler Domain Hiltaba Suite granites are themselves deformed indicating strain also continued post *c.* 1585 Ma in this region (Teasdale, 1997). Therefore, while the region of the central Gawler Craton in the vicinity of Tarcoola remained in the upper crust, permitting the preservation of the volcanic successions of the Gawler Range Volcanics, regions to the west underwent subsequent deformation in order to juxtapose the *c.* 1580 Ma mid- to lower crustal rocks of the southern Nawa Domain and Coober Pedy Ridge at the same crustal level as upper crustal volcanics. The timing of this deformation is constrained in part by $^{40}Ar/^{39}Ar$ analyses from micas within mylonitic rocks within the shear zones of the western and northern Gawler Craton. The $^{40}Ar/^{39}Ar$ thermochronology data indicate cooling of the region below biotite closure temperatures of ~300 °C had occurred by *c.* 1530 Ma across much of the region (Fraser and Lyons, 2006; Forbes et al., 2012; Fraser et al., 2012). In some instances, $^{40}Ar/^{39}Ar$ data can be interpreted to record the new growth of micaceous minerals within mylonites of the western Gawler Craton (Fraser and Lyons, 2006), suggesting not only regional cooling occurred at around this time, but that at *c.* 1460 – 1440 Ma during the Coorabie Orogeny (Hand et al., 2007), several of the major shear zones including the Karari and Tallacootra shear zones were reactivated at this time. This *c.* 1450 Ma deformation event is also recorded in metamorphic monazites from the central Nawa Domain (Howard, 2011).

2.8 Cover sequences of the western Gawler Craton: Officer Basin and Eucla Basin

The Officer Basin is a Neoproterozoic to Devonian intracratonic sedimentary basin situated to the west of the Gawler Craton and south of the Musgrave Province (Fig. 6; Preiss et al., 1993). The Officer Basin extends far into Western Australia and has a maximum thickness of sediment ~10 km (Jackson and van de Graaff, 1981). Neoproterozoic units in South Australia are dominated by carbonate (dolomite), sandstone and glacial tillite, with local mafic volcanics (Wantapella Volcanics). The Neoproterozoic succession in the Officer Basin is not as complete as the extensive sequences preserved in the Adelaide Geosyncline , and stratigraphic correlation between these Neoproterozoic successions is hampered by sparse outcrop and drilling in the Officer Basin (Preiss et al., 1993). An erosive unconformity separates the Neoproterozoic from Cambrian units (Marla Group), with the latter deposited in elongate troughs and being dominated by red bed successions of fluvial to marginal marine affinity. Mild deformation may have occurred in the north-eastern Officer Basin during the Ordovician Delamerian Orogeny (Morton and Drexel, 1997). Ordovician to Devonian deposition of shallow marine to fluvial sandstones occurred to the north as a thick wedge, thickening against the Musgrave Block and terminated by the Alice Springs Orogeny. Although no commercial hydrocarbon accumulations have been discovered within the Officer Basin, it preserves hydrocarbon shows and retains some potential for future discoveries (Morton and Drexel, 1997; Ghori, 2002).

The Eucla Basin is an intracratonic basin developed on the margins of the Gawler Craton, the southern Musgrave Province and the Yilgarn Craton and overlying the Officer Basin. The Eucla Basin comprises both onshore and offshore marginal marine to shelf deposits, the onshore portion of which extends some 200 km east-west and up to 500 km north-south, making it is one of the world's largest Cenozoic basins (Fig. 6; Benbow et al., 1995; Hou et al., 2008). The Eucla Basin is characterised by basal sandstone units (Hampton Sandstone, Pidinga Formation) of Middle Eocene age that are overlain by a series of transgressive platform carbonate units. These units include the Wilson Bluff Limestone (Late Eocene), Abrakurrie Limestone and Nullarbor Limestone (both Miocene), which form the base of the flat geomorphological feature that is the Nullarbor Plain. The Wilson Bluff Limestone has extensive, temporarily equivalent, marginal marine to paleobeach, estuarine and associated paleochannel deposits, which are preserved in the Pidinga Formation and in two major barrier systems, the Barton and Ooldea ranges. The paleobeach sediment associated with these high energy depositional environments are host to significant accumulations

Figure 6 *Extent of the Officer and Eucla basins within South Australia with respect to the deep crustal seismic line 13GA-EG1E.*

of mineral sands, which are some of the most zircon-rich heavy mineral deposits in the world (Hou et al., 2011). Internal to and behind the two barrier systems lies an extensive paleochannel network filled by predominantly estuarine deposits and, in some instances, follows a drainage network established during the Cretaceous and Permian (Benbow, 1990; Benbow et al., 1995; Hou et al., 2003).

The Eucla Basin has undergone mild Late Miocene to Pleistocene basin inversion as a result of overall north-east side down tilting of the Australian continent (Hou et al., 2008; Sandiford et al., 2009). This exhumation resulted in some 150 m of relative movement across the western versus eastern portions of the basin. Miocene shore line facies deposits transgress the Eocene barrier sands in the Gawler Craton region, yet equivalent aged sediment is regressive in deposits that overly the Albany-Fraser Orogen in Western Australia. This continental-scale tilting is an example of dynamic topography associated with interaction between the broadly east-west compressive stress field, and the relatively fast moving Australian continent and the underlying mantle (Sandiford, 2007).

3 Summary

The western Gawler Craton a long-lived history of sedimentary, magmatic and tectonic events. The geological history begins with deposition and volcanism within a sedimentary basin that was to become the Mulgathing Complex and subsequent metamorphism and deformation during the early Paleoproterozoic Sleafordian Orogeny. The Mulgathing Complex then became the crystalline basement to a number of Paleoproterozoic volcano-sedimentary basins that formed across the Gawler Craton, one portion of which is now preserved within the intensely reworked region of the Fowler Domain, and another portion of which is represented by the metasedimentary rocks of the Nawa Domain, including the Moondrah Gneiss. Extensive deformation followed basin formation at *c.* 1720 – 1680 Ma, as part of the Kimban Orogeny. Widespread, predominantly felsic magmatism following the Kimban Orogeny resulted in the formation of the largely post-tectonic Tunkillia Suite.

Subsequent to the Kimban Orogeny there was localised basin development in the central Gawler Craton represented by the Tarcoola Formation and indirect evidence for sedimentation in the Nuyts Domain as recorded by *c.* 1630 Ma metasedimentary enclaves within S-type granites of the *c.* 1585 Ma Munjeela Suite. Magmatism also occurred in the Nuyts Domain at *c.* 1630 Ma as preserved within the Nuyts Volcanics, however, these units are recorded across a very limited spatial extent. More voluminous magmatism occurred at *c.* 1620 – 1605 Ma with the formation of the juvenile and potentially subduction-related St Peter Suite. The St Peter Suite occupies the major portion of the Nuyts Domain and given its unusual geochemistry may have played an important role in priming the crust for the extensive early Mesoptoterozoic felsic and mafic magmatism that formed the Gawler Range Volcanics, Hiltaba Suite and the S-type Munjeela Suite. Gold and gold-silver mineralisation associated with this magmatic event is present in the Central Gawler Gold Province.

The region underwent significant deformation and metamorphism following this early Mesoproterozoic magmatic and metallogenic event, however, this deformation was spatially partitioned into the regions to the west of the central Gawler Craton. Indeed, the region to the north of the Karari Shear Zone, including the Coober Pedy Ridge and southern Nawa Domain, underwent very high temperature metamorphism broadly synchronous with the Gawler Range Volcanics-Hiltaba Suite magmatic event. Early Mesoproterozoic cooling as recorded in thermochronology data from the western Gawler Craton likely indicate deformation continued along several of the major shear zones at *c.* 1450 Ma as part of the Coorabie Orogeny, the final major phase in the evolution of the Gawler Craton.

Subsequent intracratonic basin formation during the Neoproterozoic permitted deposition of the basal units of the Officer Basin, which continued to be a depocentre onlapping the western Gawler Craton into the Cambrian. The region is also covered by sediment of the Eucla Basin, which includes significant heavy mineral accumulations and whose limestone deposits form the vast, low relief expanse of the Nullarbor Plain.

Acknowledgements

Wayne Cowley and Stacey McAvaney (GSSA) are thanked for comments and reviews on this abstract.

References

Allen, S. R., McPhie, J., Ferris, G., and Cadd, A. G., 2008, Evolution and architecture of a large felsic igneous province in western Laurentia: The 1.6 Ga Gawler Range Volcanics, South Australia: Journal of Volcanology and Geothermal Research, v. 172, p. 132-147.

Allen, S. R., Simpson, C. J., McPhie, J., and Daly, S. J., 2003, Stratigraphy, distribution and geochemistry of widespread felsic volcanic units in the Mesoproterozoic Gawler Range Volcanics, South Australia: Australian Journal of Earth Sciences, v. 50, no. 1, p. 97-112.

Armit, R., Betts, P. G., and Schaefer, B. F., 2010, Lu-Hf isotope characteristics of the marginal terranes of the northern Gawler Craton, in Korsch, R. J., and Kositcin, N., eds., GOMA (Gawler Craton-Officer Basin-Musgrave Province-Amadeus Basin) Seismic and MT Workshop 2010, Geoscience Australia, Record, 2010/39, p. 118-127.

Baines, G., Giles, D., Betts, P. G., and Backé, G., 2011, Locating a major Proterozoic crustal boundary beneath the Eastern Officer Basin, Australia: Precambrian Research, v. 191, no. 3–4, p. 120-140.

Benbow, M. C., 1990, Coastal dunes of the Eucla Basin, Australia: Geomorphology, v. 3, p. 9-29.

Benbow, M. C., Lindsay, J. M., and Alley, N. F., 1995, Eucla Basin and palaeodrainage, in Drexel, J. F., and Preiss, W. V., eds., The Geology of South Australia, Vol. 2 The Phanerozoic, Volume Bulletin 54, Mines and Energy South Australia, p. 178-186.

Betts, P. G., Armit, R., Baines, G., Giles, D., and Schaefer, B. F., 2010, Crustal boundaries of the marginal terranes of the northern Gawler Craton, in Korsch, R. J., and Kositcin, N., eds., GOMA (Gawler Craton-Officer Basin-Musgrave Province-Amadeus Basin) Seismic and MT Workshop 2010, Geoscience Australia, Record, 2010/39, p. 128-137.

Birt, T., and Reid, A. J., 2007, Archaean gold systems of South Australia: MESA Journal, v. 46, p. 29-33.

Blissett, A. H., Creaser, R. A., Daly, S., Flint, D. J., and Parker, A. J., 1993, Gawler Range Volcanics, in Drexel, J. F., Preiss, W. V., and Parker, A. J., eds., The geology of South Australia. Vol 1. The Precambrian: Adelaide, Geological Survey of South Australia, Bulletin 54, p. 107-131.

Budd, A. R., and Fraser, G. L., 2004, Geological relationships and 40Ar/39Ar age constraints on gold mineralisation at Tarcoola, central Gawler gold province, South Australia: Australian Journal of Earth Sciences, v. 51, p. 685-700.

Budd, A. R., and Skirrow, R. G., 2007, The nature and origin of gold deposits of the Tarcoola goldfield and implications for the central Gawler gold province, South Australia: Economic Geology, v. 102, no. 8, p. 1541-1563.

Constable, S., Fairclough, M. C., and Gum, J., 2005, Nickel mineralisation models in the Fowler Domain and Musgrave Province - applying the Thompson Nickel Belt as an analogue: MESA Journal, v. 39, p. 14-21.

Cutts, K., Hand, M., and Kelsey, D. E., 2011, Evidence for early Mesoproterozoic (ca. 1590 Ma) ultrahigh-temperature metamorphism in southern Australia: Lithos, v. 124, p. 1-16.

Cutts, K. A., Kelsey, D. E., and Hand, M., 2013, Evidence for late Paleoproterozoic (ca 1690–1665Ma) high- to ultrahigh-temperature metamorphism in southern Australia: Implications for Proterozoic supercontinent models: Gondwana Research, v. 23, no. 2, p. 617-640.

Daly, S. J., 1993, Tarcoola Formation, in Drexel, J. F., Preiss, W. V., and Parker, A. J., eds., The geology of South Australia; Volume 1, The Precambrian, Volume Geological Survey of South Australia. Bulletin 54, p. 68-69.

Daly, S. J., Fairclough, M. C., Fanning, C. M., and Rankin, L. R., 1995, Tectonic evolution of the western Gawler Craton: a Palaeoproterozoic collision zone and likely plate margin, Structural Geology and Tectonics Specialist Group, Clare Valley Conference, Geological Society of Australia. Abstracts 40, p. 35-36.

Daly, S. J., and Fanning, C. M., 1993, Archaean, in Drexel, J. F., Preiss, W. V., and Parker, A. J., eds., The geology of South Australia; Volume 1, The Precambrian: Adelaide, South Australia, Australia, Geological Survey of South Australia. Bulletin 54, p. 32-49.

Daly, S. J., Fanning, C. M., and Fairclough, M. C., 1998, Tectonic evolution and exploration potential of the Gawler Craton, South Australia: AGSO Journal of Australian Geology & Geophysics, v. 17, p. 145-168.

Daly, S. J., Horn, C. M., and Fradd, W. P., 1990, Tarcoola Goldfield, in Hughes, F. E., ed., Geology of the mineral deposits of Australia and Papua New Guinea, Volume 14, Australasian Institute of Mining and Metallurgy. Monograph Series, p. 1049-1053.

Daly, S. J., and Martin, A. R., 1989, Nundroo 1, 2 and 3 - well completion report: South Australia. Department of Mines and Energy, v. Report Book 89/39.

Daly, S. J., Tonkin, D. G., Purvis, A. C., and Shi, Z., 1994, Colona drilling program, South Australia. Department of Mines and Energy. Open file Envelope, 8768 (unpublished).

Daly, S. J., and van der Stelt, B. J., 1992, Archaean metabasic diamond drilling project, South Australia. Department of Mines and Energy. Open file Envelope 8541 (unpublished).

Drown, C. G., 2003, The Barns Gold Project - discovery in an emerging district: MESA Journal, v. 28, p. 4-9.

Dutch, R. A., and Hand, M., 2009, EPMA monazite geochronological constraints on the timing of ultra-high temperature reworking in the western Gawler Craton, South Australia. Department of Primary Industries and Resources. Report Book, 2009/2.

Fanning, C. M., Flint, R. B., Parker, A. J., Ludwig, K. R., and Blissett, A. H., 1988, Refined Proterozoic evolution of the Gawler Craton, South Australia, through U-Pb zircon geochronology: Precambrian Research, v. 40/41, p. 363-386.

Fanning, C. M., Reid, A. J., and Teale, G., 2007, A geochronological framework for the Gawler Craton, South Australia, South Australia Geological Survey. Bulletin 55.

Ferris, G. M., and Schwarz, M. P., 2003, Proterozoic gold province of the Central Gawler Craton: MESA Journal, v. 30, p. 4-12.

Ferris, G. M., Schwarz, M. P., and Heithersay, P., 2002, The geological framework, distribution and controls of Fe-oxide and related alteration, and Cu-Au mineralisation in the Gawler Craton, South Australia. Part I: geological and tectonic framework, in Porter, T. M., ed., Hydrothermal iron oxide copper-gold and related deposits: a global perspective, Volume 2: Adelaide, PGC Publishing, p. 9-31.

Flint, R. B., Rankin, L. R., and Fanning, C. M., 1990, Definition; the Palaeoproterozoic St. Peter Suite of the western Gawler Craton: Quarterly Geological Notes - Geological Survey of South Australia, v. 114, p. 2-8.

Forbes, C. J., Giles, D., Jourdan, F., Sato, K., Omori, S., and Bunch, M., 2012, Cooling and exhumation history of the northeastern Gawler Craton, South Australia: Precambrian Research, v. 200–203, no. 0, p. 209-238.

Fraser, G., and Lyons, P., 2006, Timing of Mesoproterozoic tectonic activity in the northwestern Gawler Craton constrained by 40Ar/39Ar geochronology: Precambrian Research, v. 151, p. 160-184.

Fraser, G., Reid, A., and Stern, R., 2012, Timing of deformation and exhumation across the Karari Shear Zone, north-western Gawler Craton, South Australia: Australian Journal of Earth Sciences, v. 59, no. 4, p. 547-570.

Fraser, G. L., and Reid, A. J., 2007, Time-Space evolution of the Gawler Craton, in Neumann, N. L., and Fraser, G. L., eds., Geochronological synthesis and Time-Space plots for Proterozoic Australia, Geoscience Australia Record 2007/06, p. 3-33.

Ghori, K. A. R., 2002, Modelling the hydrocarbon generative history of the Officer Basin, Western Australia: PESA Journal, v. 29, p. 29-43.

Hand, M., Reid, A., and Jagodzinski, E., 2007, Tectonic framework and evolution of the Gawler Craton, South Australia: Economic Geology, v. 102, p. 1377-1395.

Hoatson, D. M., Sun, S.-S., Duggan, M. B., Davies, M. B., Daly, S. J., and Purvis, A. C., 2005, Late Archaean Lake Harris Komatiite, central Gawler Craton, South Australia: geologic setting and geochemistry: Economic Geology, v. 100, p. 349-374.

Hou, B., and Alley, N., 2003, A model for gold and uranium dispersion and concentration in residual and transported regolith along palaeodrainage systems; a case study from the central Gawler Craton: MESA Journal, v. 30, p. 49-53.

Hou, B., Frakes, L., Sandiford, M., Worrall, L., Keeling, J., and Alley, N. F., 2008, Cenozoic Eucla Basin and associated palaeovalleys, southern Australia - climatic and tectonic influences on landscape evolution, sedimentation and heavy mineral accumulation: Sedimentary Geology, v. 203, p. 112-130.

Hou, B., Frakes, L. A., Alley, N. F., and Clarke, J. D. A., 2003, Characteristics and evolution of the Tertiary palaeovalleys in the northwest Gawler Craton: Australian Journal of Earth Sciences, v. 50, p. 215-230.

Hou, B., Keeling, J., Reid, A. J., Warland, I., Belousova, E., Frakes, L., Hocking, R., and Fairclough, M., 2011, Heavy mineral sands in the Eucla Basin, Southern Australia: deposition and province-scale prospectivity: Economic Geology, v. 106, p. 687-712.

Howard, K., Hand, M., Barovich, K., and Belousova, E., 2011a, Provenance of late Palaeoproterozoic cover sequences in the central Gawler Craton: Exploring stratigraphic correlations in eastern Proterozoic Australia using detrital zircon ages, Hf and Nd isotopic data: Australian Journal of Earth Sciences, v. 58, p. 475-500.

Howard, K., Hand, M., Barovich, K. M., Payne, J. L., Cutts, K. A., and Belousova, E. A., 2011b, U-Pb zircon, zircon Hf and whole-rock Sm-Nd isotopic constraints on the evolution of Paleoproterozoic rocks in the northern Gawler Craton: Australian Journal of Earth Sciences, v. 58, p. 615-638.

Howard, K. E., 2011, Geotectonics in the Gawler Craton: Constraints from geochemistry, U-Pb geochronology and Sm-Nd and Lu-Hf isotopes, unpublished PhD thesis, The University of Adelaide, 197 p.:

Howard, K. E., Hand, M., Barovich, K. M., Payne, J. L., and Belousova, E. A., 2011c, U-Pb, Lu-Hf and Sm-Nd isotopic constraints on provenance and depositional timing of metasedimentary rocks in the western Gawler Craton: Implications for Proterozoic reconstruction models: Precambrian Research, v. 184, p. 43-62.

Hughes, F. J., 1998, Perseverance gold deposit, Tarcoola, in Berkman, D. A., and Mackenzie, D. H., eds., Geology of Australian and Papua New Guinean Mineral Deposits Australasian Institute of Mining and Metallurgy - Monograph 22, p. 395-400.

Jackson, M. J., and van de Graaff, W. J. E., 1981, Geology of the Officer Basin, Western Australia, Bulletin 206. Bureau of Mineral Resources, Geology and Geophysics, Canberra.

Korsch, R. J., Blewett, R. S., Giles, D., Reid, A. J., Neumann, N., Fraser, G. L., Holzshuh, J., Costelloe, R. D., Roy, I. G., Kennett, B. L. N., Cowley, W. M., Baines, G., Carr, L. K., Duan, J., Milligan, P. R., Armit, R., Betts, P. G., Preiss, W. V., and Bendall, B. R., 2010, Geological interpretation of the deep seismic reflection and magnetotelluric line 08GA-OM1: Gawler Craton-Officer Basin-Musgrave Province-Amadeus Basin (GOMA), South Australia and Northern Territory, in Korsch, R. J., and Kositcin, N., eds., GOMA (Gawler Craton-Officer Basin-Musgrave Province-Amadeus Basin) Seismic and MT Workshop 2010, Geoscience Australia, Record 2010/39, p. 63-86.

Kositcin, N., 2010, Geodynamic Synthesis of the Gawler Craton and Curnamona Province, Geoscience Australia, Record, 2010/27.

McFarlane, C. R. M., 2006, Palaeoproterozoic evolution of the Challenger Au deposit, South Australia, from monazite geochronology Journal of Metamorphic Geology, v. 24, p. 75-87.

McFarlane, C. R. M., Mavrogenes, J. A., and Tomkins, A. G., 2007, Recognizing hydrothermal alteration through a granulite facies metamorphic overprint at the Challenger Au deposit, South Australia: Chemical Geology, v. 243, p. 64-89.

McGee, B., Giles, D., Kelsey, D., and Collins, A. S., 2010, Protolith heterogeneity as a factor controlling the feedback between deformation, metamorphism and melting in a granulite-hosted gold deposit: Journal of the Geological Society, v. 167, p. 1089-1104.

Morris, B. J., Hill, P. W., and Ferris, G., 1994, Barton bedrock drilling project, South Australia. Department of Primary Industries and Resources. Report Book, 1994/019.

Morton, J. G. G., and Drexel, J. F., 1997, The petroleum geology of South Australia. Vol 3: Officer Basin, South Australia Department of Mines and Energy Resources. Report Book, 97/19.

Payne, J., 2008, Palaeo- to Mesoproterozoic evolution of the Gawler Craton, Australia: geochronological geochemical, and isotopic constraints: University of Adelaide, PhD thesis (unpublished), 188 p.

Payne, J., Barovich, K., and Hand, M., 2006, Provenance of metasedimentary rocks in the northern Gawler Craton, Australia: Implications for Palaeoproterozoic reconstructions: Precambrian Research, v. 148, p. 275-291.

Payne, J., Hand, M., Barovich, K., and Wade, B., 2008, Temporal constraints on the timing of high-grade metamorphism in the northern Gawler Craton: implications for assembly of the Australian Proterozoic: Australian Journal of Earth Sciences, v. 55, p. 623-640.

Payne, J., Reid, A., Hand, M., and Barovich, K., 2010a, Definition of the Munjeela Suite, Gawler Craton: MESA Journal, v. 58, p. 31-35.

Payne, J. L., Ferris, G., Barovich, K. M., and Hand, M., 2010b, Pitfalls of classifying ancient magmatic suites with tectonic discrimination diagrams: An example from the Paleoproterozoic Tunkillia Suite, southern Australia: Precambrian Research, v. 177, p. 227-240.

Poustie, T., Bamford, P., and Daly, S., 2002, Challenger; South Australia's first Archaean gold mine: MESA Journal, v. 27, p. 4-8.

Preiss, W. V., Belperio, A., Cowley, W. M., and Rankin, L. R., 1993, Neoproterozoic, in Drexel, J. F., Preiss, W. V., and Parker, A. J., eds., The Gology of South Australia. Volume 1. The Precambrian, Geological Survey of South Australia, Adelaide, p. 171-203.

Rankin, L. R., and Flint, D. J., 1991, STREAKY BAY, South Australia, South Australia. Department of Mines and Energy, 1:250000 Geological series - explanatory notes, 40 p.:

Rankin, L. R., Flint, R. B., and Fanning, C. M., 1990, Palaeoproterozoic Nuyts Volcanics of the western Gawler Craton, South Australia. Department of Primary Industries and Resources. Report Book, 90/00060 17 p.:

Reid, A. J., and Daly, S. J., 2009, The Mulgathing and Sleaford complexes of the Gawler Craton: a historical perspective of the geology and mineral potential: MESA Journal, v. 52, p. 4-12.

Reid, A. J., Jagodzinski, E. A., Armit, R. J., Dutch, R. A., Kirkland, C. L., Betts, P. G., and Schaefer, B. F., 2014a, U-Pb and Hf isotopic evidence for Neoarchean and Paleoproterozoic basement in the buried northern Gawler Craton, South Australia: Precambrian Research, v. 250, no. 0, p. 127-142.

Reid, A. J., Jagodzinski, E. A., Fraser, G. L., and Pawley, M. J., 2014b, SHRIMP U–Pb zircon age constraints on the tectonics of the Neoarchean to early Paleoproterozoic transition within the Mulgathing Complex, Gawler Craton, South Australia: Precambrian Research, v. 250, no. 0, p. 27-49.

Sandiford, M., 2007, The tilting continent: a new constraint on the dynamic topographic field from Australia: Earth and Planetary Science Letters, v. 261, p. 152-163.

Sandiford, M., Quigley, M., de Broekert, P., and Jakica, S., 2009, Tectonic framework for the Cenozoic cratonic basins of Australia: Australian Journal of Earth Sciences, v. 56, no. S5-S18.

Stewart, J. R., Betts, P. G., Collins, A. S., and Schaefer, B. F., 2009, Multi-scale analysis of Proterozoic shear zones: An integrated structural and geophysical study: Journal of Structural Geology, v. 31, p. 1238–1254.

Swain, G., Barovich, K., Hand, M., Ferris, G., and Schwarz, M., 2008, Petrogenesis of the St Peter Suite, southern Australia: arc magmatism and Proterozoic crustal growth of the South Australian Craton: Precambrian Research, v. 166, p. 283-296.

Swain, G., Woodhouse, A., Hand, M., Barovich, K., Schwarz, M., and Fanning, C. M., 2005, Provenance and tectonic development of the late Archaean Gawler Craton, Australia; U-Pb zircon, geochemical and Sm-Nd isotopic implications: Precambrian Research, v. 141, p. 106-136.

Teasdale, J., 1997, Methods for understanding poorly exposed terranes: the interpretive geology and tectonothermal evolution of the western Gawler Craton: The University of Adelaide, unpublished PhD thesis, 183 p.

Tomkins, A. G., 2002, Evolution of the granulite-hosted Challenger Gold Deposit, South Australia: implications for ore genesis: Australian National University, unpublished PhD thesis, 222 p.

Tomkins, A. G., Dunlap, W. J., and Mavrogenes, J. A., 2004, Geochronological constraints on the polymetamorphic evolution of the granulite-hosed Challenger gold deposit: implications for assembly of the northwest Gawler Craton: Australian Journal of Earth Sciences, v. 51, p. 1-14.

Tomkins, A. G., and Mavrogenes, J. A., 2002, Mobilization of gold as a polymetallic melt during pelite anatexis at the Challenger Deposit, South Australia; a metamorphosed Archean gold deposit: Economic Geology, v. 97, no. 6, p. 1249-1271.

Wade, C. E., Reid, A. J., Wingate, M. T. D., Jagodzinski, E. A., and Barovich, K., 2012, Geochemistry and geochronology of the c. 1585 Ma Benagerie Volcanic Suite, southern Australia: Relationship to the Gawler Range Volcanics and implications for the petrogenesis of a Mesoproterozoic silicic large igneous province: Precambrian Research, v. 206–207, p. 17-35.

FURTHER INFORMATION

Anthony Reid and **Rian Dutch**
Anthony.Reid@sa.gov.au
Geological Survey of South Australia,
Department of State Development.
GPO Box 320, Adelaide, South Australia 5001

Interpretation of the western Gawler Craton section of seismic line 13GA-EG1

M.P. Doublier[1], R.A. Dutch[2], D. Clark[1], M.J. Pawley[2], G.L. Fraser[1], T.W. Wise[2], B.L.N. Kennett[3], A.J. Reid[2], C.V. Spaggiari[4], A.J. Calvert[5], S. van der Wielen[2], H. Dulfer[1], B.R. Bendall[2], S. Thiel[2], and J. Holzschuh[1]

1 Resources Division, Geoscience Australia
2 Geological Survey of South Australia, Department of State Development
3 Research School of Earth Sciences, The Australian National University
4 Geological Survey of Western Australia, Department of Mines and Petroleum
5 Department of Earth Sciences, Simon Fraser University

1 Introduction

As part of the National Geoscience Agreement, Geoscience Australia, in collaboration with the Geological Survey of South Australia, the Geological Survey of Western Australia and AuScope, acquired 834 km of vibroseis-source, deep-seismic reflection data in a single, west- to east transect across Western and South Australia from November 2013 to February 2014. For acquisition details see Holzschuh (2015, this volume). The transect follows the Trans-Australian Railway, and is referred to here as the Eucla-Gawler seismic survey, or 13GA-EG1. In the west it starts at Haig in the Madura Province, where it connects to the eastern end of seismic line 12GA-AF3 (Spaggiari et al., 2014). To the east, the line transects the Coompana Province and ends in the central Gawler Craton at Tarcoola, ~1.5 km south of the southern end of seismic line 08GA-OM1 (Fig. 1; 'GOMA' line; Korsch et al., 2010). While the Gawler Craton has some very limited exposures in the vicinity of the seismic line, the Madura and Coompana provinces are not exposed and overlain by younger rocks of the Eucla, Bight and/or Officer basins (e.g., Drexel et al., 1993; Drexel and Preiss, 1995).

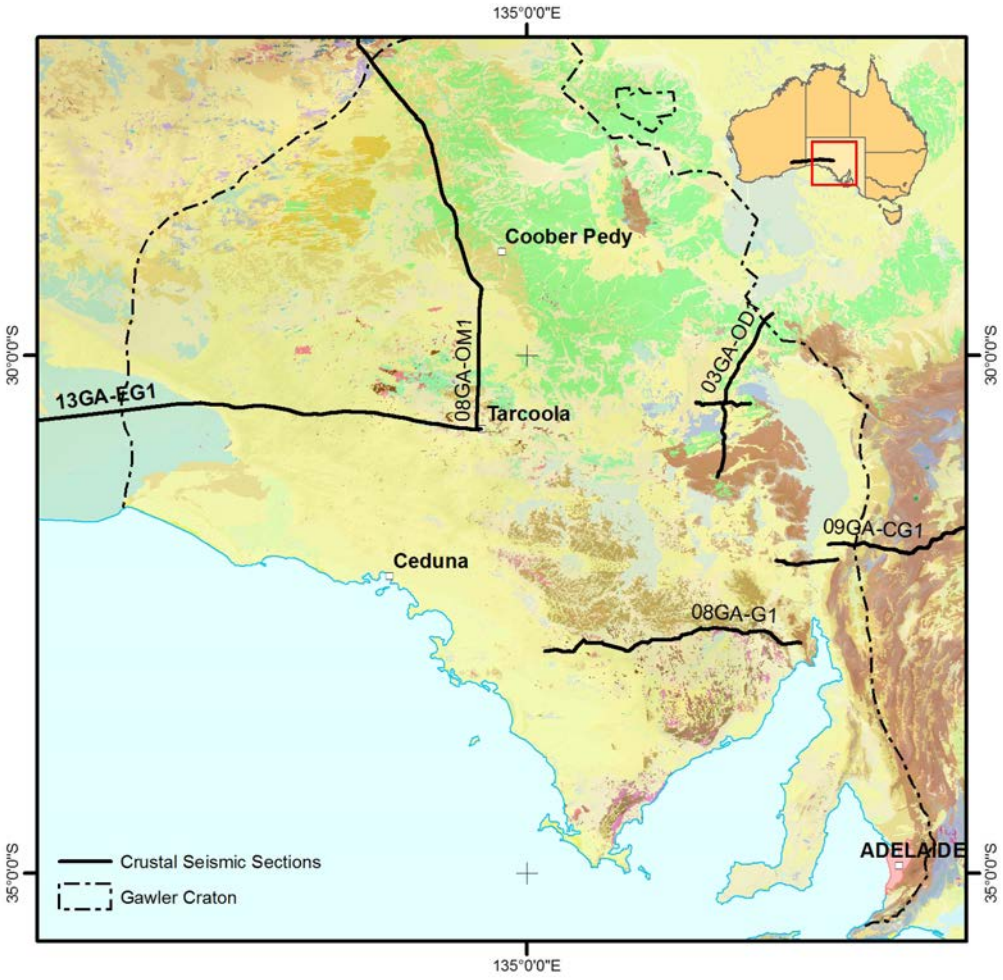

Figure 1 *Map showing the surface geology of the region covered by seismic section 13GA-EG1. Also shown is seismic line 08GA-OM1 (GOMA) and the other seismic lines collected in the region. The surface geology is from the 1:2 000 000 scale geology map of South Australia (Cowley, 2001 with latest updates as at 20/02/2015 [digital Edition] available via SARIG (https://sarig.pir.sa.gov.au/). The reader is referred there for full stratigraphic descriptions).*

The key aim of the Eucla-Gawler seismic survey was to image the crustal architecture of the unexposed basement rocks of the region. More specifically, the survey aimed to:

- define the boundaries and extents of the Madura Province, Coompana Province and the western Gawler Craton;
- investigate the contact relationships between the different geological provinces, and their internal crustal architecture, with a view to developing a better understanding the geological evolution of the Australian continent;
- image the geometries of major faults and shear zones recognized in potential field data (Plate 1; Figs 2 and 3); and,
- consider the implications of the crustal architecture for mineral systems understanding and mineral exploration strategies.

Here we provide an interpretation of the eastern part of the line 13GA-EG1, encompassing ~360 km between CDP 24950, ~38 km east of Cook, and the eastern end of the line at Tarcoola. This section of the line starts in the easternmost part of the Coompana Province, and traverses the Nawa, Christie and parts of the Wilgena domains of the western and central Gawler Craton (Figs 2-4), and is referred to here as 13GA-EG1E. In this contribution we describe the seismic interpretation process and the interpretation itself, with a focus on the seismic characteristics of the different geological entities that were imaged. The regional geological context and geological implications are described in companion papers by Reid and Dutch (2015; this volume) and Dutch et al. (2015; this volume), respectively.

2 Interpretation workflow and methodology

The interpretation of the deep-seismic reflection data was carried out by the team of authors during two intensive workshops in Canberra and Adelaide, and ongoing interpretation between and after the workshops to generate the interpretation presented here. This interpretation is preliminary and may be modified based on the interpretation of the remainder of the line.

The approach combined traditional hardcopy interpretation on large paper plots of both processed and dip moveout (DMO) stack seismic images with interpretation in a digital (ArcGIS) environment, where digital line work was generated. In practice, the two approaches are complementary. The paper plots are essential for interpretation of large scale features such as major faults, and also particular smaller features of interest within

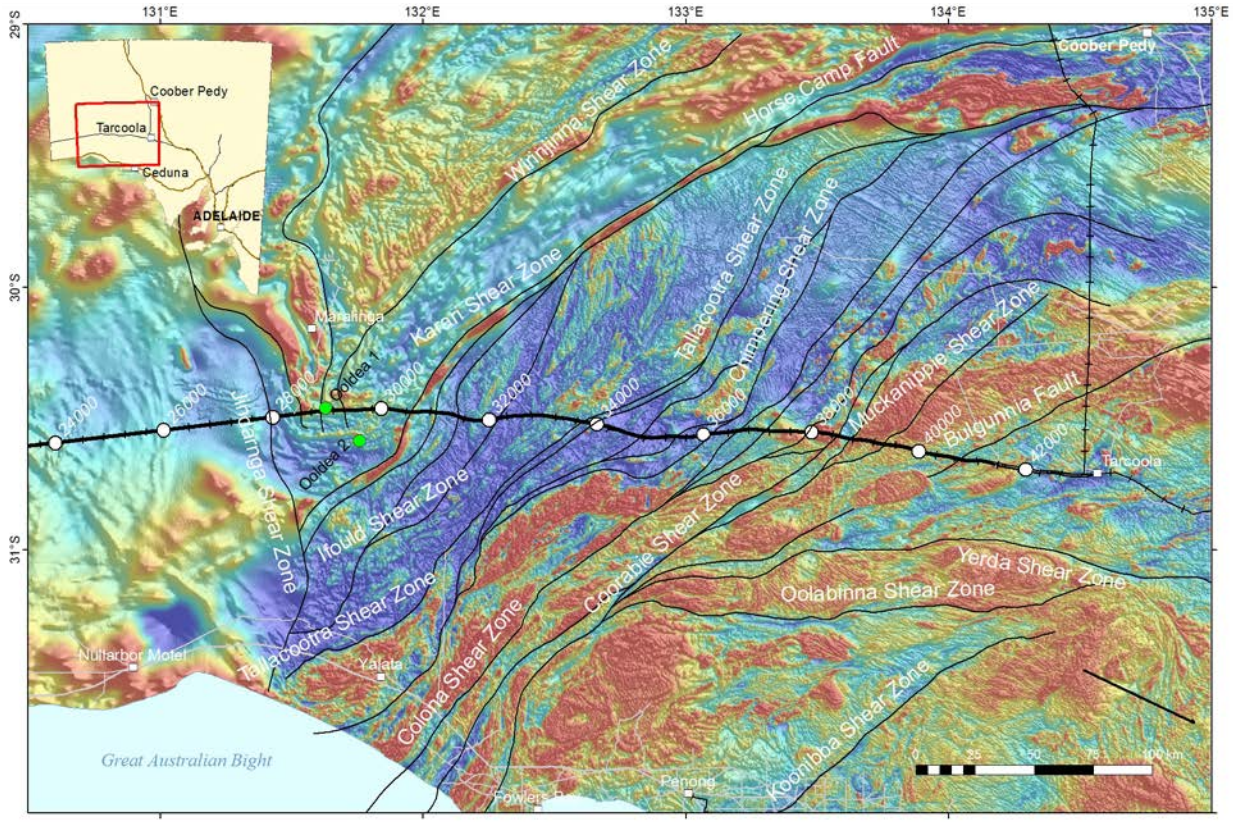

Figure 2 *Map showing regional aeromagnetic data for the area transected by seismic section 13GA-EG1E (data from Department of State Development). Warm colours are high magnetic intensities; cool colours are low magnetic intensities. Also shown are the interpreted major structures. The seismic line 13GA-EG1E has CDP stations labelled.*

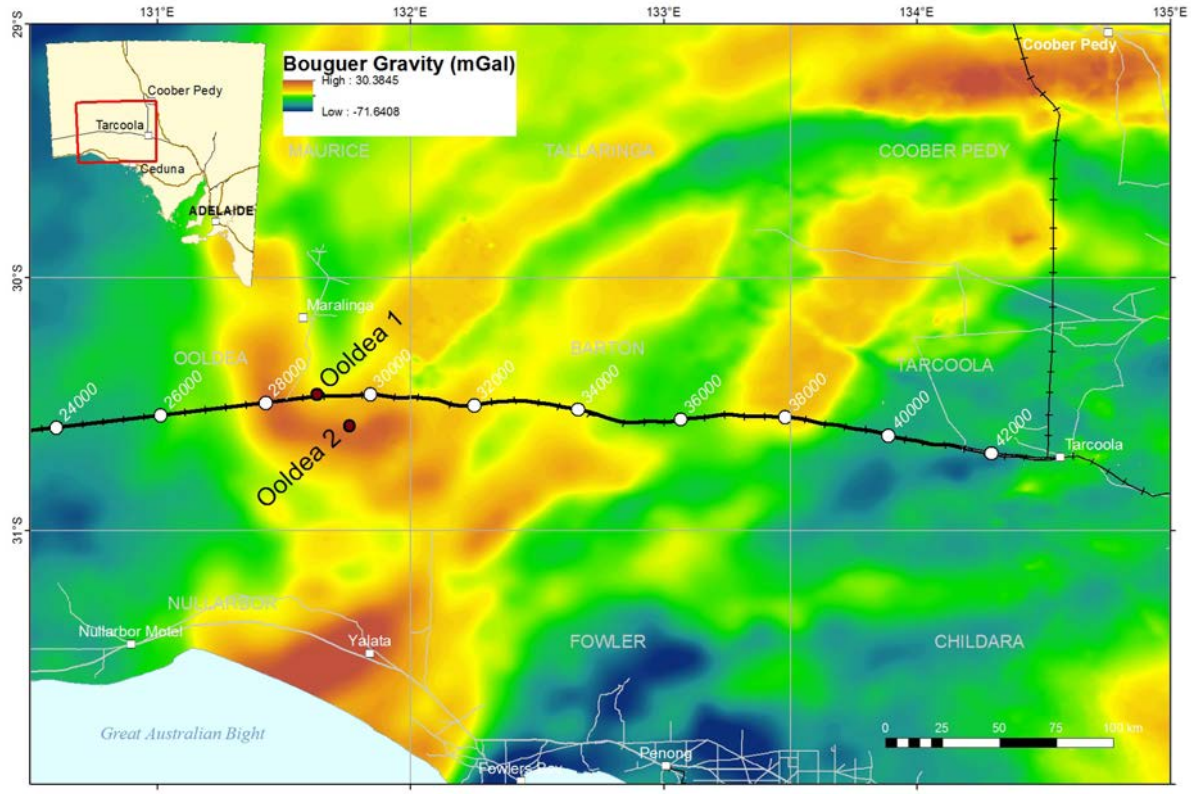

Figure 3 *Map showing regional gravity image for the area covered by seismic section 13GA-EG1E (data from Department of State Development). Warm colours are gravity highs; cool colours are gravity lows.*

context at an appropriate scale. The implementation of digital techniques into the interpretation process yields the following benefits:

- Zooming in or out allows the recorded section to be looked at in different ways
- It is possible to easily overlay and compare different image types (Fig. 5). Images used include (i) the DMO stack and processed images as used for the hardcopy interpretation, (ii) different versions of the final processed data (e.g., with different gain or contrast), and (iii) other types of images which emphasize certain aspects and or regions of the data (e.g., the lower crust and Moho, Fig. 5c), but are less suitable for whole line interpretation. One example is the interpretation of the Hiltaba Suite granite intrusions, which are well defined in high contrast images (Fig. 6).
- As the line work is digital, comparisons between different interpretations and exchange of interpretation line work between team members is easy.
- During each stage of the interpretation (including early stages) the digital line work can be converted for use in 3D software (e.g. GOCAD) and potential field modelling software (e.g. ModelVision; van der Wielen et al., 2015, this volume) allowing further assessment. Gravity modelling was carried out during various stages of the interpretation process, and the insights gained from the modelling were used to feed back into the interpretation process.

The interpretation of the faults and shear zones has been carried out using criteria such as (i) the termination or truncation of distinct sets of seismic reflectors; (ii) changes in the orientation of coherent packages across discrete zones as, for example, delineated in the change of orientation of form lines; (iii) changes of seismic character (e.g. between lower and middle crust). Due to weak seismic reflectivity some structures are not well defined/imaged in the middle crust, and hence are shown as 'inferred' (e.g., sections of the Chimpering Shear Zone, a new name after Chimpering Rock Hole that is ~17 km south of the seismic line at CDP ~32600; the Beella Shear Zone, a new name after the Beella Rock Hole that is ~36 km north of the seismic line at CDP ~35570, the Tallacootra Shear Zone, and the Ifould Shear Zone; Fig. 7 and Plate 1).

3 Regions of low reflectivity along the line

While the quality of the seismic reflection data along 13GA-EG1E is generally good, there are some areas with low reflectivity, particularly in the lower and middle crust. Two broader zones showing lower reflectivity are located between CDP ~29800 and CDP ~31700, at the contact between the Christie Domain and the Nawa Domain, and between CDP ~38400 and CDP~39300, underneath the western Wilgena Domain (Figs 4 and 7). There are also several zones with low reflectivity in the western part

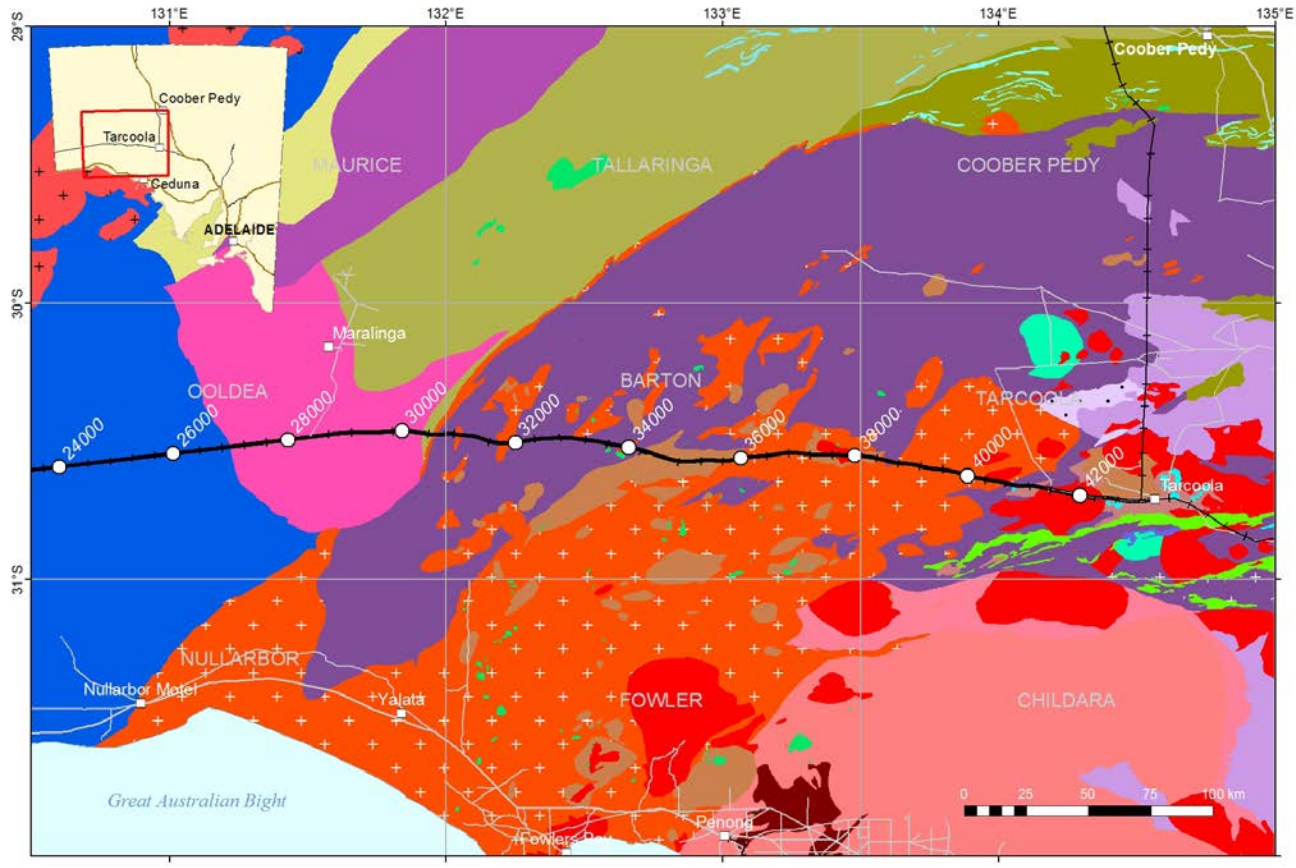

Reference

MESOPROTEROZOIC
- ?Mp *PITJANTJATJARA SUPERSUITE*

MESOPROTEROZOIC
- Mj *MUNJEELA SUITE*
- Mh *HILTABA SUITE*
- Mh6 *Mafic to felsic plugs*
- Ma *GAWLER RANGE VOLCANICS*
- Ma10 *Upper Gawler Range Volcanics*
- Ma8 *Lower Gawler Range Volcanics*
- M40 *Basement rocks of Coompana Block*

PALAEO-MESOPROTEROZOIC
- LM14 *Deformed gabbro to granite and metamorphic rocks*

PALAEOPROTEROZOIC
- L44 *St Peter Suite, St Francis Suite*
- L32 *Tarcoola Formation, Labyrinth Formation and Eba Formation*
- Ln *TUNKILLIA SUITE*
- L36 *Syn-Kimban Orogeny granitoids*
- Lu *MUCKANIPPIE SUITE*
- L-d *MOONDRAH GNEISS*
- L38 *Undifferentiated metasediments of Nawa Domain*
- L40 *Schist, granitic gneiss and granite of Nawa Domain*
- L39 *Iron formations of Nawa Domain*
- L37 *Iron formation in Mount Woods, Coober Pedy and Olympic Domains*
- L-i *WILGENA HILL JASPILITE*
- Lq *MOUNT WOODS COMPLEX*

ARCHAEAN-MESOPROTEROZOIC
- AM1 *Undifferentiated Archaean to Mesoproterozoic rocks of Nawa Domain*

ARCHAEAN-PALAEOPROTEROZOIC
- ALm *MULGATHING COMPLEX*
- ALm7 *Lake Harris Komatiite, acid volcanics, metasediments*
- ALmg *GLENLOTH GRANITE*

Figure 4 *Map showing the solid geology for the area covered by seismic section 13GA-EG1E. The solid geology is from Cowley (2006).*

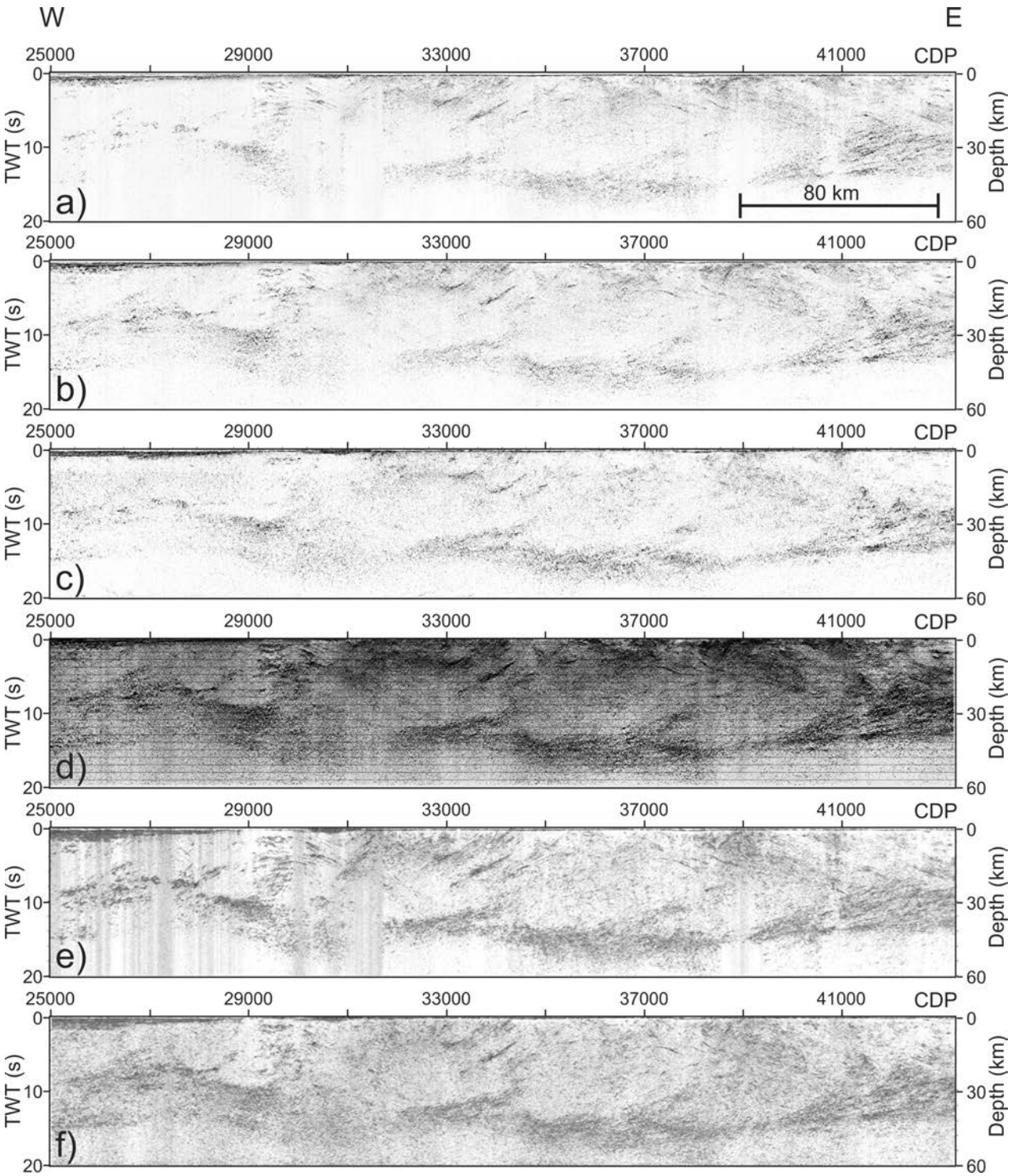

Figure 5 *The figure shows some of the different image types of seismic line 13GA-EG1E used in the interpretation process:* ***a)*** *field stack;* ***b)*** *final migrated DMO stack with 20 m CDP spacing and 150 nominal fold;* ***c)*** *migrated NMO stack with 100 m CDP spacing and a nominal fold of 750. Note the improvement for imaging of the lower crust (Holzschuh, 2015, this volume);* ***d)*** *Image processed to increase contrast and enhance the distinction between regions of differing seismic character by applying (i) Gaussian blur was applied (1 or 1.6 standard deviations) to enhance the continuity of reflections; (ii) a low pass filter to enhance the long wavelength character of the image (highlighting the reflectivity of packages rather than individual reflections); and (iii) a histogram stretch to increase final contrast between packages of varying reflective character;* ***e)*** *Image of the stack section processed by coherency enhancement processing and CDP trace equalisation;* ***f)*** *Image of the migrated section processed by coherency enhancement processing and CDP trace equalisation.*

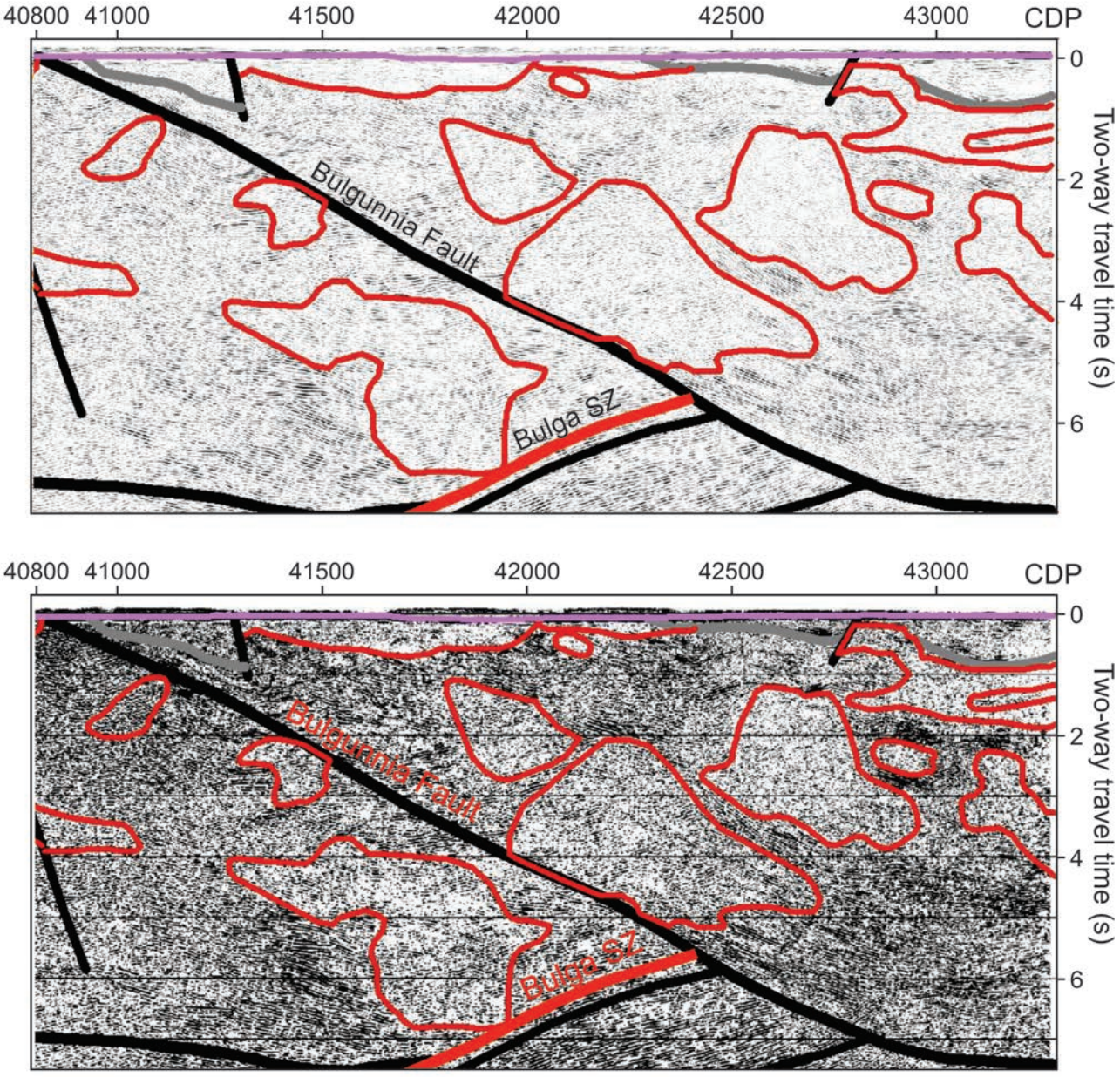

Figure 6 *Detail of line 13GA-EG1E between CDP ~40800 and CDP ~ 43500 showing the Hiltaba Suite intrusions (red outline) as interpreted on a) the final migrated DMO stack with 20 m CDP spacing; and b) the high contrast image.*

of 13GA-EG1E overlain by the Eucla Basin between CDP ~25000 and CDP ~29000. These zones of low reflectivity are most obvious in the DMO stack images (Fig. 5a), and the coherency-enhanced stack images (Fig. 5e) where they appear as vertical corridors of low (coherent) reflectivity. The reasons for these zones include the presence of major sand dunes and/or deep weathering which may impede the source energy transfer into the ground, or the dense Nullarbor Limestone which may impede reflected energy from reaching the surface or limit the effectiveness of refraction static corrections (see Holzschuh, 2015, this volume).

4 Seismic interpretation of 13GA-EG1E

4.1. Moho

Other than the areas of low reflectivity described above, the Mohorovčić discontinuity (Moho) is reasonably well imaged in most parts of line 13GA-EG1E as a discontinuity between a reflective lower crust and underlying largely non-reflective material interpreted to represent the upper mantle. It shows considerable topography, defining two regions of crust >52 km thick underneath the Gawler Craton (Fig. 7). These two regions have the shape of 'bulges' with relatively steep edges, and have a lateral extent of ~68 km and ~28 km along the bottom where the Moho is nearly flat (Fig. 7).

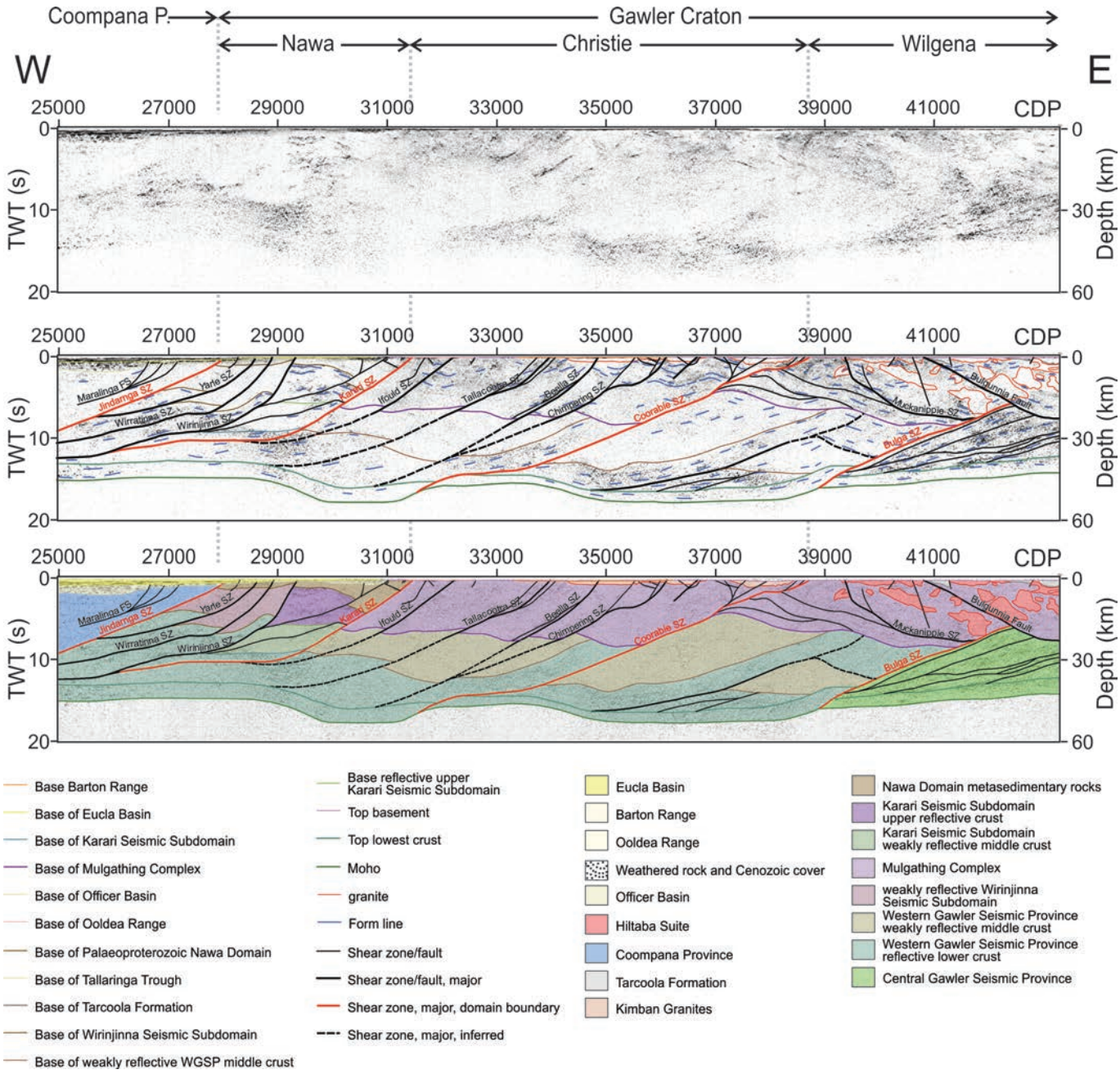

Figure 7 *Migrated section of line 13GA-EG1E, showing both uninterpreted (upper image) and interpreted versions (middle and lower images). Display is to 60 km depth, and shows vertical scale equal to horizontal scale, assuming a crustal velocity of 6000 m/s. See also Plate 1 (Wise et al., 2015, this volume).*

The Moho is shallowest at the eastern end of the line at 14 s two-way travel time (TWT, ~42 km depth) and progressively deepens towards the west to 15.7s at CDP ~38900, before reaching 17.2 s at CDP ~38000. This relatively sharp increase of 1.5 s TWT over a distance of ~18 km defines the eastern edge of the eastern bulge under the western Wilgena Domain and eastern Christie Domain, which continues to ~CDP 34600 and reaches the deepest point at 17.6 s TWT (~53 km depth) at CDP ~36300. The interpretation of the Moho presented here is conservative, and consideration of some deeper, weaker reflectors as part of the crust would increase the depth by up to 1 s TWT (~3 km). The Moho shallows to a depth of 15.1 to 15.5 s TWT under the western Christie Domain between CDP ~34000 and CDP ~31700, before deepening again to 17.5 s TWT underneath the Nawa Domain between CDP ~31100 and CDP ~29700. Further to the west the Moho shallows again to 14.5 s TWT (~43.5 km depth) at CDP ~28500, and continues relatively flat, ending at 14.8 s at the western end of 13GA-EG1E (CDP ~24950).

4.2. Crustal architecture

Seismic line 13GA-EG1E crosses two Precambrian geological provinces; the western part of the Gawler Craton to the east, and the eastern part of the Coompana Province to the west (Fig. 4; for a detailed description of the regional geology see Reid and Dutch, 2015, this volume). These provinces are, in part, overlain by sedimentary basins and thin Cenozoic cover. In the vicinity of the seismic line, the upper crust of the Gawler Craton can be subdivided into several domains, based on interpretation of potential field data, geochronology constraints, lithostratigraphy and tectonic history. These domains are from east to west the Wilgena Domain, the Christie Domain, and the Nawa Domain (Figure 2 of Reid and Dutch, 2015, this volume). The Fowler Domain has not been imaged in seismic section 13GA-EG1E, as it does not extend as far north as the seismic line.

In the central part of the seismic section, under both the Christie Domain and most of the Wilgena Domain, the crust consists of three layers, all of which have a distinct seismic character: (i) a reflective lower crust; (ii) middle crust that is weakly to non-reflective; and (iii) an upper crustal layer that shows some variation but is overall moderately reflective.

Reflective lower crust is present throughout the seismic section, and becomes thicker and occurs at higher structural levels towards both the eastern and western ends of the section. The weakly to non-reflective middle crust is largely absent under the easternmost part of the Wilgena Domain, and its presence under the Nawa Domain is discussed in greater detail below. For the middle to lower crust we distinguish the Central Gawler Seismic Province and the Western Gawler Seismic Province (Figs 7 and 8), which are described in greater detail below. The term 'seismic province' describes a discrete volume of middle-lower crust, which cannot be traced to the surface and whose seismic reflectivity is different from that of vertical or horizontally adjoining provinces (Korsch et al., 2010).

Only the easternmost part of the Coompana Province is imaged in seismic section 13GA-EG1E, forming a westward thickening wedge in the hanging wall of the westerly dipping Jindarnga Shear Zone (new name after the Jindarnga Rock Hole, which is ~34 km to the north of the seismic line and overlies the proposed trace of the shear zone).

With the exception of the upper crustal Wilgena Domain, the structural architecture along 13GA-EG1E is dominated and controlled by typically listric, westerly dipping shear zones defining ramp- and/or apparent thrust duplex-like geometries, although apparent extensional offsets are also observed (Fig. 7). While some structures are restricted to a particular crustal level, others are interpreted as crustal scale features, extending from

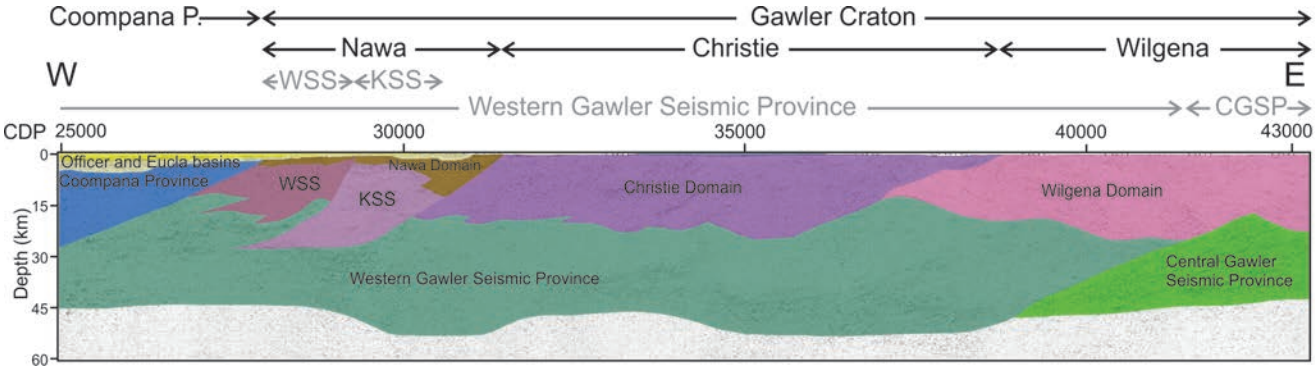

Figure 8 *Migrated section of line 13GA-EG1E, showing the distribution of basins, domains and provinces. Extend of seismic subdomains and provinces are shown in grey. Display is to 60 km depth, and shows vertical scale equal to horizontal scale, assuming a crustal velocity of 6000 m/s. WSS - Wirinjinna Seismic Subdomain; KSS - Karari Seismic Subdomain.*

the surface through the crust, soling into the lower crust or Moho. Of these crustal scale shear zones, the Coorabie Shear Zone and the Karari Shear Zone represent boundaries of upper crustal domains, being the eastern and western boundaries of the Christie Domain, respectively.

To the east of the Karari Shear Zone, our interpretation suggests a structural decoupling between upper crust and the middle to lower crust along the base of the upper crust (i.e., the base of the Mulgathing Complex) during some stage of the tectonic evolution. While the deformation of the middle to lower crust appears focused along the shear zones described above, which control the topography and distribution of the lower and middle crust, deformation in the upper crust involved a combination of discrete shear zones and open folding.

As described in greater detail by Dutch et al. (2015, this volume), we interpret that many of the structures have a protracted history of repeated movement, possibly reflecting the different orogenic events that are preserved in the geological record (e.g., Hand et al., 2007; Payne et al., 2008; Reid and Dutch, 2015, this volume). In that regard it is important to be cognisant that many of these structures may have formed or been reactivated under a transpressional and/or transtensional regime, involving major strike-slip displacement (e.g., Stewart and Betts, 2010). This implies substantial out-of-plane movement with respect to the seismic section 13GA-EG1E, and care must be taken with respect to the kinematic analysis, as offsets of particular horizons (e.g. the base of the upper crust) across these structures imaged in the seismic section will be apparent offsets only.

The following sections describe the major geological entities and related structures as imaged in the seismic section, starting at the eastern end of the section and stepping progressively west.

4.3. Gawler Craton

4.3.1. Upper crust of the Gawler Craton

4.3.1.1 Wilgena Domain

The crust of the Wilgena Domain shows some variation in seismic character. Overall the crust is moderately reflective with discontinuous, curviplanar reflectors that generally dip shallowly to the east, and define upright open folds with wavelengths between 10 km and 20 km (Fig 7). We interpret this moderately reflective package to represent the gneisses of the Neoarchean to early Proterozoic Mulgathing Complex (Reid and Dutch, 2015, this volume). The lower boundary of the Mulgathing Complex has been interpreted as the lower limit of the moderately reflective package (Fig. 7b; Plate 1). This boundary defines the lower limit of the upper crust, and represents both a structural and lithological boundary. It may in parts also represent the top of an Archaean basement substrate to the Mulgathing Complex. In the eastern and central parts of the domain, the moderately reflective character is disturbed by bland zones that vary in shape and size, but can reach a thickness of up to 3 s TWT (~9 km thick; Fig. 6). Locally, the bland zones also form thin, flat-bottomed bodies at the surface. These zones are interpreted to represent granite intrusions of the Hiltaba Suite. In the eastern part of the domain, we interpret shallow basins of the Palaeoproterozoic Tarcoola Formation, which reaches a maximum thickness of 0.8 s TWT (~2.4 km depth; Fig. 7b).

At the surface, the Wilgena Domain extends from the eastern end of the seismic line to the Coorabie Shear Zone at CDP ~38700, and is interpreted to extend farther to the west in the footwall of the Coorabie Shear Zone where it wedges out at CDP ~36890 at a depth of 4.6 s TWT (~14 km). The domain reaches its maximum thickness of just over 8 s TWT (~24 km depth) between CDP ~41400 and CDP ~40200. To the east, where it is underlain by the Central Gawler Seismic Province, the lower boundary of the Wilgena Domain is represented by two shear zones; a westerly dipping mid- to lower crustal shear zone that forms the upper boundary of the Central Gawler Seismic Province (the Bulga Shear Zone, see section 4.3.2.), and the Bulgunnia Fault (Fig. 7). The Bulgunnia Fault reaches the surface at CDP ~40800 and dips moderately to the east to reach 7.4 s TWT (~22 km depth) at the eastern limit of the seismic section.

The Wilgena Domain is remarkable from a structural point of view, as it is the only upper crustal region along 13GA-EG1E with an easterly dipping structural grain. This is illustrated by easterly dipping shear zones, such as the listric Muckanippie Shear Zone a splay of which reaches the surface at CDP ~39360. This part of the line also contains a series of blind shallowly east-dipping faults that are sub-parallel to the base of the Mulgathing Complex.

4.3.1.2 Christie Domain

At the surface, the Christie Domain is bounded by the Coorabie Shear Zone to the east and by the Karari Shear Zone to west (at CDP ~31440; Fig. 7b). The domain is slightly thicker in the east, and the overall thickness varies between 6 s to 8 s TWT (~18 km to 24 km). In common with the Wilgena Domain, the Christie Domain has a moderately reflective seismic character, which is dominated by sub-horizontal to shallowly dipping reflectors that define upright, open folds. This package is interpreted to represent the gneisses of the Mulgathing Complex. Several shallow, flat-bottomed bodies in the eastern part of the domain are interpreted as tabular granites of Kimban Orogeny (*c.* 1730 – 1690 Ma) or Tunkillia Suite (*c.* 1680 Ma) age. A thin veneer comprising Eocene sands of the Ooldea Range and Barton Range, which host mineral sand deposits, overlie weathered Mulgathing Complex basement.

The domain is segmented by several west-dipping crustal-scale shear zones that appear to offset both the bottom of the Mulgathing Complex and the top of the reflective lower crust. From east to west these shear zones are the Chimpering Shear Zone, the Beella Shear Zone, the Tallacootra Shear Zone, and

the Ifould Shear Zone (Fig. 7). In most cases, the structures show several fault splays. Due to weak seismic reflectivity some structures are not well defined/imaged in the middle crust, and hence their continuation is shown as 'inferred' in order to reflect the higher uncertainty involved in their interpretation.

In contrast to the Wilgena Domain, the Christie Domain shows a westerly dipping fault and shear zone architecture. The Christie Domain is also apparently devoid of Hiltaba Suite granite intrusions and the Palaeoproterozoic Tarcoola Formation.

4.3.1.3 Nawa Domain

Along 13GA-EG1E the Nawa Domain is imaged between the Karari Shear Zone at CDP ~31440 and the Jindarnga Shear Zone at CDP ~27960, which we interpret as the eastern boundary of the Coompana Province. Most of the domain is overlain by cover sequences containing sedimentary rocks of the Officer Basin and Eucla Basin. In the hanging wall of a westerly dipping splay of the Karari Shear Zone at CDP ~31000, the Tallaringa Trough (eastern Officer Basin) is imaged to a depth of 0.6 s TWT, and gradually thins towards the west. Constraints on the cover thickness in this area are provided by the drill hole Ooldea 1 (Fig. 2), which is located about 1 km to the north of the seismic line at CDP ~28980. This hole intersected ~28 m of the Eucla Basin (Miocene Nullarbor Limestone) and ~ 259 m of sedimentary rocks, predominantly sandstone, of the Officer Basin, before reaching the granulitic basement gneisses at ~287 m depth (Meyer, 1979; Swain et al., 2005). To the west of Ooldea 1, both basins increase in thickness, with the maximum thickness of the Officer Basin observed over the Coompana Province at 1.8 s TWT. Nevertheless, it is possible that the lower sequence of reflections (about 0.6 s TWT) in the basin are seismic multiples (i.e., seismic reflectors due to multiple bounce paths in the section), and that the basin is shallower. Additional constraints from the area farther to the west will help to resolve these uncertainties.

The upper part of the Nawa Domain is represented by a zone of low seismic reflectivity, which thickens towards the east and reaches its deepest point in the hanging wall of the Karari Shear Zone at a depth of 4 s TWT (~12 km depth). We interpret this zone to represent a package of Palaeoproterozoic metasedimentary rocks, which includes the Moondrah Gneiss intersected in drillhole Ooldea 2, located about 13 km to the south of the seismic line (Fig. 2; e.g. Fraser and Reid, 2007; Fraser et al., 2012), and the granulites in drillhole Ooldea 1 (Swain et al., 2005). This unit contains some strongly magnetised lithologies, which are obvious in aeromagnetic images where they display complex short-wavelength patterns (Fig. 2).

The portions of the Nawa Domain that underlie the Palaeoproterozoic metasedimentary rocks show a large diversity of seismic character. This suggests a composite character of the Nawa Domain, consistent with observations in seismic line 08GA-OM1 ('GOMA'; Korsch et al., 2010), and allows for the distinction of two seismic subdomains, each bounded by crustal scale faults or shear zones. Following the convention of naming the seismic subdomains after the fault in the footwall (Korsch et al., 2010), we recognise the Karari Seismic Subdomain in the east, and the Wirinjinna Seismic Subdomain in the west.

4.3.1.3.1 Karari Seismic Subdomain

In the Karari Seismic Subdomain, the Palaeoproterozoic metasedimentary rocks are underlain by a strongly reflective package up to 5 s TWT thick (~15 km). The seismic reflectors are subhorizontal to shallowly dipping in the western part of the seismic subdomain, but steepen towards the Karari Shear Zone. We refer to this package as the upper reflective crust of the Karari Seismic Subdomain. It is underlain by a package of poor reflectivity in the middle crust that is up to 3.5 s TWT thick (~10.5 km), and transected by a west-dipping sigmoidal shear that bridges between the Karari and Wirinjinna shear zones.

The Karari Seismic Subdomain is underlain by reflective middle to lower crust interpreted to represent the lower, reflective part of the Western Gawler Seismic Province. It is possible that the poorly reflective package corresponds to the upper, non-reflective part of the Western Gawler Seismic Province. However, as it is overlain by a distinctly different upper crust we refer to it as 'non-reflective middle crust' of the Karari Seismic Subdomain.

4.3.1.3.2 Wirinjinna Seismic Subdomain

The Wirinjinna Seismic Subdomain is located between the Wirinjinna and Jindarnga shear zones (Fig. 7). It is covered by a thin layer (less than 1 s TWT) of Palaeoproterozoic metasedimentary rocks of the Nawa Domain. The lower boundary of this package is poorly constrained, but has been interpreted as the lower boundary of a package with some coherent subhorizontal to shallowly west-dipping reflectors (Fig. 7).

The Wirinjinna Seismic Subdomain consists of a package of poorly reflective crust, up to 5 s TWT thick (~15 km), which in turn overlies reflective middle to lower crust interpreted to represent the lower, reflective part of the Western Gawler Seismic Province. Hence, it is possible that the poorly reflective Wirinjinna Seismic Subdomain package corresponds to the upper, non-reflective part of the Western Gawler Seismic Province as observed under the Christie and Wilgena domains. However, as the Wirinjinna Seismic Subdomain is overlain by Palaeoproterozoic metasedimentary rocks (similar to the Karari Seismic Subdomain) rather than Mulgathing Complex, and there are no further constraints, we refer to this middle package as the 'non-reflective mid- to upper crust' of the Wirinjinna Seismic Subdomain.

The Wirinjinna Seismic Subdomain is cut by two crustal-scale, listric, west-dipping structures; the eastern Wirratinna Shear Zone that reaches the surface at CDP ~28890 (new name after

Wirratinna Rockhole located ~11 km north of the seismic line and 1 km east of the interpreted trace of this structure), and the western Yarle Shear Zone that reaches the surface at CDP ~28580 (new name after Yarle Lakes located ~26 km north of the seismic line along the interpreted trace of this structure). Both of these shear zones penetrate the subdomain, with the Yarle Shear Zone apparently overlain by the Officer Basin without continuing into this unit. The Wirratinna Shear Zone is sub-parallel to the Wirinjinna Shear Zone and can be traced to the western end of the seismic section, where it reaches a depth of about 10.3 s TWT (~31 km depth). The Yarle Shear Zone flattens out at 7 s TWT(~21 km depth) and appears to be cut by the Jindarnga Shear Zone at CDP ~25700.

4.3.2 Lower and middle crust of the Gawler Craton

The lower and middle crust of the Gawler Craton can be divided into several major parts. The lowermost part of the crust is characterised by a reflective package with reflectors that are aligned parallel to the Moho, forming a coherent package that can be traced continuously along the seismic section. This layer is termed the 'lowermost reflective crust' and has a thickness between 1.2 s and 2 s TWT (~3.5 km to ~6 km; Fig. 7). The top of this zone appears to represent a rheological boundary, with many shear zones interpreted to sole onto this horizon.

Above the lowermost reflective crust, the 'reflective lower crust' and the overlying weakly to non-reflective middle crust have a complex geometry where we are able to distinguish two provinces in the middle to lower crust, the Central Gawler Seismic Province and the Western Gawler Seismic Province (Fig. 8). These provinces will be described below.

4.3.2.1 Central Gawler Seismic Province

The Central Gawler Seismic Province forms a westward thinning wedge underlying the Wilgena Domain (Fig. 8). The wedge is 8.7 s TWT thick (~26 km) at the eastern end of the section, tapering away by CDP ~38850. Reflectors in the overlying Mulgathing Complex and middle crust to the west are truncated by, and deflected with an apparent extensional drag against the top of the wedge, which is interpreted as a structure called the Bulga Shear Zone (new name after the Bulga Well, which is just north of the seismic line at CDP ~42270) and represents the western boundary of the Central Gawler Seismic Province. The seismic province is made of several coherent reflective packages, which are separated by low angle, anastomosing and partly sigmoidal shear zones. Both shear zones and the reflective packages are cut by the overlying Bulgunnia Fault. The Moho is deeper on the western side of the Bulga Shear Zone (i.e., its hanging wall), suggestive of a normal displacement along it. However, it has to be kept in mind that this area is one of the zones of low seismic reflectivity mentioned above, which hinders interpretation.

4.3.2.2. Western Gawler Seismic Province

The Western Gawler Seismic Province extends from the contact with the Central Gawler Seismic Province and at least as far as the western end of seismic section 13GA-EG1E. It is of variable thickness, ranging from about 13.5 s TWT (~40.5 km) in the footwall of the Coorabie Shear Zone to about 7.7 s (~23 km) in the footwall of the Tallacootra Shear Zone at CDP ~33300 (Figs 7 and 8).

The Western Gawler Seismic Province features a reflective lower crust and the overlying weakly to non-reflective middle crust, arranged in a complex geometry. The reflective lower crust generally forms a layer that can be traced along the lower part of the crust. However, in three places the reflective lower crust appears to extend into the middle-crust, with the seismic reflectors aligned parallel to the bounding, west dipping shear zones. The crust between these packages forms irregular, elongate bland zones that are characterised by poor reflectivity. The emerging picture is one of lower- to mid-crustal ramps and duplexes which (i) may emplace lower crust on top of middle crust (e.g. in the hanging wall of the Coorabie Shear Zone between CDPs ~33800 and ~35650); (ii) cause substantial lateral thickness variations of the lower and/or middle crust along the seismic section, and (iii) may transport the lower crust into higher structural levels, in particular in the western part of the section (e.g., in the footwall of the Jindarnga Shear Zone at CDP ~27200, where the top of the reflective lower crust is interpreted at 3.7 s TWT (~11 km depth).

There is uncertainty in the interpretation of the eastern part of the seismic province, between CDP ~38500 and CDP ~41400. In this area, slight changes in seismic character and also in the dip of reflectors east of about CDP ~39300 could indicate a duplex-like geometry, while a ramp-like geometry would be more consistent with the tectonic style further to the west (Fig. 9). However, as this region is a zone of low reflectivity the data are not conclusive.

The main differences between the two seismic provinces are that the Central Gawler Seismic Province is; (i) slightly more reflective, and (ii) is not overlain by a weakly to non-reflective middle crust. As the latter could be structurally detached (e.g. truncated by the Bulgunnia Fault), and the reflective character could be related to a more refractive character (related to the Hiltaba Suite magmatism) and/or a slightly different orientation, it is possible that the Central Gawler Seismic Province represents the eastern continuation of the Western Gawler Seismic Province.

4.4 Coompana Province

The easternmost part of the Coompana Province is imaged on seismic section 13GA-EG1E, forming a wedge that thickens to the west reaching 9 s TWT (~27 km depth) at the western end of 13GA-EG1E at CDP ~24950. The eastern boundary of

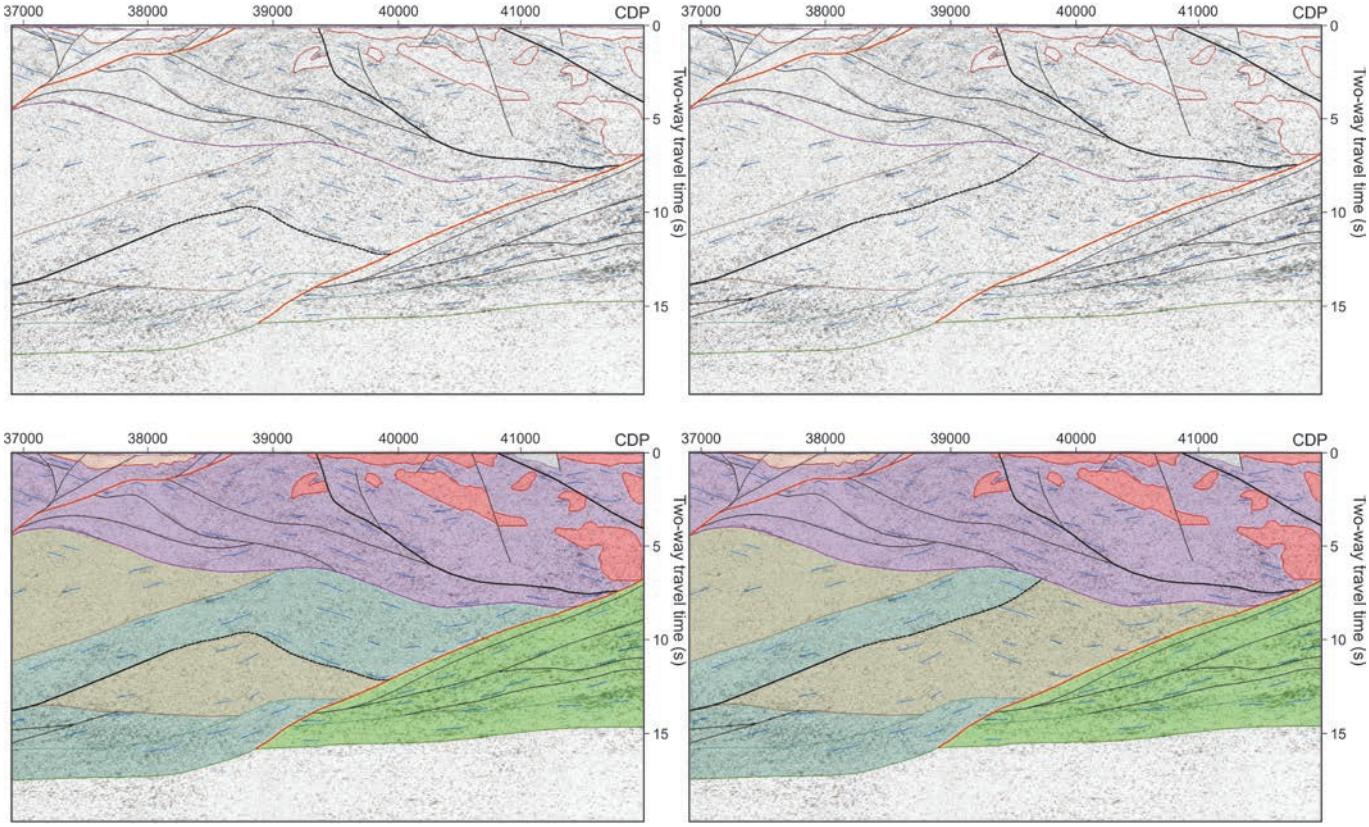

Figure 9 *Migrated section of the western end of the Western Gawler Seismic Province between CDP ~37000 and CDP ~41900, showing two alternative interpretations discussed in the text as a ramp-like (right hand side) and duplex-like (left hand side) architecture.*

the province is interpreted to be the Jindarnga Shear Zone, a relatively planar, west dipping structure that extends into the lower part of the Officer Basin, but not the Eucla Basin, at CDP ~27960. The Coompana Province is overlain by the Officer and Eucla basins, which both thicken to the west reaching maximum thicknesses of 1.8 s TWT and 0.6 s TWT, respectively, although the Officer Basin may be shallower (see above in section 4.3.1.1. on the Nawa Domain). The part of the Coompana Province imaged on seismic section 13GA-EG1E shows weak seismic reflectivity, with few reflectors shallowly dipping to the west. The province is segmented by a series of west-dipping, listric second-order faults between CDP ~26620 and CDP ~27150, called the Maralinga Fault System (new name after the Maralinga Blowhole that is ~1.4 km south of the seismic line at CDP ~26920), which offset the basal reflectors of the Officer Basin, but do not appear to extend into the overlying Eucla Basin.

The Coompana Province and the architecture of the Gawler Craton to Coompana Province transition will be assessed in detail during the interpretation of the western part of seismic line 13GA-EG1, referred to as 13GA-EG1W.

5 Summary

This chapter provides a brief description of the interpretation of seismic section 13GA-EG1E, focussing on subdivision of the crust according to seismic character and the geometry of first and second order structures. A summary of the different datasets and the workflow used to produce the interpretation is also provided. The reader is now referred to the companion paper by Dutch et al. (2015, this volume), which integrates the interpretation presented here into the regional geological framework, discusses implications, and investigates some of the uncertainties in the interpretation.

Acknowledgements

Richard Blewett and Richard Chopping (Geoscience Australia) are thanked for thoughtful reviews of this abstract.

References

Cowley, W. M., 2001, Geological Map of South Australia 1:2,000,000 scale: Department of Primary Industries and Resources. South Australia.

Cowley, W. M., compiler, 2006, Solid geology of South Australia. South Australia Department of Primary Industries and Resources, Mineral Exploration Data Package 15.

Drexel, J. F., Preiss, W. V., and Parker, A. J., 1993, The geology of South Australia: Vol. 1, The Precambrian. South Australia Geological Survey Bulletin 54, 242pp.

Drexel, J. F., and Preiss, W. V., 1995, The geology of South Australia: Vol. 2, the Phanerozoic. South Australia Geological Survey Bulletin 54, 347pp.

Dutch, R. A., Doublier, M. P., Pawley, M. J., Wise, T. W., Reid, A. J., Clark, D., Kennet, B. L. N., Fraser, G. L., Thiel, S., van der Wielen, S., Chopping, R., and Bendall, B., 2015, Geological and Geodynamic implications for the western Gawler Craton section of Seismic line 13GA-EG1, *in* Dutch, R. A., Pawley, M. J., and Wise, T. W., eds., What lies beneath the western Gawler Craton? 13GA-EG1E Seismic and Magnetotelluric Workshop 2015, Report Book 2015/00029. Department of State Development, South Australia, Adelaide.

Fraser, G. L., and Reid, A. J., 2007, Time-Space evolution of the Gawler Craton, *in* Neumann, N. L., and Fraser, G. L., eds., Geochronological synthesis and Time-Space plots for Proterozoic Australia. Geoscience Australia Record 2007/06, 3–33.

Fraser, G. L., Reid, A. J., and Stern, R. A., 2012, Timing of deformation and exhumation across the Karari Shear Zone, north-western Gawler Craton, South Australia: Australian Journal of Earth Sciences, v. 59, p. 547-570.

Hand, M., Reid, A., and Jagodzinski, L., 2007, Tectonic Framework and Evolution of the Gawler Craton, Southern Australia: Economic Geology, v. 102, p. 1377-1395.

Holzschuh, J., 2015, 13GA–EG1 Eucla-Gawler Seismic Survey – Acquisition and Processing of the western Gawler Craton section, *in* Dutch, R. A., Pawley, M. J., and Wise, T. W., eds., What lies beneath the western Gawler Craton? 13GA-EG1E Seismic and Magnetotelluric Workshop 2015, Report Book 2015/00029. Department of State Development, South Australia, Adelaide.

Korsch, R. J., Blewett, R. S., Giles, D., Reid, A. J., Neumann, N. L., Fraser, G. L., Holzschuh, J., Costelloe, R. D., Roy, I. G., Kennett, B. L. N., Cowley, W. M., Baines, G., Carr, L. K., Duan, J., Milligan, P. R., Armit, R., Betts, P. G., Preiss, W. V., and Bendall, B. R., 2010, Geological interpretation of the deep seismic reflection and magnetotelluric line 08GA–OM1: Gawler Craton–Officer Basin–Musgrave Province–Amadeus Basin (GOMA), South Australia and Northern Territory, *in* Korsch, R. J., and Kositcin, N. eds., GOMA (Gawler Craton–Officer Basin–Musgrave Province–Amadeus Basin) Seismic and MT Workshop 2010: Extended Abstracts. Geoscience Australia, Record 2010/39, 63-86.

Payne, J. L., Hand, M., Barovich, K. M., and Wade, B. P., 2008, Temporal constraints on the timing of high-grade metamorphism in the northern Gawler Craton: implications for assembly of the Australian Proterozoic: Australian Journal of Earth Sciences, v. 55, p. 623-640.

Raymond, O. L., coordinator, 2009, Surface geology of Australia 1:1million scale digital geology data. Geoscience Australia digital map.

Reid, A. J., and Dutch, R. A., 2015, Lithostratigraphy, structure and metamorphic architecture of a reworked Paleoproterozoic continental rift in the western Gawler Craton, *in* Dutch, R. A., Pawley, M. J., and Wise, T. W., eds., What lies beneath the western Gawler Craton? 13GA-EG1E Seismic and Magnetotelluric Workshop 2015, Report Book 2015/00029. Department of State Development, South Australia, Adelaide.

Spaggiari, C. V., Occhipinti, S. A., Korsch, R. J., Doublier, M. P., Clark, D. J., Dentith, M. C., Gessner, K., Doyle, M. G., Tyler, I. M., Kennett, B. L. N., Costelloe, R. D., Fomin, T., and Holzschuh, J., 2014, Interpretation of Albany–Fraser seismic lines 12GA-AF1, 12GA-AF2 and 12GA-AF3: implications for crustal architecture, *in* Albany–Fraser Orogen seismic and magnetotelluric (MT) workshop 2014: extended abstracts compiled by Spaggiari, C. V., and Tyler, I. M., Geological Survey of Western Australia, Record 2014/6, p. 28-51.

Stewart, J. R., and Betts, P. G., 2010, Implications for Proterozoic plate margin evolution from geophysical analysis and crustal-scale modeling within the western Gawler Craton, Australia. Tectonophysics, v. 483, p. 151-177.

Swain, G. M., Hand, M., Teasdale, J., Rutherford, L., and Clark, C., 2005, Age constraints on terrane-scale shear zones in the Gawler Craton, southern Australia, Precambrian Research, v. 139, p. 164-180.

Van der Wielen, S., Goodwin, J., Nicoll, M., and Keeping, T., 2015, Potential Field Investigation of the western Gawler Craton Section of Seismic Reflection Line 13GA-EG1E, *in* Dutch, R. A., Pawley, M. J., and Wise, T. W., eds., What lies beneath the western Gawler Craton? 13GA-EG1E Seismic and Magnetotelluric Workshop 2015, Report Book 2015/00029. Department of State Development, South Australia, Adelaide.

Wise, T. W., Doublier, M. P., Dutch, R. A., Clark, C., Pawley, M. J., Fraser, G. L., Kennett, B. L. N., Reid, A. J., Spaggiari, C. V., Calvert, A. J., van der Wielen, S., Dulfer, H., Bendall, B., Thiel, S., Holzschuh, J., 2015, Geological Interpretation of the Gawler Craton section of the Eucla-Gawler Seismic Line (13GA-EG1E) Plate 1 *in* Dutch, R. A., Pawley, M. J., and Wise, T. W., eds., What lies beneath the western Gawler Craton? 13GA-EG1E Seismic and Magnetotelluric Workshop 2015, Report Book 2015/00029. Department of State Development, South Australia, Adelaide.

FURTHER INFORMATION

Michael Doublier
Michael.Doublier@ga.gov.au
Resources Division, Geoscience Australia,
GPO Box 378, Canberra, ACT, 2601

Potential-field investigation of the seismic reflection line 13GA-EG1E

Simon van der Wielen[1,2,3], James Goodwin[4], Malcolm Nicoll[4] and Tim Keeping[2]
1 Deep Exploration Technologies Cooperative Research Centre
2 Geological Survey of South Australia, Department of State Development
3 School of Physical Sciences
4 Resources Division, Geoscience Australia

1 Introduction

13GA-EG1 is an east-west, deep-crustal seismic reflection line, over 800 km long. The line was acquired in 2013-14 from Haig, Western Australia, to Tarcoola, South Australia, and follows the transcontinental railway. This study deals with the eastern ~360 km portion of 13GA-EG1 in SA and will be referred to throughout the abstract as 13GA-EG1E to distinguish it from any future potential-field study of the entire seismic line. The objective of 13GA-EG1E was to image the western boundary of the Gawler Craton, determine the nature and character of the crust underlying the Eucla and Officer Basins, and map variations in the Moho. Petrophysical data was compiled to run forward models and constrain geophysical inversions over the region imaged in the seismic reflection survey to objectively test the accuracy of the geological interpretation and understand the processes governing variations in density and magnetic susceptibility in the subsurface. An interpretation of potential-field data for the eastern portion of 13GA-EG1E is given here, in three sections:

1. Summary of relevant petrophysical data,
2. Description of the forward modelling of the initial geological interpretation,
3. Description of the potential-field inversion.

2 Petrophysics

The Geological Survey of South Australia (GSSA) routinely collects and compiles petrophysical data for the state. There are currently 12 180 density and 71 008 magnetic susceptibility measurements from 1702 drill holes in the database. The data can be accessed and downloaded freely by the public through the South Australian Resources Information Geoserver (SARIG; https://sarig.pir.sa.gov.au/Map). Representative bulk petrophysical properties were derived for selected provinces and geological units (Tables 1 and 2). Histograms and scatter plots were calculated for density and magnetic susceptibility (Figs 1 and 2). This petrophysical compilation provided a key input for the forward modelling.

3 Forward modelling

Forward modelling of the 13GA-EG1E seismic line was undertaken to highlight inconsistencies with the preliminary geological interpretation and make the final interpretation internally consistent with the potential-field data. The forward modelling was not intended to produce an alternate interpretation that precisely matches the potential-field data. To this end we used the actual geological interpretation provided by Doublier, et al. (2015) and Dutch, et al. (2015) of 13GA-EG1E in the forward modelling rather than using a geophysicist's representation of the geology.

Table 1 *Summary statistics of density data from the SARIG petrophysical database for selected basement units and the overlying cover sequences.*

	Minimum	Median	Maximum	Count	Mean	Standard Deviation	Variance
Cenozoic sediments	1.390	1.84	2.86	49	1.86	0.3085	0.0951
Officer Basin	1.84	2.39	3.17	942	2.41	0.1778	0.0316
Hiltaba Suite	2.07	2.67	4.10	329	2.68	0.1342	0.0180
Mulgathing Complex	2.44	2.85	3.68	274	2.91	0.2835	0.0024

Table 2 *Summary statistics of magnetic susceptibility data from the SARIG petrophysical database for selected basement units and the overlying cover sequences.*

	Minimum	Median	Maximum	Count	Mean	Standard Deviation	Variance
Cenozoic sediments	0.00000	0.00008	0.43600	8651	0.00077	0.01109	0.00012
Officer Basin	0.00000	0.00002	0.00085	531	0.00005	0.00007	0.00000
Hiltaba Suite	0.00001	0.00028	0.46211	1066	0.00358	0.01903	0.00036
Mulgathing Complex	0.00001	0.00008	3.10000	3237	0.04014	0.24691	0.06097

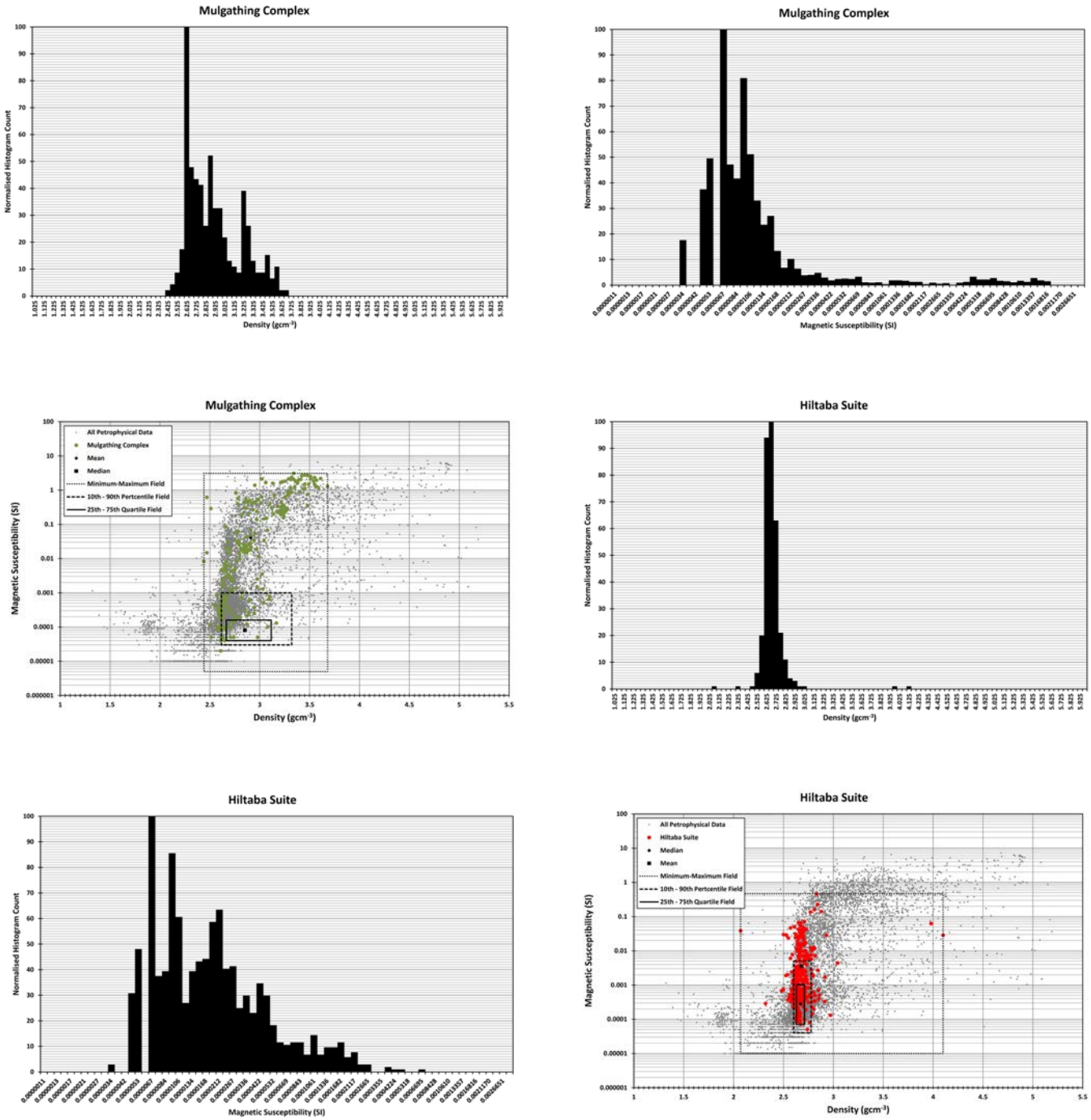

Figure 1 *Histograms of density and magnetic susceptibility data for selected basements units from the SARIG petrophysics database. The magnetic susceptibility data exhibit lognormal distribution and therefore have been converted into logarithmic space. Collocated density and magnetic susceptibility data have been plotted on a scatter plot for selected basement units. The minimum-maximum, 10th-90th percentile and 25th-75th quartile fields were calculated on the complete density and magnetic susceptibility dataset for selected basement units and cover sequences and not just collocated data.*

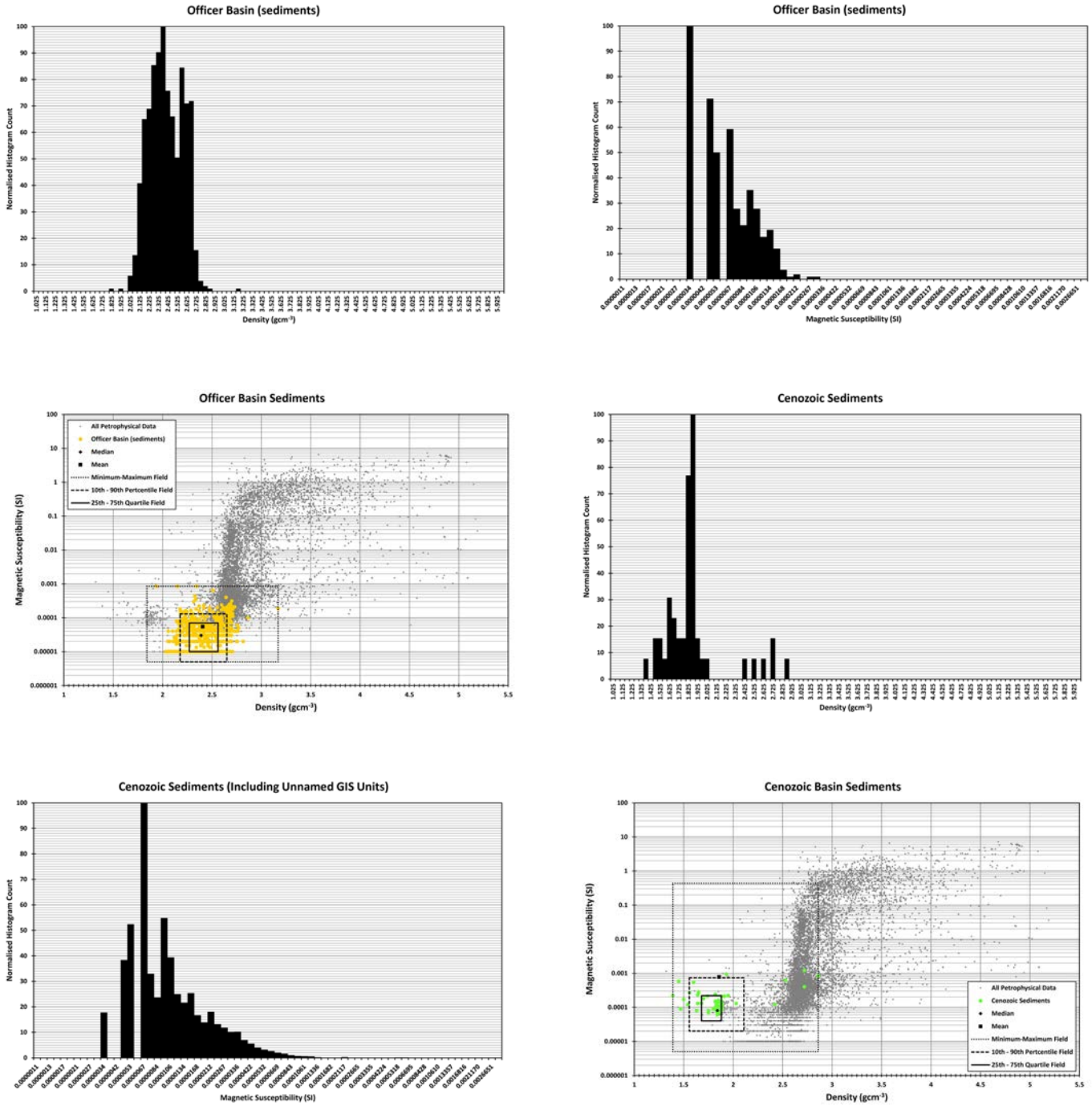

Figure 2 *Histograms of density and magnetic susceptibility data for cover sequences from the SARIG petrophysics database. The magnetic susceptibility data exhibit lognormal distribution and therefore have been converted into logarithmic space. Collocated density and magnetic susceptibility data has been plotted on a scatter plot for selected basement units. The minimum-maximum, 10th-90th percentile and 25th-75th quartile fields were calculated on the complete density and magnetic susceptibility dataset for selected basement units and cover sequences and not just collocated data.*

The initial forward model (Fig. 3) was run using the median values of density from the petrophysical compilation (Table 1). Median values are preferred over the mean as the median is less affected by outliers. For units that had no petrophysical data in SARIG the Australian Seismological Reference Model (AuSREM) (Kennett and Salmon, 2012) was queried to determine the most relevant density value to use (Table 3). After the initial forward model, density values of the polygons were varied to reduce the mismatch (Fig. 4). Generally, first order features are modelled adequately, however the revised model has highlighted two major discrepancies with the interpretation.

1. The density required to model the Kimban Granite was 2.8 5gcm^{-3}. This is anomalously high for a granite body as they typically have a bulk density between 2.60-2.70 gcm^{-3} (e.g., Telford et al., 1990, Dentith and Mudge, 2014). However 2.85 gcm^{-3} is consistent with the Mulgathing Complex.
2. In the western 40-60 km of the line (Fig. 4) there is a low density feature that could not be forward modelled by changing the densities of the existing geological interpretation. The most likely explanation for the discrepancy is low density heterogeneities within the Coompana Province.

4 Potential-field Inversions

Inversions of geophysical data produce three dimensional (3D) rock property models that estimate the distribution of physical properties in the subsurface. Inversion results can also be integrated with other subsurface data. For inversions of gravity data, the models portray the density distribution of the Earth, whilst inversions of magnetic data produce models of the magnetisation distribution of the Earth. Inversion models are non-unique; few of the possible solutions will be geologically realistic, and even fewer will be consistent with specific geological and petrophysical observations from the study area. Potential-field inversions from the UBC Geophysical Inversion Facility (UBC-GIF: Li and Oldenburg, 1996; Li and Oldenburg, 1998a) were run using the National Computational Infrastructure (NCI) High Performance Computing (HPC) facility at the Australian National University (Goodwin et al., 2012; Goodwin et al., 2015).

The inversion process can be guided towards models that are most realistic by adding geological and petrophysical constraints. A 3D geological model was constructed from SeeBase™ (FrOG Tech, 2005; FrOG Tech, 2006), AusMoho (Kennett et al., 2011) and Curie depth (Chopping and Kennett, 2013) datasets. Geological interpretations were converted into a reference model for the inversion by assigning density and magnetic susceptibility values for each of the geological units.

Density and magnetic susceptibility profiles were extracted from the inversions along the seismic line 13GA-EG1E. Doublier, et al. (2015) have produced a detailed geological interpretation of 13GA-EG1E (Fig. 5). The majority of the density anomalies along the section occur in the upper crust (Figs 6 and 7) and represent changes in lithology. The most prominent feature in the magnetic inversion profile (Fig. 8) is a strong, east-dipping magnetic body that is present in the eastern portion of the 13GA-EG1E line. This feature corresponds to the Wilgena Domain in the Mulgathing Complex. There is a moderately magnetic body in the western third of the seismic line that corresponds to the Moondrah Gneiss in the Nawa Domain. This feature also corresponds with a conductive body in the magnetotelluric data (Thiel et al., 2015).

Table 3 *Density values used in the initial and final forward models.*

Unit	Specific Gravity – Initial	Specific Gravity – Final	RGB Colour
Eucla Basin	1.84	2.30	255, 255, 0
Officer Basin	2.39	2.60	255, 170, 0
Hiltaba Suite	2.67	2.58-2.67	255, 0, 0
Kimban Granite	2.60	2.85	255, 85, 0
Granite (unknown age)	2.6	2.56	180, 0, 0
Tarcoola Formation	2.70	2.70	168, 112, 0
Mulgathing Complex	2.85	2.79-2.85	151, 173, 157
Nawa Domain Metasediments	2.70	2.68-2.78	209, 255, 115
Nawa Middle Crust	2.70	2.70-2.85	68, 137, 112
Nawa Reflective Seismic Province	2.70	2.80	115, 178, 115
Coompana Upper Crust	2.76	2.80	114, 137, 68
Central Gawler Seismic Province	2.76	2.76	0, 132, 168
Non Reflective Middle Crust	2.70	2.70-2.82	122, 182, 245
Reflective Mid to Lower Crust	2.80	2.80	122, 245, 202
Mantle	3.30	3.30	85, 255, 0

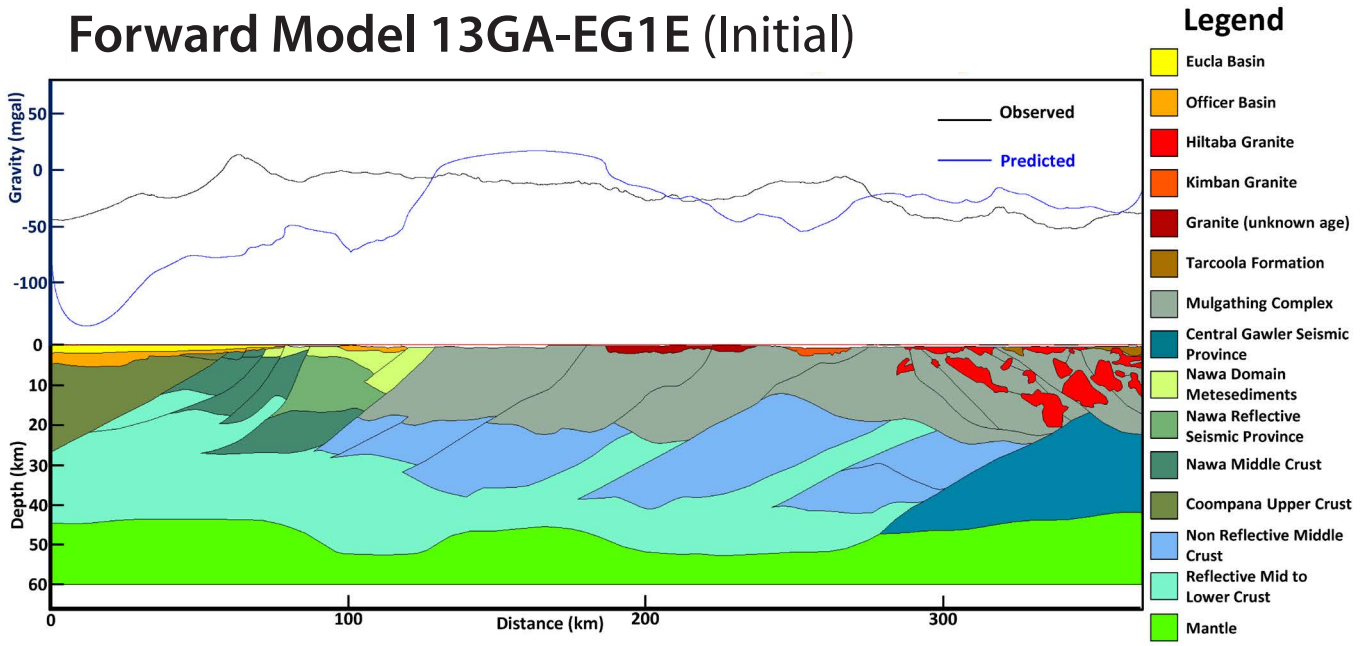

Figure 3 *Initial gravity forward model of 13GA-EG1E using density values obtained from the petrophysical compilation.*

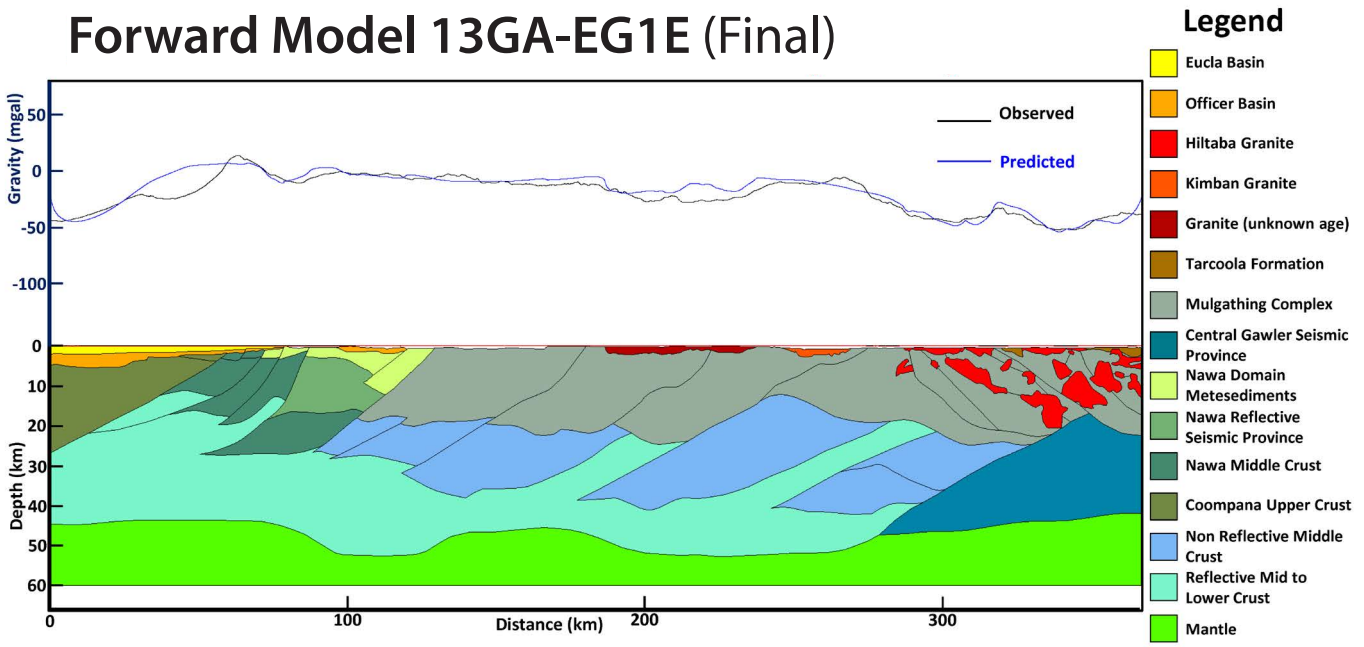

Figure 4 *Final gravity forward model for 13GA-EG1E with density values adjusted to obtain a better fit to the observed data.*

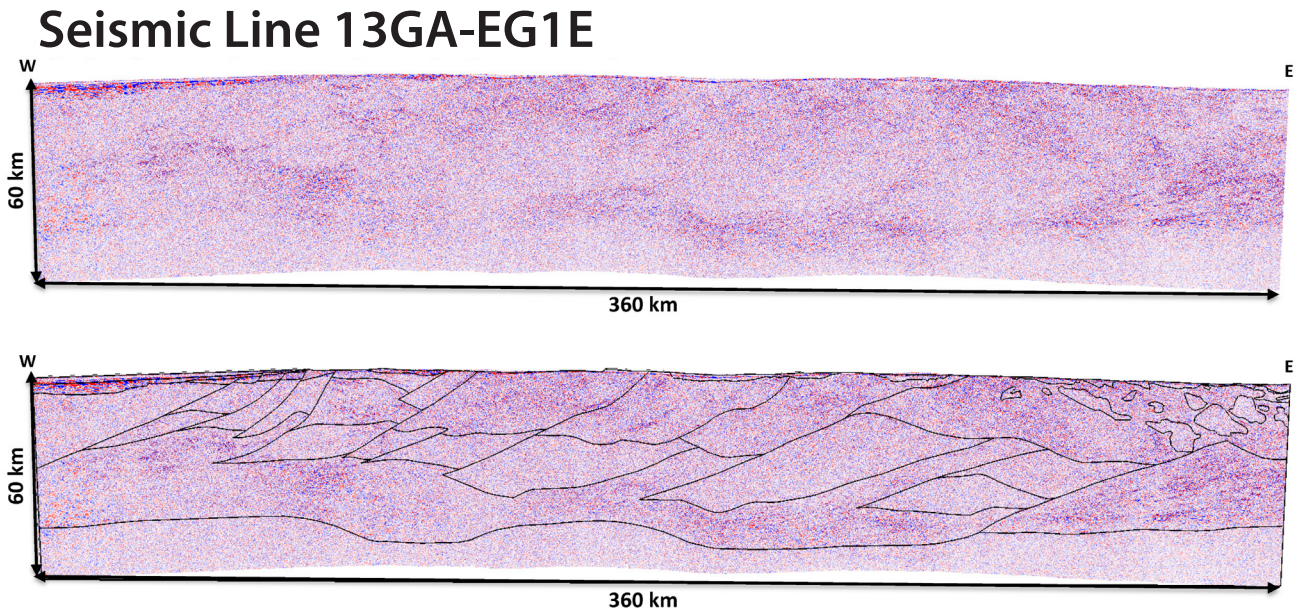

Figure 5 *Reflection seismic line 13GA-EG1E (migrated), with and without the geological interpretation overlayed.*

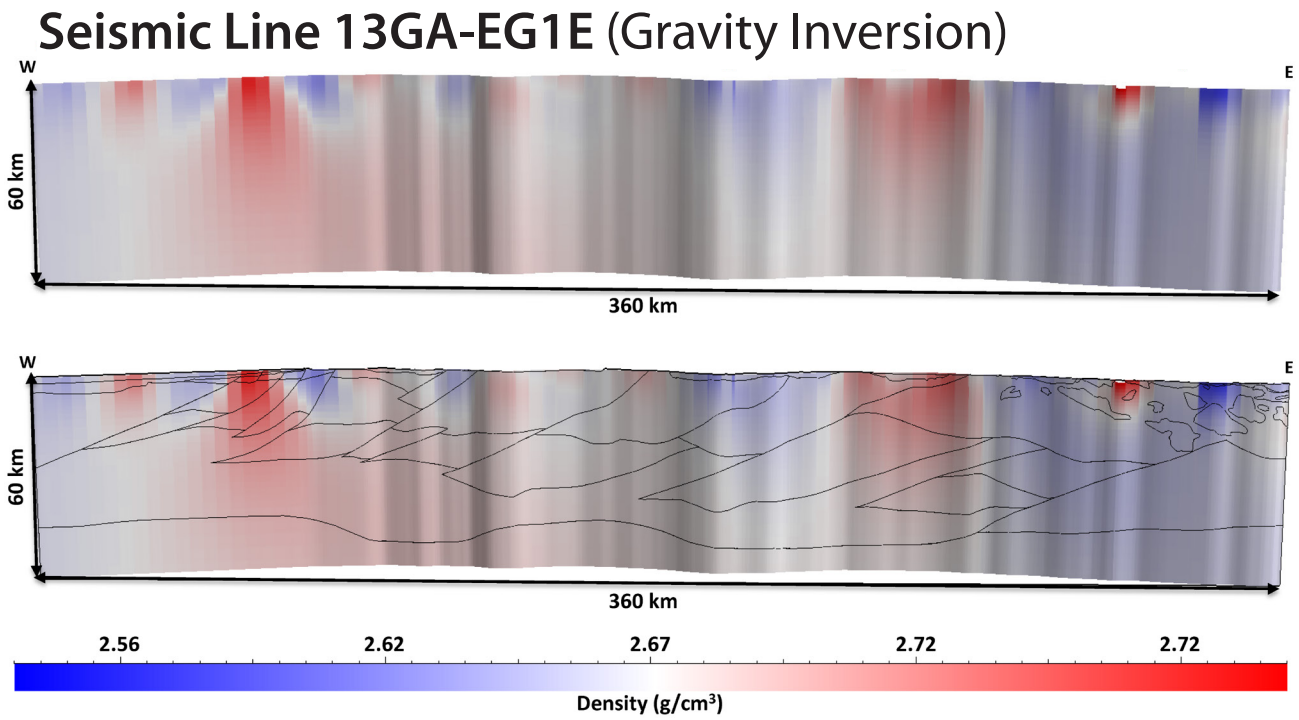

Figure 6 *East-west slice through the gravity inversion along seismic line 13GA-EG1E, with and without the interpretation overlayed.*

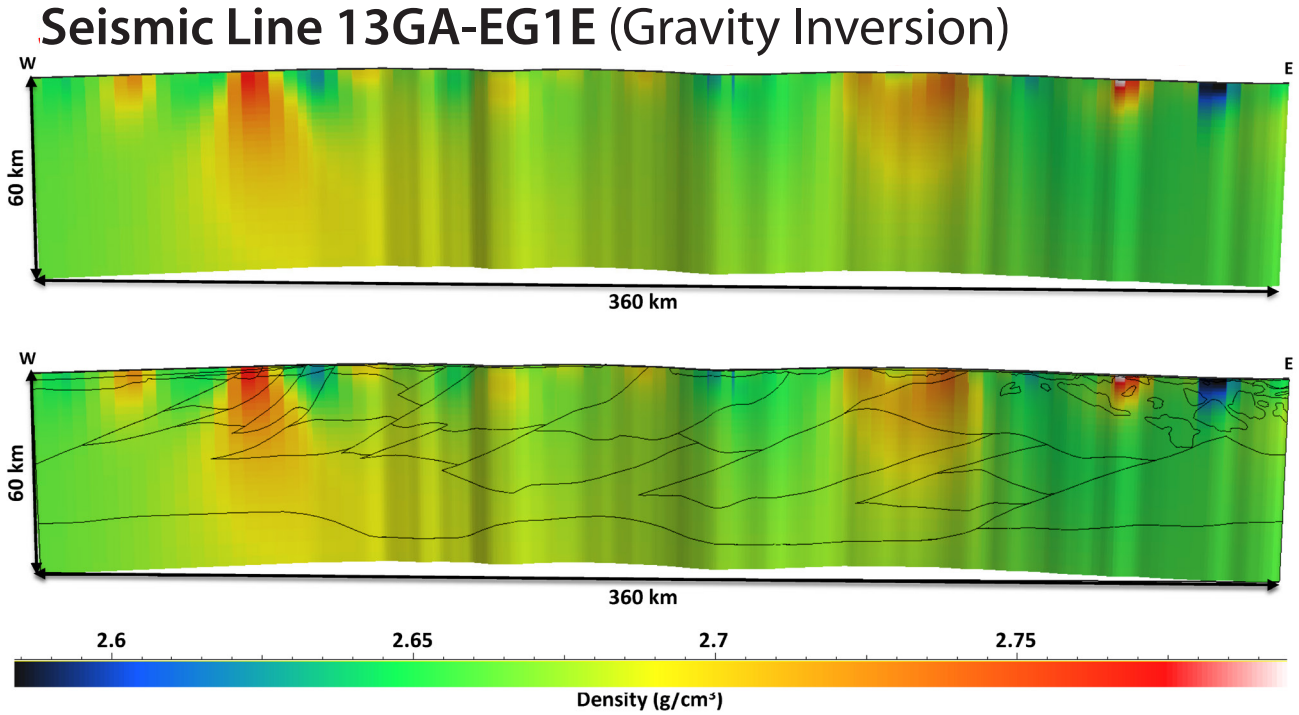

Figure 7 *Slice through the gravity inversion with an alternate colour ramp to enhance different features along seismic line 13GA-EG1E, with and without the interpretation overlayed.*

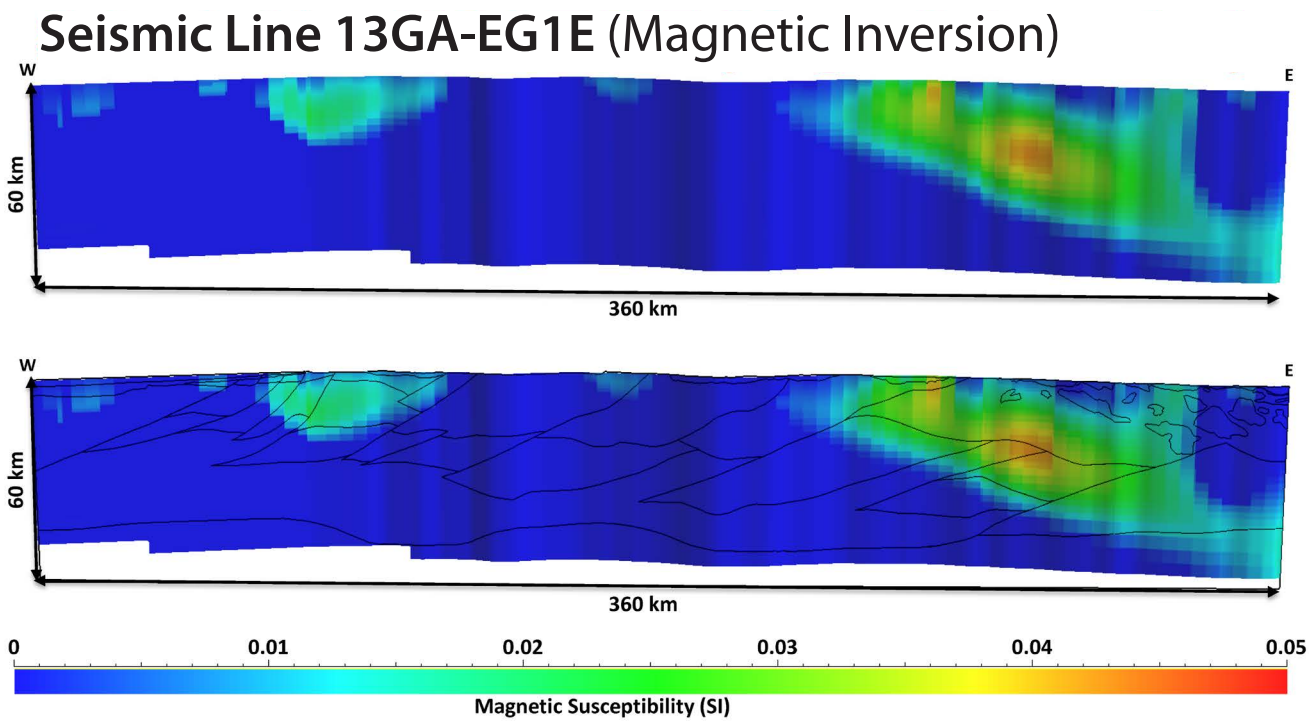

Figure 8 *Slice through the magnetic inversion along seismic line 13GA-EG1E, with and without the interpretation overlayed.*

5 Conclusions

Potential-field and petrophysical data from publicly available datasets were used in forward modelling of 13GA-EG1E and geophysical inversions. The results of the modelling show features corresponding with known geological elements in the crust. This robust interpretation is consistent with all available datasets and shows the usefulness of potential-field data for producing rigorous geological interpretations of crustal seismic lines.

Acknowledgments

James Goodwin and Malcolm Nicoll publish with permission of the CEO of Geoscience Australia. Simon van der Wielen publishes with permission of the CEO of Deep Exploration Technologies Collaborative Research Centre. Access to the NCI was provided by Geoscience Australia without which this project would not have been possible. Stephanie McLennan is thanked for her considered comments on the manuscript.

References

Chopping, R., and Kennett, B.L.N., 2013, The Curie depth of Australia, and its uncertainty. ASEG Extended Abstracts 2013, 1–3, DOI: http://dx.doi.org/10.1071/ASEG2013ab199.

Dentith, M., and Mudge, S.T., 2014, Geophysics for the Mineral Exploration Geoscientist. Cambridge University Press, Cambridge, pp 438.

Doublier, M. P., Dutch, R. A., Clark, D., Pawley, M. J., Fraser, G. L., Wise, T. W., Kennett, B. L. N., Reid, A. J., Spaggiari, C. V., Calvert, A. J., van der Wielen, S., Dulfer, H., Bendall, B., Thiel, S., and Holzschuh, J., 2015, Interpretation of the western Gawler Craton section of Seismic line 13GA–EG1, *in* Dutch, R. A., Pawley, M. J., and Wise, T. W., eds., What lies beneath the western Gawler Craton? 13GA-EG1E Seismic and Magnetotelluric Workshop 2015, Report Book 2015/00029. Department of State Development, South Australia, Adelaide.

Dutch, R. A., Doublier, M. P., Pawley, M. J., Wise, T. W., Reid, A. J., Clark, D., Kennett, B. L. N., Fraser, G. L., Thiel, S., van der Wielen, S., Chopping, R., and Bendall, B., 2015a, Geological and Geodynamic implications for the western Gawler Craton section of Seismic line 13GA-EG1, in Dutch, R. A., Pawley, M. J., and Wise, T. W., eds., What lies beneath the western Gawler Craton? 13GA-EG1E Seismic and Magnetotelluric Workshop 2015, Report Book 2015/00029. Department of State Development, South Australia, Adelaide.

FrOG Tech, 2005, OZ SEEBASE Phanerozoic Basins Study. Public domain report to Shell Development Australia by FrOG Tech Pty Ltd.

FrOG Tech, 2006, OZ SEEBASE Proterozoic Basins Study. Public domain report to Shell Development Australia by FrOG Tech Pty Ltd.

Goodwin, J., Hackney, A. R., and Williams, N. C., 2015, 3D Geophysical inversion modelling of the Wallaby Plateau: evidence for continental crust and seaward-dipping reflectors. Record 2015/01. Geoscience Australia, Canberra, DOI: http://dx.doi.org/10.11636/Record.2015.001.

Goodwin, J., Williams, N. C., and Oldenburg, D. W., 2012, High-resolution regional-scale 3D inversion modelling using the National Computational Infrastructure. ASEG Extended Abstracts 2012, 1–4, DOI: http://dx.doi.org/10.1071/ASEG2012ab406.

Hornby, P., Boschetti, F., and Horowitz, F., 1999, Analysis of potential field data in the wavelet domain: Geophysical Journal International, 137, 175-196, DOI: 10.1046/j.1365-246x.1999.00788.x.

Kennett, B.L.N., and Salmon, M., 2012, AuSREM: Australian Seismological Reference Model: Australian Journal of Earth Sciences, 59, 1091-1103, DOI: 10.1080/08120099.2012.736406

Kennett, B.L.N, Salmon, M., Saygin, E., and AusMoho Working Group, 2011, AusMoho: the variation of Moho depth in Australia: Geophysical Journal International, 187, 946-958, DOI: 10.1111/j.1365-246X.2011.05194.x

Li, Y., and Oldenburg, D.W., 1996, 3-D inversion of magnetic data: Geophysics, 61, 394-408.

Li, Y., and Oldenburg, D.W., 1998, 3-D inversion of gravity data: Geophysics, 63, 109-119.

Telford, W.M., Geldart, L.P., and Sheriff, R.E., 1990, Applied Geophysics (Second Edition). Cambridge University Press, Cambridge, pp 770.

Thiel, S., Duan, J., and Wise, T. W., 2015, Crustal resistivity structure of the western Gawler Craton and margins derived from the 13GA-EG1E magnetotelluric profile, in Dutch, R. A., Pawley, M. J., and Wise, T. W., eds., What lies beneath the western Gawler Craton? 13GA-EG1E Seismic and Magnetotelluric Workshop 2015, Report Book 2015/00029. Department of State Development, South Australia, Adelaide.

FURTHER INFORMATION

Simon van der Wielen
Simon.vanderWielen@sa.gov.au
Deep Exploration Technologies Cooperative Research Centre
Box 66, Export Park, Adelaide Airport, SA, 5950

Eucla MT profile and modelling

Stephan Thiel[1], Tom Wise[1], Jingming Duan[2]
1 Geological Survey of South Australia, Department of State Development
2 Resources Division, Geoscience Australia

1 MT method

Magnetotellurics is a passive electromagnetic technique measuring natural variations of the Earth's magnetic and electric fields at the surface of the Earth (Cagniard, 1953). Interactions between the solar plasma with the Earth's ionosphere and magnetosphere (Frequency f<10 Hz or its inverse period T>10 s) or global lightning activity (f>10 Hz) cause magnetic field variations, which act as a source for the induction of electric eddy currents in the Earth.

In the field, the MT systems sample time series of the horizontal electric field $\{E_x,E_y\}$ and the three-component magnetic field $\{B_x,B_y,B_z\}$, with {x,y,z} denoting geographic north, east, and vertically down, respectively. The time series convert into the frequency domain using robust remote referencing processing schemes. The frequency of the signal as well as the bulk resistivity of the subsurface determines the penetration depth δ of the signal via the skin-depth relationship (in m):

$$\delta = 503\sqrt{\rho \cdot T}$$

The complex ratio of the horizontal electric to magnetic field, as a function of period T, yields the impedance tensor Z via:

$$[E_x \quad E_y] = \begin{bmatrix} Z_{xx} & Z_{xy} \\ Z_{yx} & Z_{yy} \end{bmatrix} \cdot \begin{bmatrix} B_x \\ B_y \end{bmatrix}$$

Each component of Z=X + iY can be expressed as a magnitude ρ_a and phase ϕ as follows:

$$\rho_a = \frac{1}{\omega\mu_0}|Z_{ij}|^2$$

Where ω denotes the angular frequency, and μ_0 the magnetic permeability.

$$\phi = \tan^{-1}\frac{\Im Z_{ij}}{\Re Z_{ij}}$$

Where $\Im$ and $\Re$ denote the imaginary and real part of Z_{ij}, respectively. An alternative way to represent the impedance tensor information is the galvanic distortion free magnetotelluric phase tensor.

$$\Phi = X^{-1}Y$$

Its representation as an ellipse readily shows the dimensionality and strike of the impedance tensor. One-dimensional resistivity distributions are characterized by a circle. Ellipses denote 2D or 3D structure, with a non-zero value of the phase tensor skew $\beta = \frac{1}{2}\tan^{-1}\frac{\phi_{12}-\Phi_{21}}{\phi_{11}+\Phi_{22}}$ pointing to 3D structures. The principal components of the phase tensor denote the transverse electric and transverse magnetic polarization phases in 2D and are therefore parallel or perpendicular to the geoelectric strike.

2 MT data

2.1 Acquisition and processing

In 2014, Geoscience Australia, the Geological Survey of Southern Australia, and the Geological Survey of Western Australia in collaboration collected 167 broadband MT sites along ~840 km profile. The survey was conducted within a corridor either side of the Trans-Australian railway line from Western Australia into South Australia (Fig. 1). Here we present analysis and modelling of the 13GA-EG1E beginning at MT station 90 and progressing east to the end of the line at Tarcoola.

The data were acquired by a mixture of Phoenix and Metronix MT systems at various sample rates for approximately 40 hours. The Phoenix system used an MTU-5A data recorder with MTC-50 (for B_x and B_y) and MTC-80H (B_z) magnetic induction coils. The Metronix system used an ADU-07e recorder with MFS-06e induction coils.

The electric dipoles for both instruments were typically 100 m in length. The electric field was measured using non-polarizing Pb/PbCl2 electrodes in a cross layout. The position of each electrode was recorded with 10 cm accuracy by the LandPak GPS.

Time-series data were processed by using commercial software from the Phoenix and Metronix companies. The data processing fundamentally involves a Fourier transformation with robust remote-reference (Gamble et al., 1979) approach for deriving the impedance tensor of the subsurface. Then apparent resistivity and phase were calculated. The processed data (0.025 s – 2000 s) was in good quality generally.

The impedance data have very good data quality, resulting in generally smooth responses across the frequency spectrum (Fig. 2). Increased error bars and unstable responses are observed at some stations in the period dead-band around 10 s. These data points were masked prior to further analysis and inverse modelling. Figure 2 illustrates the strong influence of the sediments of the Eucla Basin with low resistivities of typically less than 10 Ωm for T < 1 s (site EGC095A). Further east along the profile, the cover is much thinner with apparent resistivities increasing from short periods (T < 0.01s) to high resistivities exceeding 1000 Ωm in the crust. Responses across the Gawler Craton also show higher complexity than for stations across the Eucla, exemplified by 2D or 3D responses. Additionally, there are more rapid changes in the apparent resistivity and phase curves between adjacent stations for the Gawler part suggestive of relatively rapid variation on electrical resistivity structure of the subsurface.

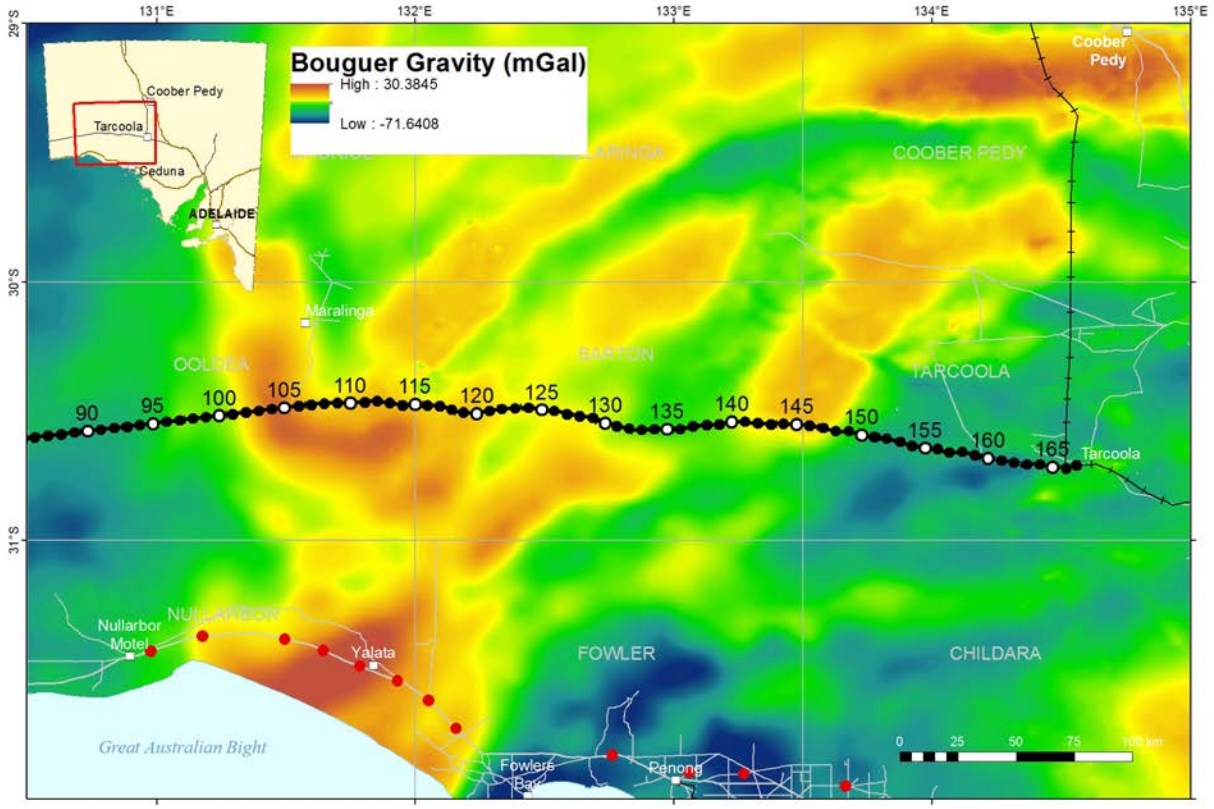

Figure 1 *Overview map of the 13GA-EG1E MT line stations on top of Bouguer gravity image. The resistivity models presented here are restricted to the section between stations EGC090 in the Eucla Basin and EGC167 in the Gawler Craton. Location of the Fowler survey (Thiel & Heinson, 2010) is shown in red.*

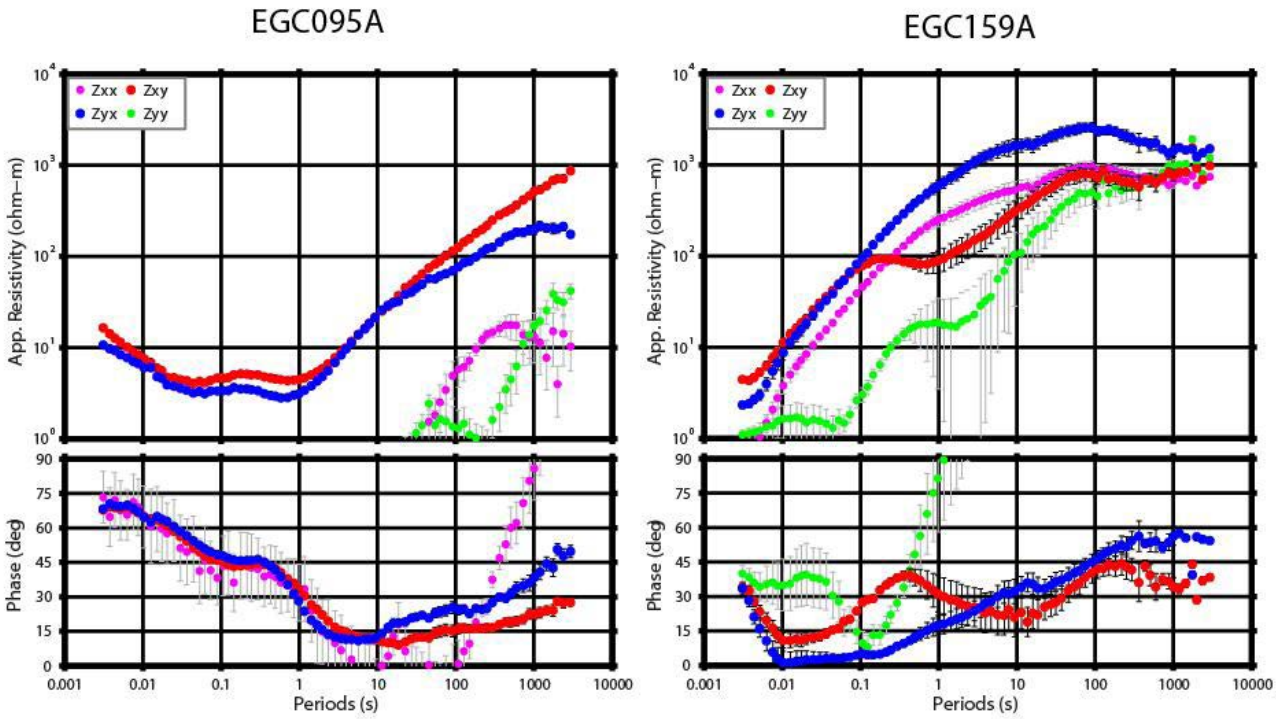

Figure 2 *Apparent resistivity and phase curve for station EGC095A (located over the Eucla basin) and EGC159A (on the Gawler Craton) further east. The thicker sediments across the Eucla Basin compared to the shallow cover of the Gawler Craton sites is apparent from the low apparent resistivities to periods of 1 s for site EGC095A.*

2.2 Effect of near surface distortion – influence of near surface structure

Galvanic and inductive distortion can have a significant influence on magnetotellurics data (Caldwell, et al., 2004; Selway, et al., 2012; McNeice and Jones, 2001; Becken and Burkhardt, 2004). The MT data of the current profile shows phases dipping below 0° in the period range between 0.1 s and 1 s for selected stations (Fig. 3). While this effect can be caused by noise and extreme 3D resistivity distributions, it is commonly observed where there are strong resistivity contrasts between a shallow and conductive overburden overlying a resistive basement (Selway, et al., 2012). The observed phases <0° typically associate with the TE-mode response for stations located on top of the shallow conductor, such as a sedimentary cover near an outcrop. Figure 4 illustrates the spatial correlation between stations exhibiting anomalous phases below 0° and boundaries between the electrically conductive cover of Quaternary dune ranges, palaeodrainage channels, and coastal sediments and the more resistive basement underlying the calcrete layers of the Nullarbor Plains.

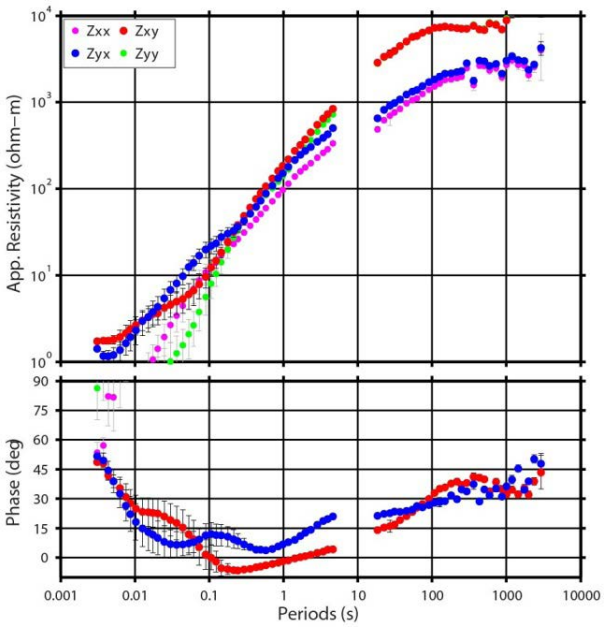

Figure 3 *Apparent resistivity and phase curves for site EGC149A. The Zxy component of the impedance tensor shows phases dipping below 0° for periods. In absence of noise, this effect is associated with very strong resistivity contrasts between shallow, bounded, and laterally extensive conductive cover over a resistive basement (Selway, et al., 2012).*

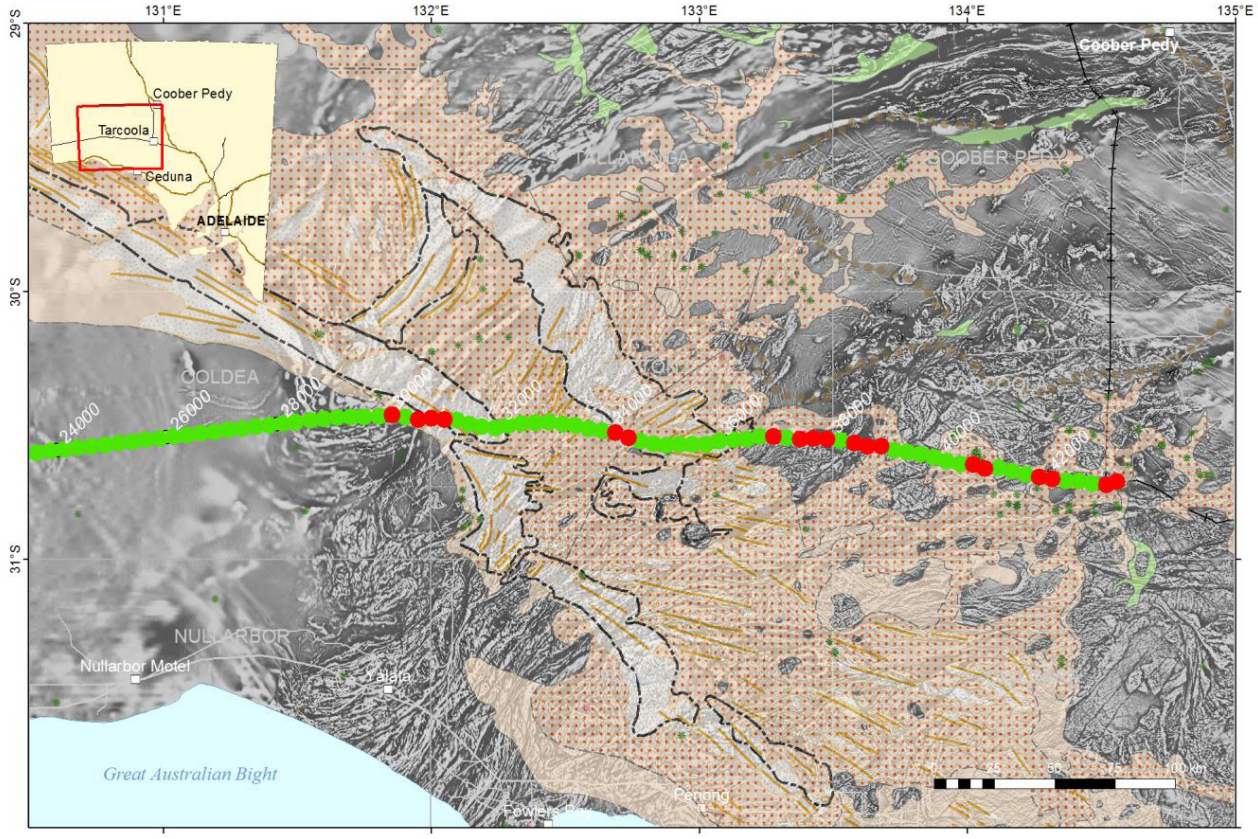

Figure 4 *MT stations of the 13GA-EG1E profile across the western Gawler Craton and margins on palaeodrainage map. Red circles indicate MT stations which have anomalous phases below 0° (Selway, et al., 2012). Dash-dotted outline denotes Quaternary dune ranges sitting between palaeodrainage channels and coastal sediments (red dots on yellow shading). Anomalous phases occur for some stations located along the margins of the dunes or palaeodrainage channels.*

2.3 Induction arrows – effects of the railway line

The close vicinity of the MT profile to the railway line due to logistical constraints leads to inductive effects of the direct current railway line dominating the tipper data (Schaefer, et al., 2011). Figure 5 illustrates the effect of the railway line on the tipper responses. The magnitude of the tipper largely exceeds 1, suggestive of a larger vertical than horizontal component. This behavior is only observed in case of extreme current channeling. The data show that the real component of the tipper points to the railway line along the profile. This behavior is verified in places where the deployment jumps from the northern to the southern side of the railway line resulting in a corresponding flip of the tipper. The imaginary part is antiparallel to the real induction arrows, which indicates a predominantly 2D response of the data to the railway line. Therefore, other inductive effects related to the subsurface play a negligible role in the tipper responses. As a consequence, the tipper information was excluded from modelling.

2.4 Strike analysis and dimensionality

Prior to any 2D inverse modelling attempts, it is crucial to identify subsets of the data that fulfil the dimensionality requirements for modelling (1D and 2D response). For this purpose, the data were analysed using the phase tensor approach (Caldwell, et al., 2004) and the ellipticity criterion (Becken and Burkhardt, 2004) to determine the dimensionality and the preferred geoelectric strike, and eliminate galvanic distortion from the data. Figure 6 shows a pseudosection of the skew angle β. Values greater than 5° are generally regarded as 3D (Thiel, et al., 2009), but smaller values have also been proposed as a stricter threshold (Booker, 2014). Skew values indicating three-dimensionality predominantly occur in the vicinity of shear zones and where phases dip below 0° across the eastern part of the profile presented in the resistivity models below. The responses attributed to the Eucla Basin sediments and the crust beneath are predominantly non-3D for stations EGC001 to EGC090.

The phase tensor pseudosection in Figure 7 displays the impedance tensor information displayed as phase tensors, free of galvanic distortion. The orientation of the ellipse major axes illustrates the direction of current flow, i.e. circles denote no preferred orientation for current flow and therefore mostly 1D electric structure. The most dominant feature is the Eucla Basin with largely circular ellipses for periods between <0.01 s and to about 1 s in the central part of the 13GA-EG1 MT line. The minimum phases (shading in red and blue color) are >45° suggesting that the shallowest sediment layers are more resistive than sediment layers at depths of a few tenths to hundreds of meters. This is further supported by the apparent resistivity and phase curves, e.g. station EGC095 in Figure 3. For the modelled profile between station EGC090 and EGC167, the phase tensors show rapidly changing orientation, which can be explained by interpreted fault zones from magnetic images (Fig. 8). It is evident that major shear zones cause a polarization in current flow and also changes in the minimum phase value for periods that are sampling depths equivalent to the upper few km depth extent of the faults. Analysis of the entire 13GA-EG1 line identifies several subsets of data that are suitable for 2D modelling as there are competing strike directions along the entire 800+ km long profile. Figure 7 shows that the strike direction changes between the Gawler Craton and margins compared to the crust beneath the Eucla Basin. The Gawler Craton shows a strike angle close to N~30°E, whereas the general strike angle for the Eucla Basin crust and uppermost mantle is around 0°N.

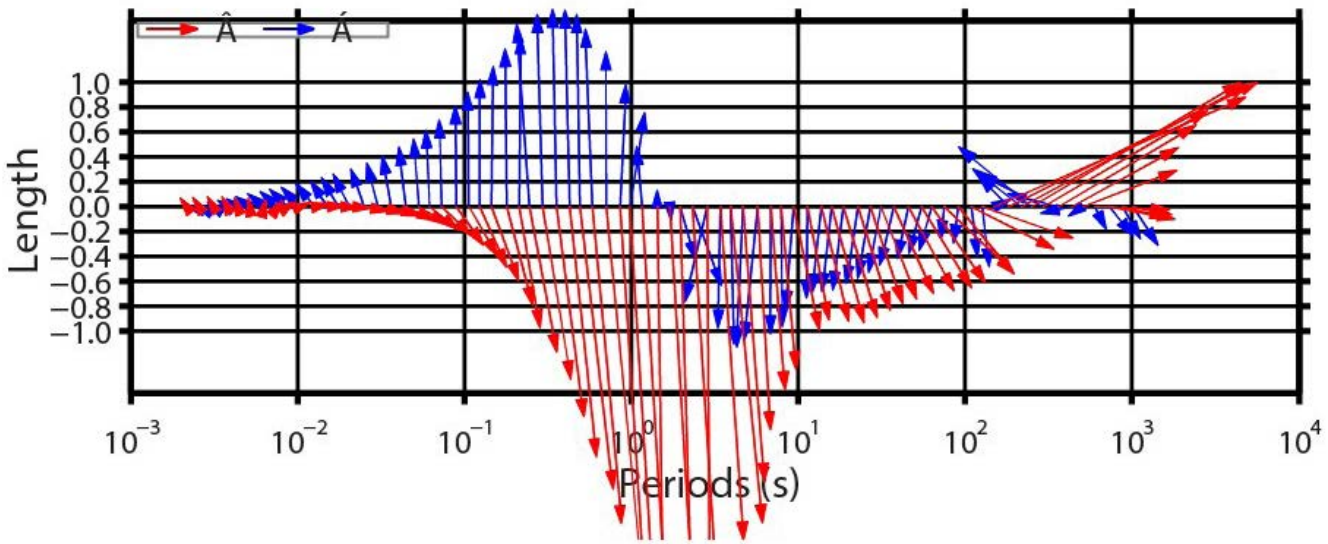

Figure 5 *Induction arrows for station EGC131A. Red and blue arrows denote the real and imaginary component of the tipper transfer function, respectively. The real part of the arrow points at the railway line a few hundred meters to the south.*

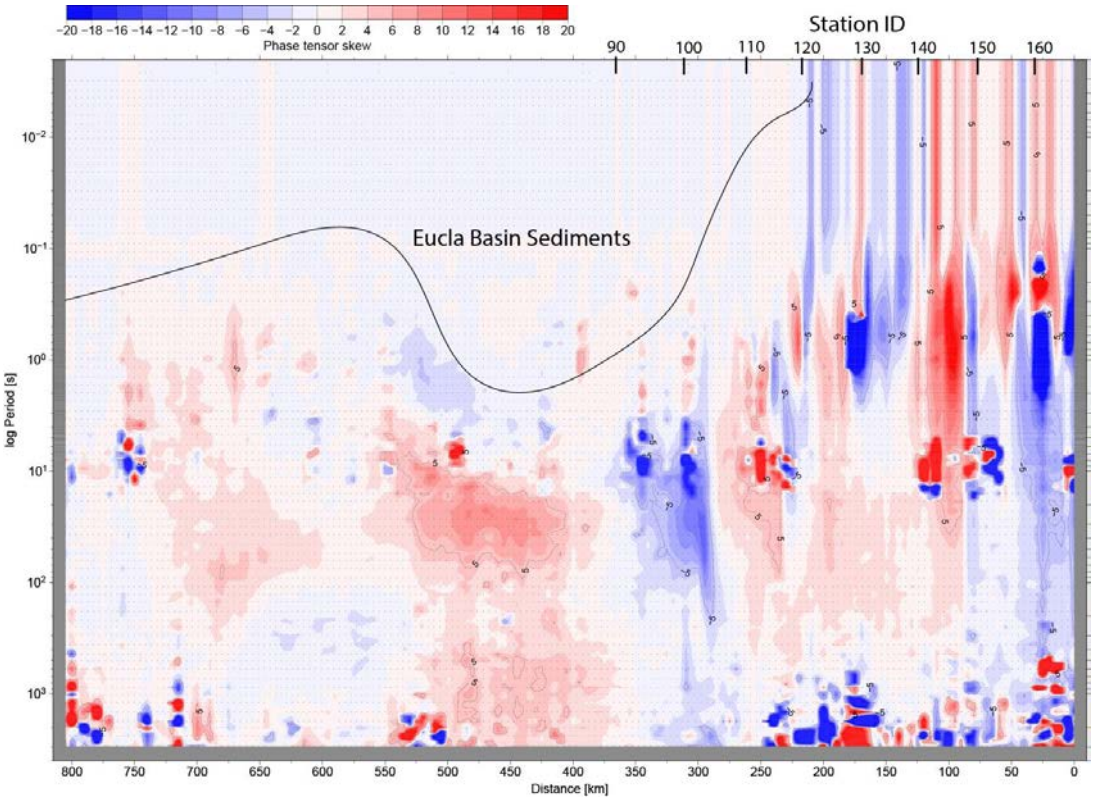

Figure 6 *Phase tensor skew pseudosection for the entire 13GA-EG1 profile. Highest degree of dimensionality is observed in the eastern part of the profile where skew values β exceed ±5°, indicative of 3D structures. Three-dimensionality is primarily associated with fault zones in the Fowler Domain.*

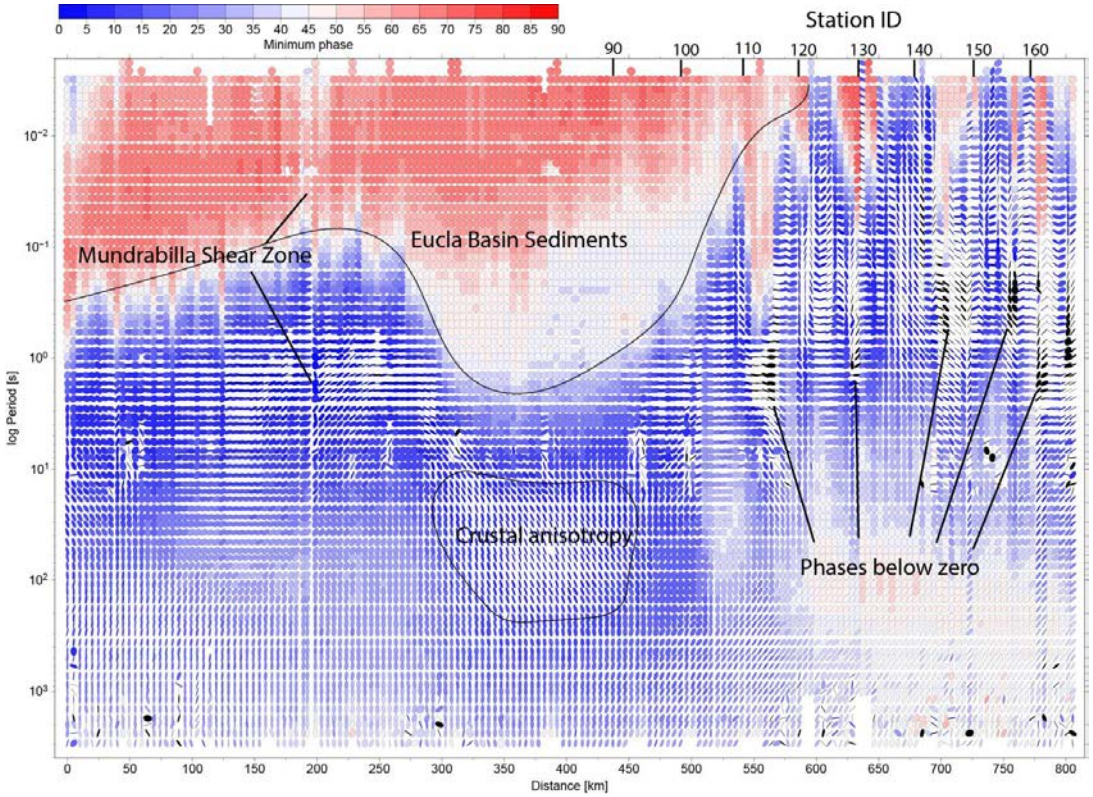

Figure 7 *Phase tensor pseudosection of the entire 13GA-EG1 profile. Shading indicates the minimum phase value of the phase tensor (Caldwell, et al., 2004). Only sites 90 to 167 were modelled in 2D due to consistent strike directions for this part of the profile and the spatial overlap with the 13GA-EG1E seismic line. Between EGC100 and the eastern end of the profile, there are rapidly changing orientation of the phase tensors indicating strong resistivity contrast of the shear zones. Black ellipses denote phases below 0°.*

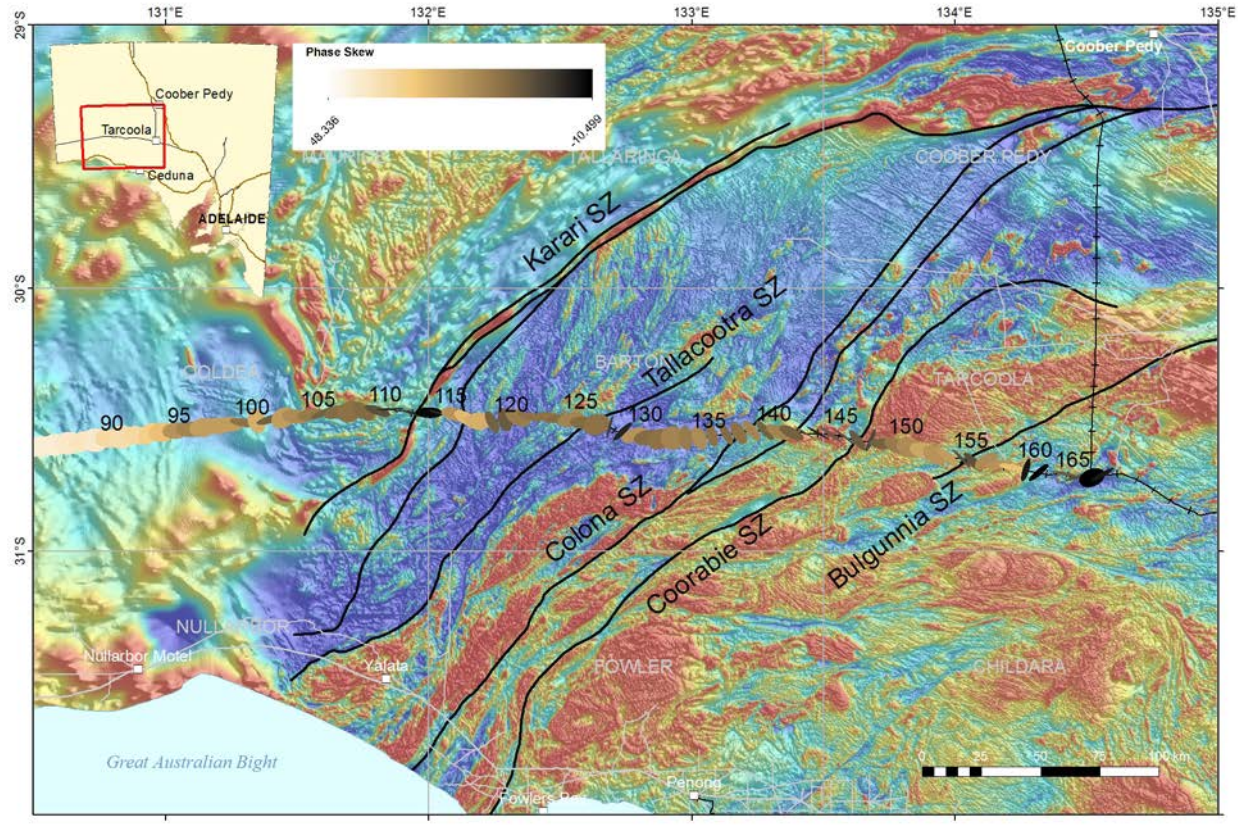

Figure 8 *Phase tensor ellipses for period of 1s on top of total magnetic intensity image and interpreted major faults.*

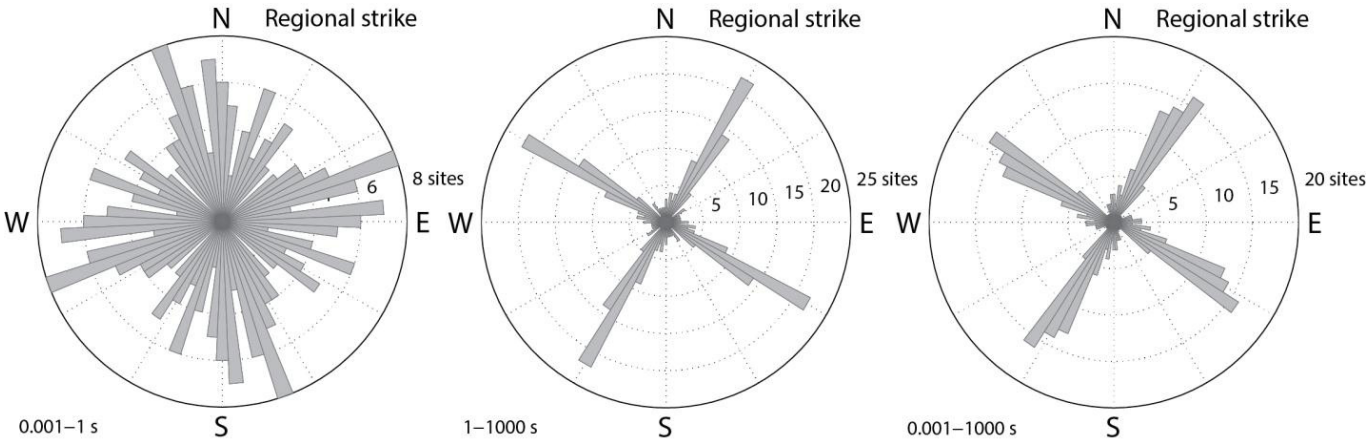

Figure 9 *Strike angle analyses for periods 0.001-1 s, 1-1000 s and 0.001-1000 s (left to right) along the 13GA-EG1E line from station EGC90A in the west to EGC167 in the east. The predominant strike direction is N27°E after phase tensor analysis (Caldwell, et al., 2004) and decomposition analysis using the ellipticity criterion (Becken and Burkhardt, 2004).*

For this reason, 2D modelling was restricted to the Gawler Craton and margins as far west as station EGC090. Phase tensor analysis and the ellipticity criterion determine a best fit overall strike angle of N27°E for the profile (Fig. 9). The upper crust appears strongly heterogeneous without a clear preferred orientation, however from periods ~1 s (equivalent to depths of a few km) and longer, the geoelectric strike is relatively uniform along profile. The N27°E orientation coincides with the strike of the faults, interpreted from TMI. Even in the absence of induction arrow data, it is then possible to assign the TE-mode to the rotated impedance tensor component, where the E-field is aligned with the geoelectric strike of N27°E. The TM-mode is perpendicular with the E-field oriented N117°E across the geoelectric strike. The galvanic distortion is minimized and error bars enlarged where data are 3D to minimize 3D effects in the modelling (Becken and Burkhardt, 2004; Becken, et al., 2008).

3 Model and discussion

After rotation of the data to the preferred strike direction of N27°E the data were inverted using a 2D smooth inversion code with Tikhonov-type regularization (Fig. 10; Rodi and Mackie, 2001). In order to test the robustness of the models and the influence of the TE- and TM-mode on the final inversion outcomes, the models were started using the TE-mode first with large error bars of 50% for the TE apparent resistivities and 20% for the TE phase. Additionally, the regularization parameter τ, which balances the trade-off between fitting the data and ensuring model smoothness was set to high values of τ=50 initially to produce smooth models but avoid getting trapped in local minima. Subsequently, the data error bars were reduced and the weighting to fitting the data emphasized by reducing τ. At this point the TM-mode apparent resistivities and phases were also introduced. The same strategy was applied to a second model starting with the TM-mode only and later introducing the TE-mode data. The TM-mode is inherently more sensitive to resistivity boundaries, placing emphasis on vertical features in the model due to the E-field aligned across geoelectric strike. The TE-mode has a higher emphasis on the actual true resistivity of the resistivity features, which explains the slightly more sub-vertical nature of the crustal conductors C2, C3 and C4 in Figure 10.

Both models converged after more than 1000 iterations with final error floors of 5% and 2.5% for the TM-mode apparent resistivities and phases, respectively. The TE-mode error floors were 16% and 4% for apparent resistivity and phase, respectively. The regularisation parameter τ had a final value of 3. The slightly higher error bars for the TE-mode down weight 3D effects (Wannamaker, et al., 1984) in the data. Static shift in the TE-mode is accommodated by larger error floors of 16% as opposed to 5% in the TM-mode.

Both models converged to a similar final rms (root mean square) of 2.39 and 2.42 for the TE-mode first and TM-mode first inversion, respectively. As expected, the differences in rms for individual stations are biggest across areas of strong resistivity contrast and where phase tensor analyses indicate three-dimensionality in the data. In areas of predominantly 1D or 2D responses, the individual station rms is within ±0.05 for each station.

Notable differences between the models are the shape of conductor C1 and the continuation of higher conductivity beneath the shallow upper-crustal conductor C6. While the continuation of low resistivity beneath C6 of the TM-mode first model may be attributed to the bias of the TM-mode to introduce sub-vertical features, it highlights the lack of resolution beneath the upper-crustal conductivity anomaly C6.

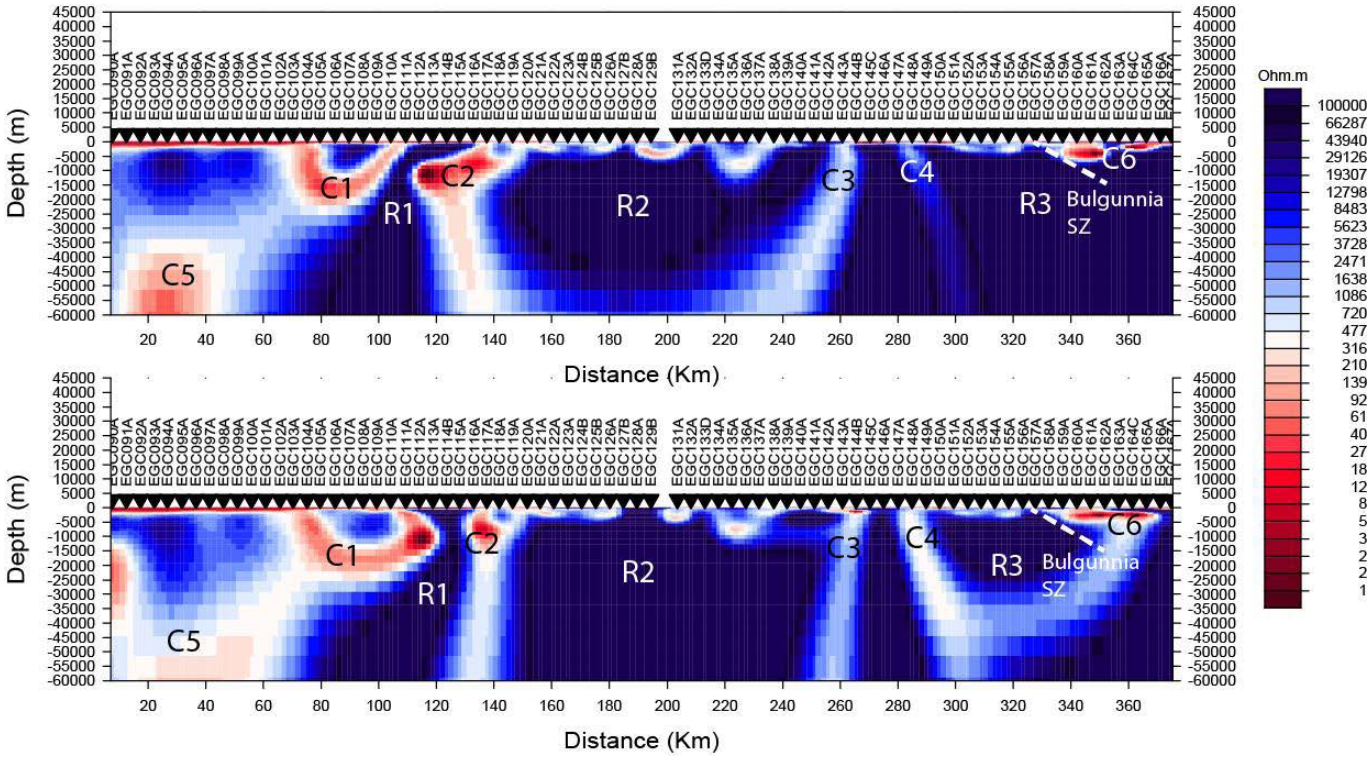

Figure10 *Final resistivity models for the crust and upper mantle (top 60 km) from MT site EGC090 in the west (Eucla Basin) to EGC167 (Gawler Craton) in the east. Top model represents starting TE-mode inversion followed by inclusion of TM-mode responses. Bottom model is the TM-mode followed by TE-mode addition. Final total rms are 2.39 and 2.42, respectively.*

Conductor C1 describes an arcuate shape coincident with a folded surface magnetic anomaly situated to the west of the Karari Shear Zone in the Nawa Domain (Fig. 11). Furthermore its position correlates with the margins of the gravity high between stations EGC102 and EGC112. C1 extends to depths of around 15 km and is connected to the thin surface conductivity layer representing the sedimentary cover of the Eucla Basin. There is no known surface outcrop, but drill samples of the adjacent Ooldea 2 hole intersected magnetite-bearing metasedimentary rocks of the Moondrah Gneiss in the top 200 m (Payne, et al., 2008; Teasdale, 1997). Magnetite has been associated with a reduction in resistivity in the field across other parts of South Australia in the Delamerian (Robertson, et al., 2015) and has the potential to form interconnected pathways in fold hinges and through shearing (Thiel, et al., 2005). The seismic reflection data have been interpreted to have a shallow (top 1 km) expression of the Moondrah Gneiss (Doublier, et al., 2015). This interpretation remains in contradiction to the large vertical extent of the conductor C1 to depths of 15 km. Either the magnetite abundance crosses lithology with varying seismic reflection character or the conductor may be a representation of out-of-profile structure. Given the high degree of three-dimensionality of sites across C1 (Fig. 6), a possibility could be that the large folded TMI structure in the Nawa Domain between sites EGC102 and EGC112 is imaged as a uniquely vertical feature in the 2D model. Further analysis, potentially with 3D modelling, is required to conclusively identify the geometry of C1.

The interface between resistor R1 and conductor C2 coincides with the surface expression of the Karari Shear Zone outcropping at site EGC116A (Fig. 11). The dip of the interface is to the west and likely to a depth of around 10 km before steepening and extending vertically into the crust. Analyses of U-Pb and $^{40}Ar/^{39}Ar$ geochronology indicate multiple stages of reworking along the Karari Shear Zone from 1780 Ma to 1450 Ma (Fraser, et al., 2012). The conductivity feature C2 appears wider than the narrow magnetic anomaly traditionally associated with the Karari Shear Zone suggesting that shearing and mineral precipitation occurred over an approximately 10 km wide corridor which is sharply truncated by the magnetic high to the west.

The Tallacootra Shear Zone does not show a significant conductivity response near the interpreted position at site EGC129 to EGC130. Station EGC 130 had to be omitted due to highly distorted responses, which may be a result of near surface expressions of the Tallacootra Shear Zone. However, adjacent stations do not require a crustal conductivity anomaly to fit the data. Along the eastern margin of the Fowler Domain, both the Colona (C3 in Fig. 10) and Coorabie shear zones (C4) are imaged as sub-vertical crustal conductors about 5 km wide. It should be noted that a finer resolution is limited by station spacing of the same dimension of 5 km. Both of these crustal conductivity structures bound a gravity high extending further north (cf. Fig. 1).

A lower crustal to upper mantle conductor labelled C5 in Figure 10 is situated beneath the western margin of the Eucla Basin. It is likely associated with an area of strong phase splits and probable electrical anisotropy (see Fig. 7).

The shallow conductor C6 to the eastern end of the profile roughly coincides with surface expressions and interpreted vertical extent of the Tarcoola Formation (Doublier, et al., 2015). The formation is a fluvial to marginal-marine clastic succession emplaced into grabens. Relevant for MT measurements is the interbedding of quartzite with laminated carbonaceous and pyritic siltstone, which is the most likely source for the low resistivity close to the surface. It is also possible that iron formations perhaps equivalent to the Wilgena Hill Jaspilite exist, and are responsible for, the aforementioned C6 conductor. Its western margin is bound by the interpreted extent of the Bulgunnia Shear Zone (Fig. 10).

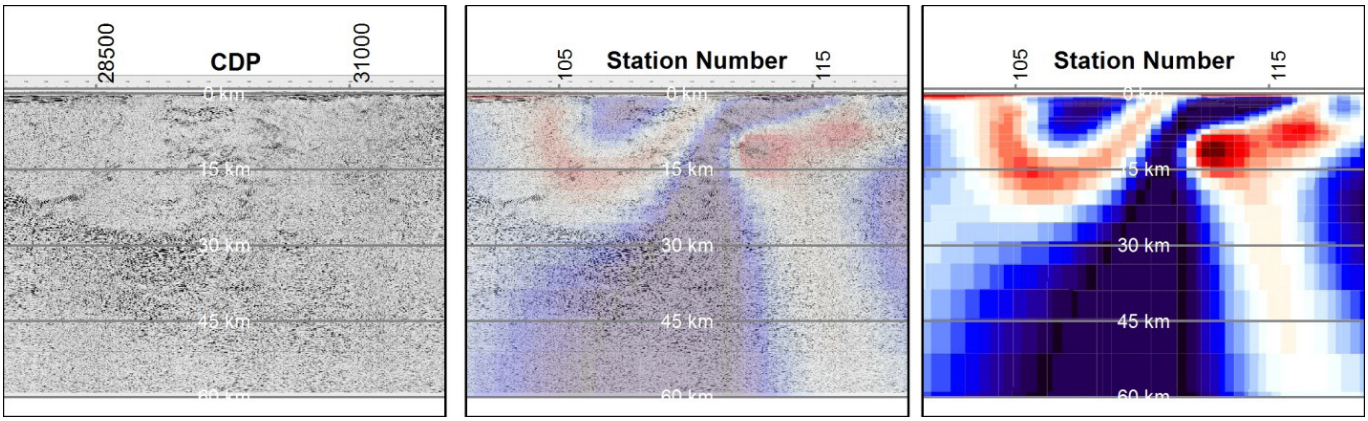

Figure11 *Close-up of conductors C1 and C2 in Figure 10 juxtaposed on the seismic reflection image. Conductive features appear to cross-cut shallow reflectors; however the western arcuate shaped conductor seems to occupy a generally low reflectivity zone truncated by a reflective lower crust at around 25 km respectively.*

4 Comparison to previous magnetotelluric studies

A long-period MT profile 100 km to the south from the edge of the Eucla Basin in the west to the eastern edge of the Nuyts Domain also crossed the Fowler Domain (Fig. 1; Thiel and Heinson, 2010). There are limitations in the resolution of upper-crustal features due to the lack of high-frequency broadband data and higher station spacing of 15 km. However, the profile imaged two sub-vertical conductivity features that were associated with the Tallacootra and Coorabie shear zones (see Fig. 11 in Thiel and Heinson 2010). Given the recent results of the 13GA MT line, the western conductivity feature (C1 in Fig. 10) may in fact be an extension of the Karari Shear Zone, as the Tallacootra Shear Zone does not show a conductive response and C1 in their study lies along the magnetic extension of the conductive feature C2 of this study, associated with the 10 km wide band of the Karari Shear Zone. The Coorabie Shear Zone is imaged in both models as a sub-vertical feature. It may be that the off-set Colona and Coorabie shear zones are imaged as a single conductor in the model of Thiel and Heinson (2010) due to the lack of resolution.

5 Conclusions

The 13GA-EG1E MT line transects the western Gawler Craton and margins. The data are approximately 2D for mid- to lower crustal levels following the strike of interpreted faults of the craton-bounding Karari shear zone and several major shear zones in the Fowler Domain. 2D inverse modelling shows that the Karari, Colona and Coorabie shear zones have a low resistivity, sub-vertical signature extending through the crust. The folded TMI feature in the Nawa Domain is imaged as an arcuate conductor extending to depths of 15 km. The low resistivity is most like caused by magnetite-rich metasediments of the Moondrah Gneiss, further supported by a magnetic high in the upper crust derived from potential field inversions (Van der Wielen, et al., 2015). The electrical conductors largely cross-cut interpreted seismic reflectors, suggesting that both techniques image different geological processes. Additionally, seismic reflection studies lack sensitivity to vertical structure which is primarily imaged with MT. The conductive anomalies coincide with margins of gravity highs and magnetic field lineaments. The dense and magnetically susceptible banded iron formations leading to the potential field expressions appear to be structurally controlled and linked to deformation zones that may be connected to Moho offsets and crustal fluid pathways. The fluid related precipitates are the result of the deformation and fluid processes and are likely the cause for the current low resistivity structure.

References

Becken, M., and Burkhardt, H., 2004, An ellipticity criterion in magnetotelluric tensor analysis: Geophysical Journal International, v. 159, p. 69-82.

Becken, M., Ritter, O., Park, S.K., Bedrosian, P.A., Weckmann, U., and Weber, M., 2008, A deep crustal fluid channel into the San Andreas Fault system near Parkfield, California: Geophysical Journal International, v. 173, no. 2, p. 718-732.

Booker, J., 2014, The Magnetotelluric Phase Tensor: A Critical Review: Surveys in Geophysics, v. 35, no. 1, p. 7-40.

Cagniard, L., 1953, Basic theory of the magneto-telluric method of geophysical prospecting: Geophysics, v. 18, p. 605-635.

Caldwell, T. G., Bibby, H. M., and Brown, C., 2004, The magnetotelluric phase tensor: Geophysical Journal International, v. 158, p. 457-469.

Doublier, M. P., Dutch, R. A., Clark, D., Pawley, M. J., Fraser, G. L., Wise, T. W., Kennett, B. L. N., Reid, A. J., Spaggiari, C. V., Calvert, A. J., van der Wielen, S., Dulfer, H., Bendall, B., Thiel, S., and Holzschuh, J., 2015, Interpretation of the western Gawler Craton section of Seismic line 13GA–EG1, in Dutch, R. A., Pawley, M. J., and Wise, T. W., eds., What lies beneath the western Gawler Craton? 13GA-EG1E Seismic and Magnetotelluric Workshop 2015, Report Book 2015/00029. Department of State Development, South Australia, Adelaide.

Fraser, G., Reid, A., and Stern, R., 2012, Timing of deformation and exhumation across the Karari Shear Zone, north-western Gawler Craton, South Australia: Australian Journal of Earth Sciences, v. 59, no. 4, p. 547-570.

McNeice, G. W., and Jones, A. G., 2001, Multisite, multifrequency tensor decomposition of magnetotelluric data: Geophysics, v. 66, p. 158-173.

Parker, A. J., 1993, Geological Framework, in Drexel, J., Preiss, W. V., and Parker, A. J., eds. The geology of South Australia. Vol. 1, The Precambrian. Geological Survey of South Australia, p. 9-31.

Payne, J. L., Hand, M., Barovich, K. M., and Wade, B. P., 2008, Temporal constraints on the timing of high-grade metamorphism in the northern Gawler Craton: implications for assembly of the Australian Proterozoic: Australian Journal of Earth Sciences, v. 55, no. 5, p. 623-640.

Robertson, K., Taylor, D., Thiel, S., and Heinson, G., 2015, Magnetotelluric evidence for serpentinisation in a Cambrian subduction zone beneath the Delamerian Orogen, southeast Australia: Gondwana Research, v. 28, no. 2, p. 601-611.

Rodi, W., and Mackie, R. L., 2001, Nonlinear conjugate gradients algorithm for 2-D magnetotelluric inversion: Geophysics, v. 66, no. 1, p. 174-187.

Schaefer, A., Houpt, L., Brasse, H., and Hoffman, N., 2011, The North German Conductivity Anomaly revisited: Geophysical Journal International, v. 187, no. 1, p. 85-98.

Selway, K., Thiel, S., and Key, K., 2012, A simple 2-D explanation for negative phases in TE magnetotelluric data: Geophysical Journal International, v. 188, no. 3, p. 945-958.

Teasdale, J., 1997, Methods for understanding poorly exposed terranes: The interpretive geology and tectonothermal evolution of the western Gawler Craton: PhD thesis, The University of Adelaide.

Thiel, S., and Heinson, G., 2010, Crustal imaging of a mobile belt using magnetotellurics: An example of the Fowler Domain in South Australia: Journal of Geophysical Research, v. 115, no. B6, p. B06102.

Thiel, S., Heinson, G., Gray, D. R., and Gregory, R. T., 2009, Ophiolite emplacement in NE Oman: constraints from magnetotelluric sounding: Geophysical Journal International, v. 176, no. 3, p. 753-766.

Thiel, S., Heinson, G., and White, A., 2005, Tectonic evolution of the southern Gawler Craton, South Australia, from electromagnetic sounding: Australian Journal of Earth Sciences, v. 52, p. 887-896.

Thiel, S., Milligan, P., Heinson, G., Boren, G., Duan, J., Ross, J., Adam, H., Dhu, T., Fomin, T., Craven, E., and Curnow, S., 2010, Magnetotelluric acqusition and processing, with examples from the Gawler Craton, Curnamona Province and Curnamona-Gawler Link transects in South Australia, in Korsch, R., and Kositcin, N., eds. South Australian Seismic and MT Workshop 2010. Geoscience Australia, Record, 2010/10, p. 11-21.

Van der Wielen, S., Goodwin, J., Nicoll, M., and Keeping, T., 2015, Potential Field Investigation of the western Gawler Craton Section of Seismic Reflection Line 13GA-EG1E, in Dutch, R. A., Pawley, M. J., and Wise, T. W., eds., What lies beneath the western Gawler Craton? 13GA-EG1E Seismic and Magnetotelluric Workshop 2015, Report Book 2015/00029. Department of State Development, South Australia, Adelaide.

Wannamaker, P., Hohmann, G., and Ward, S., 1984, Magnetotelluric responses of three-dimensional bodies in layered earths: Geophysics, v. 49, p. 1517-1533.

FURTHER INFORMATION

Stephan Thiel
Stephan.thiel@sa.gov.au
Geological Survey of South Australia,
Department of State Development,
GPO Box 320, Adelaide, South Australia, 5001

Geological and geodynamic implications of the western Gawler Craton section of seismic line 13GA-EG1

R.A. Dutch[1], M.P. Doublier[2], M.J. Pawley[1], T.W. Wise[1], A.J. Reid[1], D. Clark[2], B.L.N. Kennett[3], G. Fraser[2], S. Thiel[1], S. van der Wielen[1]

1 Geological Survey of South Australia, Department of State Development

2 Resources Division, Geoscience Australia

3 Research School of Earth Sciences, Australian National University

1 Introduction

Under the National Geoscience Agreement, Geoscience Australia, in conjunction with the Geological Survey of South Australia (funded through PACE Frontiers), the Geological Survey of Western Australia, and AuScope acquired 834 km of vibroseis-source, deep-seismic reflection data in a single, west to east transect across Western and South Australia from November 2013 to February 2014 (see Holzschuh, 2015, this volume). The transect follows the Trans-Australian Railway, and is referred to here as the Eucla-Gawler seismic survey, or as 13GA-EG1 (Fig. 1). In the west, it starts in the Madura Province at Haig, where it connects to the eastern end of seismic line 12GA-AF3 (Spaggiari et al., 2014), transects the Coompana Province and ends in the central Gawler Craton at Tarcoola, about 1.5 km south of the southern end of seismic line 08GA-OM1(Fig. 1; 'GOMA' line; Korsch and Kositcin, 2010).

In this contribution we consider some geological and geodynamic implications of the western Gawler Craton section of the 13GA-EG1 seismic line, encompassing ~ 360 km between CDP 24950, ~ 38 km east of Cook, and the eastern end of the line at Tarcoola (Fig. 2 and Plate 1). This eastern portion of line 13GA-EG1 is referred to here as 13GA-EG1E. This paper forms a companion paper to the descriptive interpretations presented in Doublier et al. (2015, this volume) and integrates the regional geology, magnetotelluric modelling and potential field modelling presented in this volume (Reid and Dutch, 2015; Thiel et al., 2015; Van der Wielen et al., 2015).

13GA-EG1E starts in the easternmost part of the Coompana Province, and traverses the Nawa, Christie and part of the Wilgena domains of the western and central Gawler Craton (Figs 3 and 4). This region records a protracted geological history of basin formation, magmatism, metamorphism and deformation spanning the Neoarchean through to the Mesoproterozoic (Daly et al., 1998; Ferris et al., 2002; Swain et al., 2005; Hand et al., 2007; Reid et al., 2008; Reid et al., 2014b; Reid and Dutch, 2015, this volume). Interpretation of the regional geology is hampered by limited basement exposure (Fig. 5), with the Wilgena and Christie domains being covered by a thin veneer of Cenozoic cover including the paleostrandlines of the Barton and Ooldea ranges (Fig. 6), which host economic heavy mineral deposits (Hou et al., 2011). The Paleoproterozoic metasediments and granites of the Nawa Domain, west of the Karari Shear Zone, are buried beneath Neoproterozoic to Cambrian and Cenozoic sedimentary rocks of the Officer and Eucla basins. These basins become progressively thicker to the west where they overlie the Mesoproterozoic basement of the Coompana Province (Figs 4 and 6).

2 Upper Crust

2.1 Wilgena and Christie Domains

The Wilgena and Christie domains form part of the Neoarchean to Paleoproterozoic core of the Gawler Craton. Lithologically they are similar, being dominated by metasedimentary and meta-igneous rocks of the Christie and Kenella gneisses of the Mulgathing Complex (Reid et al., 2014b; Reid and Dutch, 2015, this volume). Previous workers have differentiated the Christie and Wilgena domains based largely on magnetic character (e.g., Parker, 1990; Ferris et al., 2002), with the Wilgena Domain being dominated by units of high magnetic intensity and the Christie Domain having a characteristically low magnetic signature (Fig. 3). The two domains are separated by the Coorabie Shear Zone. Other differences between the two domains include the prevalence of elliptical Hiltaba-aged intrusions in the Wilgena Domain which are apparently absent from the Christie Domain, the preservation of the late Paleoproterozoic Tarcoola Formation sediments in the upper crust of the Wilgena Domain and the metamorphic grade of the early Paleoproterozoic Sleafordian Orogeny, which decreases from HT-LP granulite facies in the Christie Domain to greenschist and lower amphibolite facies in the Wilgena Domain (Fig. 7; Reid and Dutch, 2015, this volume).

The gross seismic character of these domains displays a similar, moderately reflective character dominated by rolling reflectors suggestive of open, upright folding. This conforms with the understanding that the two domains are dominated by units of the Mulgathing Complex. The new seismic data reveal that the broad structural architecture of the Wilgena Domain differs considerably from the Christie Domain, and the rest of the imaged line, in that it is dominated by east-dipping structures, which sole out at the interpreted base of the Mulgathing Complex. These structures are truncated at the western margin of the Wilgena Domain by the west-dipping listric crustal-scale Coorabie Shear Zone. We interpret the major east dipping structures in the Wilgena Domain (i.e., Bulgunnia, Muckanippie and unnamed blind shear zones) and west dipping structures in the Christie Domain (i.e., Coorabie,

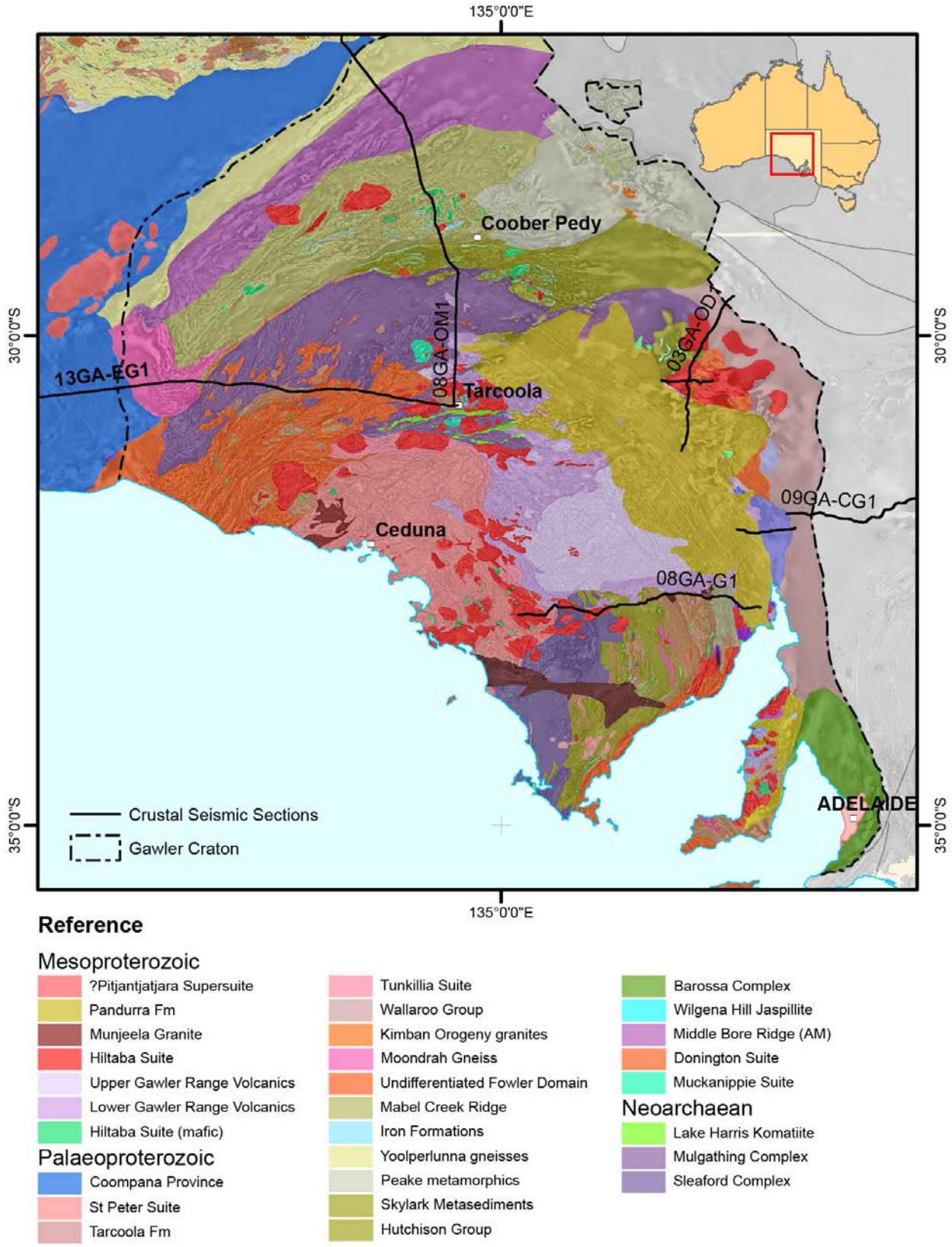

Figure 1 *Regional location map of the 13GA-EG1E seismic line on interpreted basement geology (after Cowley, 2006). Also shown are the other deep crustal seismic reflection lines on the Gawler Craton.*

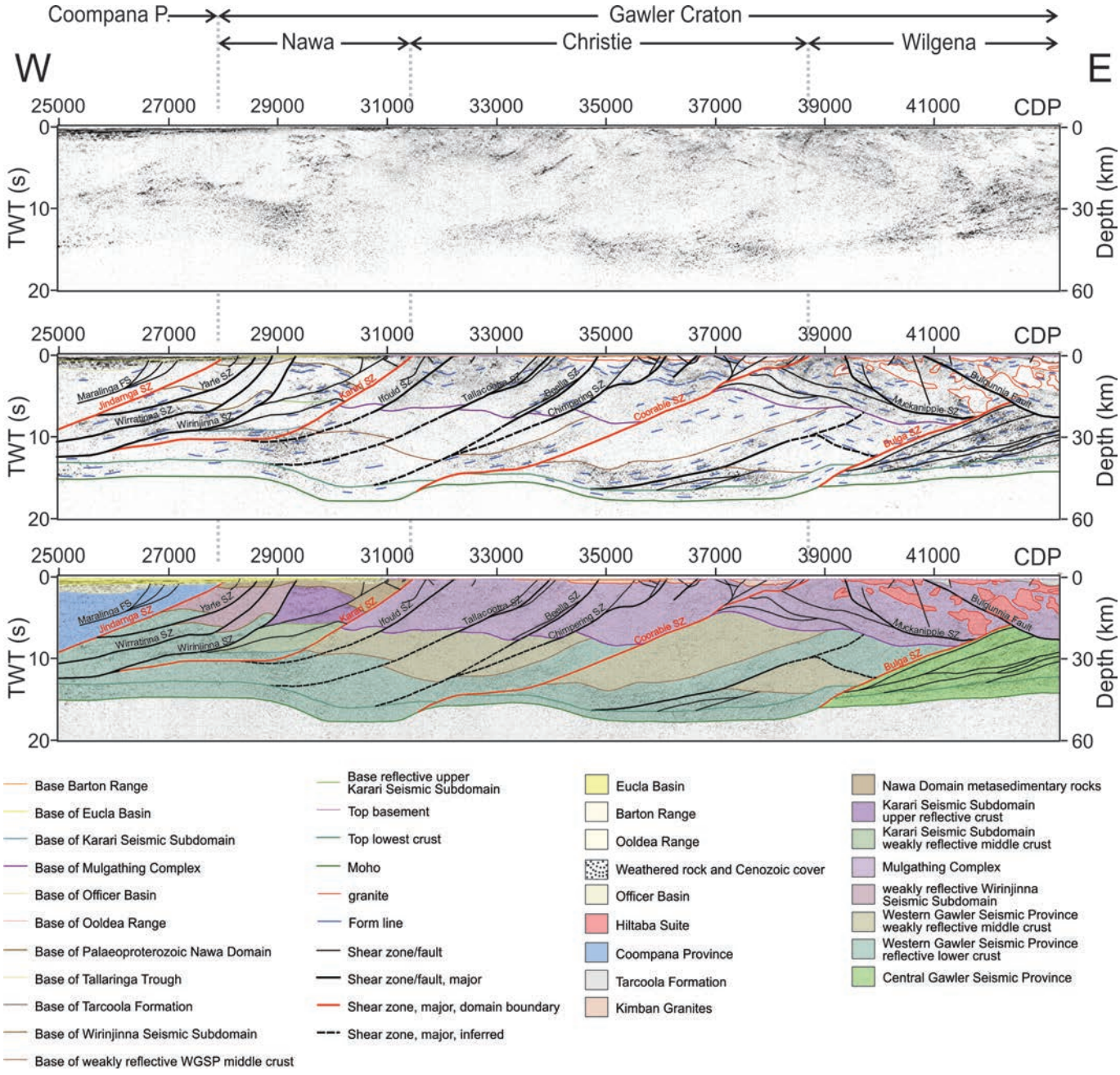

Figure 2 *13GA-EG1E seismic interpretation. Top image is the migrated stacks with no interpretation. Second image includes the interpretation described in Doublier et al. (2015, this volume). The final image includes the interpreted major structures and the interpreted domains.*

Chimpering, Beella, Tallacootra and Ifould shear zones; Fig. 2) to have originally formed as extensional structures, possibly reactivating a pre-existing Neoarchean structural architecture in the middle to lower crust, accommodating the deposition of the Mulgathing Complex in an interpreted back-arc or arc-rift setting (Swain et al., 2005; Reid et al., 2014b). Of note is a highly magnetic region modelled in the magnetic inversions (Van der Wielen et al., 2015, this volume), and mirrored by a conductor modeled in the magnetotelluric (MT) data (Thiel et al., 2015, this volume), located at the base of the Wilgena Domain between the Coorabie Shear Zone and approximately the Muckanippie Shear Zone and dipping parallel to the base of the Mulgathing Complex (figure 8 of Van der Wielen et al., 2015, this volume). This magnetic conductor may indicate a large proportion of iron formations in this part of the Mulgathing Complex.

Reactivation of the major structures likely occurred during the *c.* 2465-2410 Ma Sleafordian Orogeny (Hand et al., 2007; Reid et al., 2014b). Metamorphism during this event reached HT-LP granulite facies conditions in the central Christie Domain

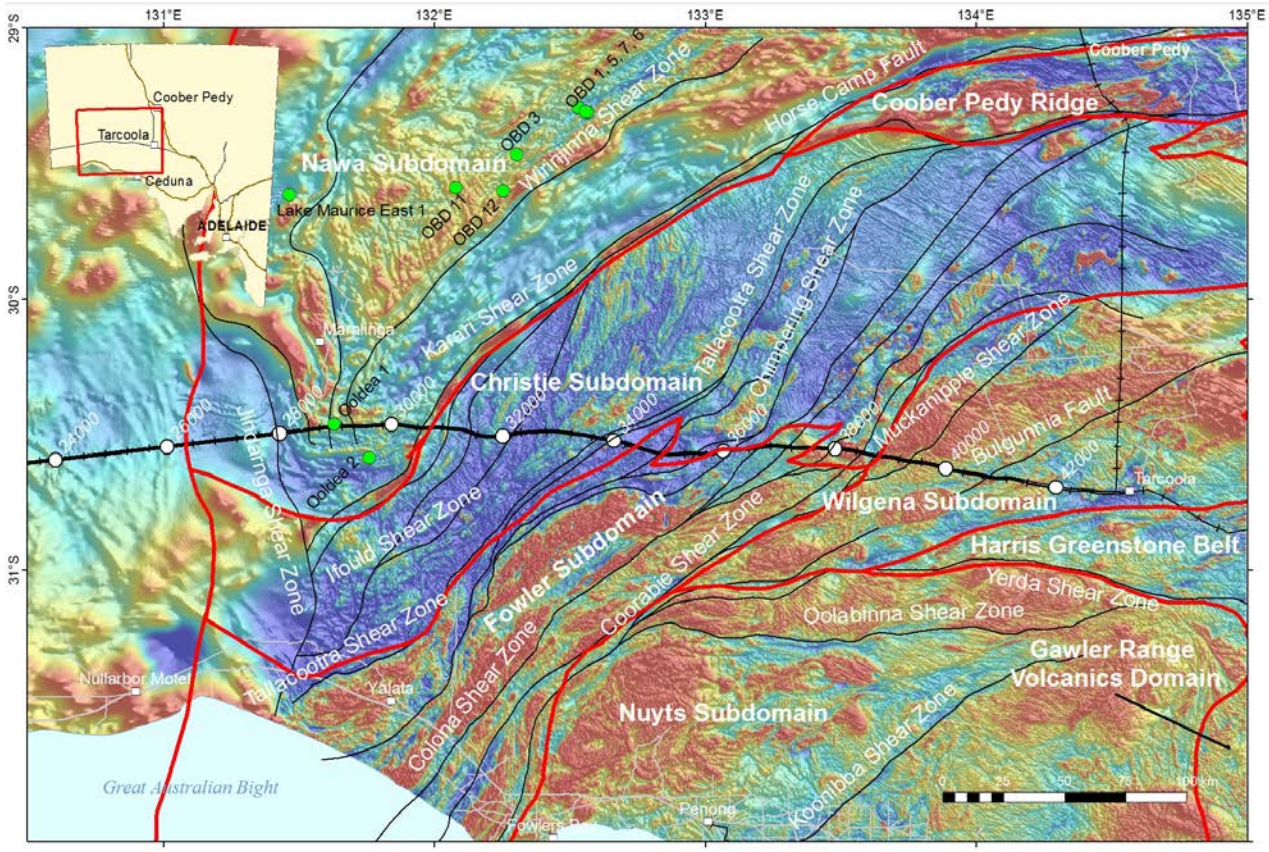

Figure 3 *Plan view of the interpreted major structures in the western Gawler Craton (black lines) on a reduced to pole total magnetic image. Also shown are the interpreted domains of the western Gawler Craton (in red) after Ferris et al. (2002) and the locations of selected drill holes (green circles) discussed in the text. CDP numbers are shown on the seismic line for reference.*

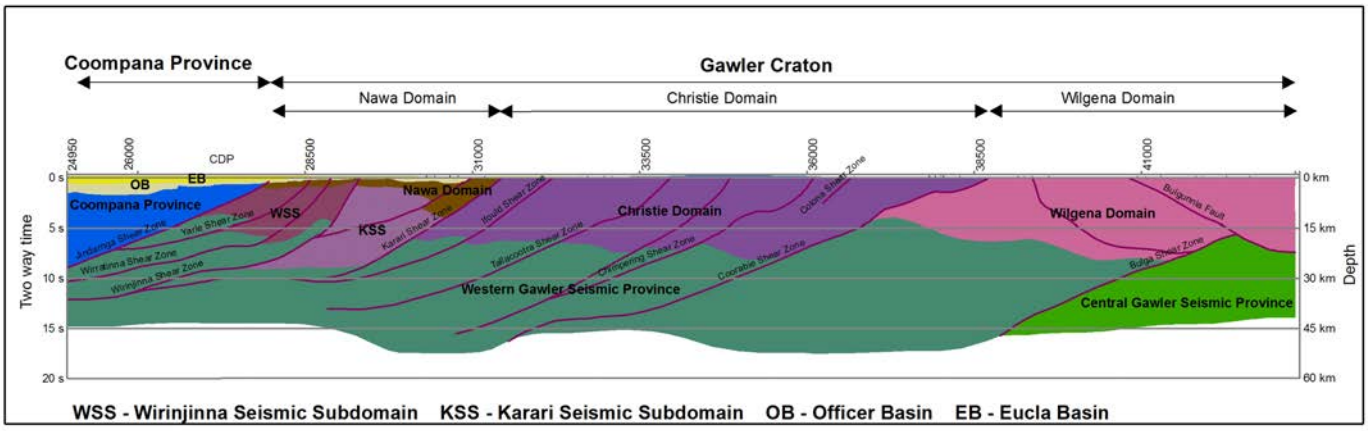

Figure 4 *Schematic map of the interpreted seismic domains of the seismic line 13GA-EG1E including the interpreted major structures.*

between the Tallacootra Shear Zone and the Coorabie Shear Zone and decreases progressively westward towards the Coompana Domain and eastward into the lower amphibolite to greenschist facies of the Wilgena Domain (Fig. 7; Teasdale, 1997; Tomkins and Mavrogenes, 2002; Reid and Dutch, 2015, this volume). The interpreted open folding imaged in the Christie and Wilgena domains likely occurred during this event. The lack of a similar folding event recorded in the middle to lower crust suggests that the upper crust was at least partially decoupled from the middle to lower crust at this time, with the base of the Mulgathing Complex acting as a décollement surface. Metamorphic monazite records a protracted age range from peak metamorphic conditions at *c.* 2450 Ma down to *c.* 2300 Ma, interpreted to represent slow cooling following the Sleafordian Orogeny (McFarlane, 2005). Biotite $^{40}Ar/^{39}Ar$ ages from within the Christie and Wilgena domains suggest

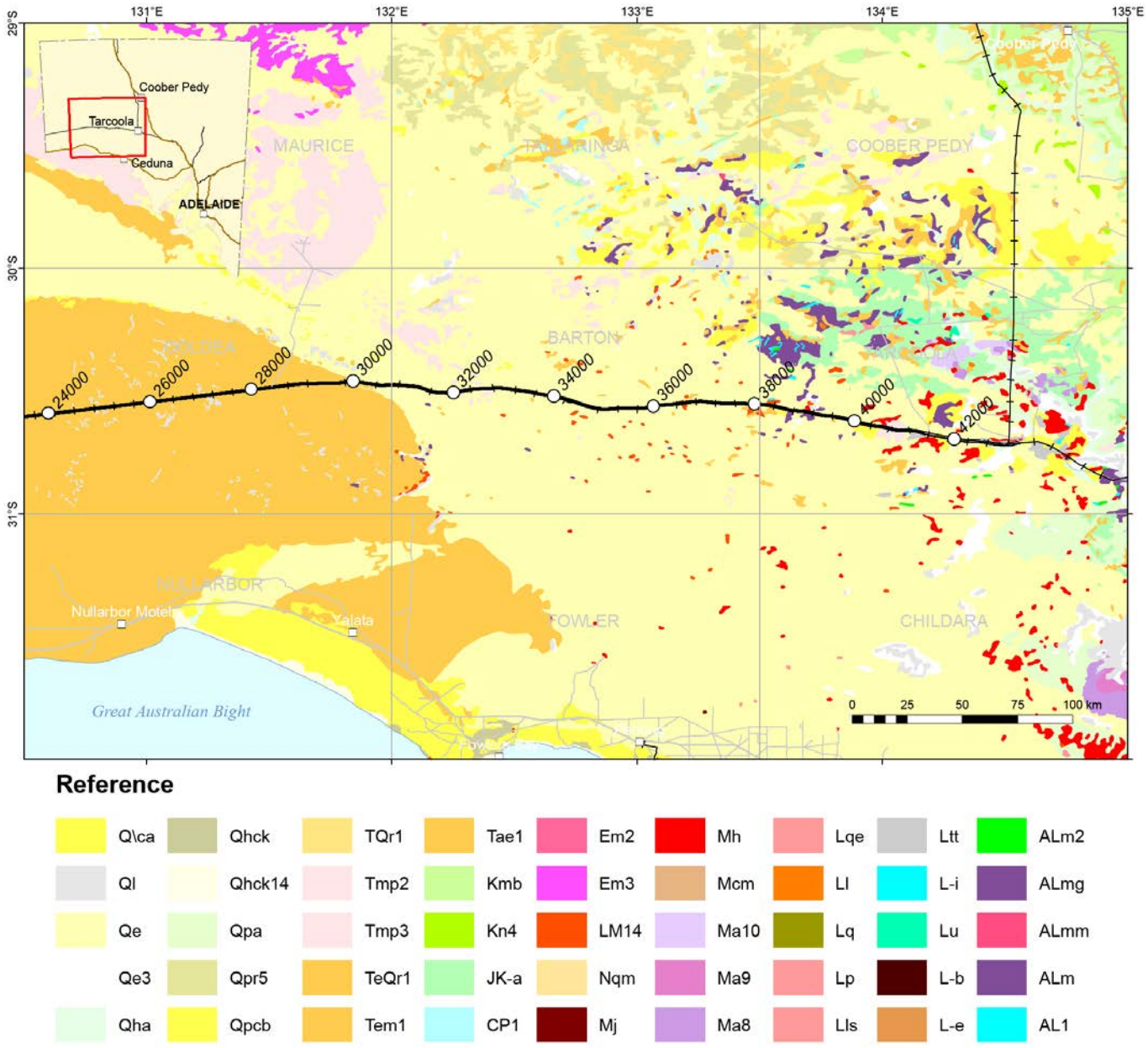

Figure 5 *Regional 1:2,000,000 generalised surface geology map of the western Gawler Craton highlighting the lack of crystalline basement out crop in the region of the seismic line (Crystalline basement map units here begin with the prefix M, L and A). Map after Cowley (2001) with latest updates as at 20/02/2015 (digital Edition) available via SARIG: www.statedevelopment.sa.gov.au/sarig. The reader is referred there for full stratigraphic descriptions.*

a complex, partitioned, exhumation history (Fig. 8; Fraser et al., 2012). Cooling ages >1800 Ma in the blocks west of the Tallacootra Shear Zone and east of the Coorabie Shear Zone are indicative of slow cooling and erosive exhumation after the Sleafordian Orogeny (McFarlane, 2005; Fraser et al., 2012). In contrast, the block between the Tallacootra and Coorabie shear zones, which contains the highest metamorphic grade has a range of $^{40}Ar/^{39}Ar$ ages of between *c.* 2000 – 1670 Ma at the Challenger Gold mine (Tomkins et al., 2004) and more broadly ages of *c.* 1650 – 1600 Ma, suggesting this block has also been exhumed in the early stages of the Kararan Orogeny (Figs 7 and 8; Reid and Dutch, 2015, this volume). Exhumation of this block was likely accommodated along the crustal scale Coorabie Shear Zone and possibly involved thick-skinned deformation including the lower and middle crust (see section 3.2 below).

The second major orogenic event to affect the western Gawler Craton was the *c.* 1730-1690 Ma Kimban Orogeny (Payne et al., 2008; Howard et al., 2011a; Howard et al., 2011b; Reid and Dutch, 2015, this volume). Evidence for deformation and high grade metamorphism during this event is recorded in the adjacent Nawa and Fowler domains (Fig. 7). However, there is little evidence of pervasive deformation or metamorphism of

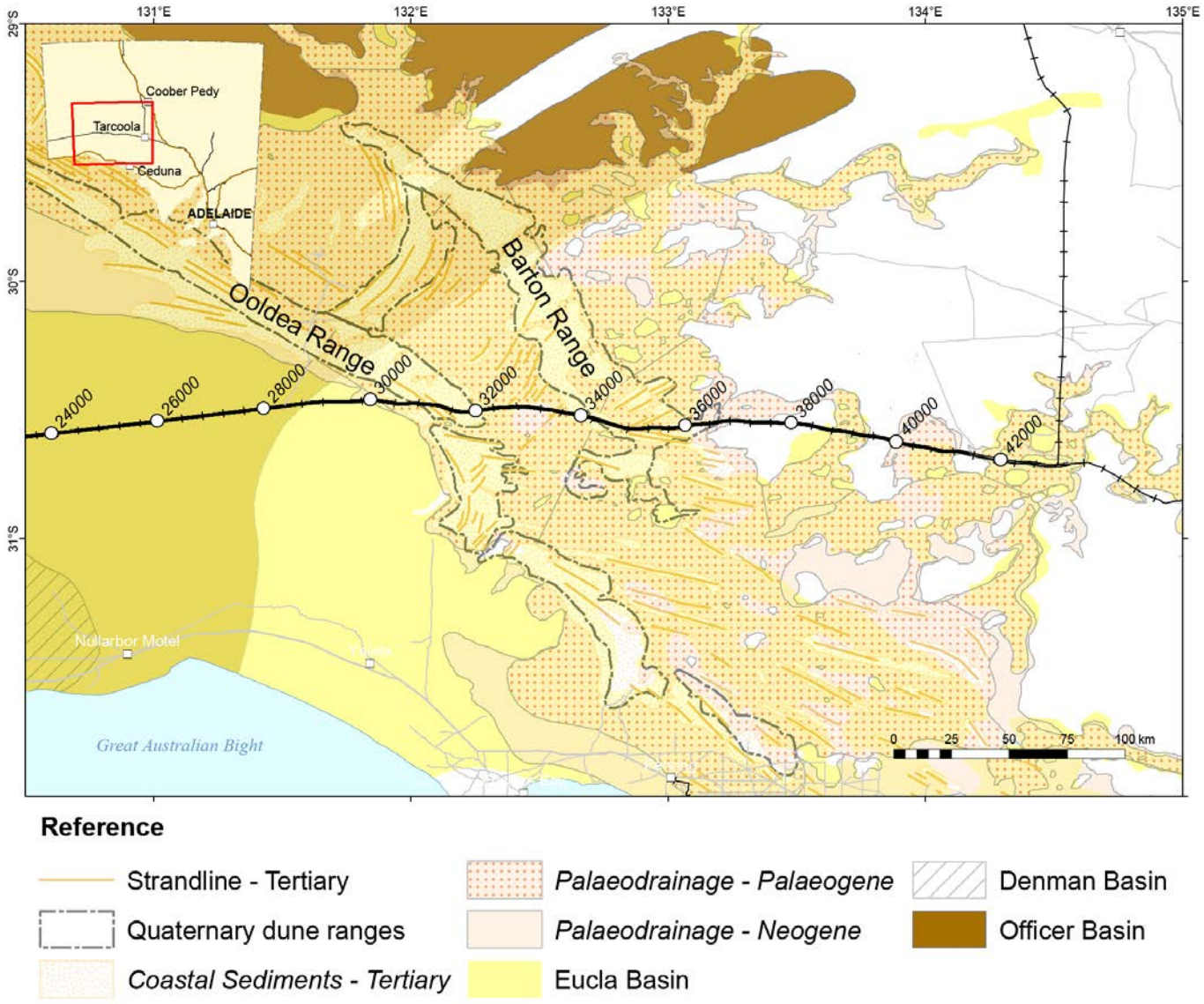

Figure 6 *Region of the 13GA-EG1E seismic line showing the extents of the Officer and Eucla Basins which overlie the western parts of the seismic line. Also shown are the extents of the Ooldea and Barton ranges.*

this age within the Mulgathing Complex. Instead it is likely that this event was strongly partitioned into predominantly strike-slip deformation and reactivation of the major shear zones in the Christie and Wilgena domains.

A number of post-Sleafordian granite suites have been interpreted to intrude into the Mulgathing Complex. In the Christie Domain, both magnetic and non-magnetic granite plutons are imaged in the potential field data between the Tallacootra and Coorabie shear zones (Fig. 3). These are interpreted to be syn- to post-Kimban granitoids and granites of the *c.* 1680 Ma Tunkillia Suite (Fanning et al., 2007). The proximity of these granite intrusions to the major shear zones suggests these structures facilitated magma transfer and emplacement. Potentially the presence of these syn- to post-Kimban-aged intrusives in the same crustal block, and at the same crustal level, as the HT-LP Sleafordian granulites, provides a second indicator that these rocks have been exhumed subsequent to granite emplacement (i.e., after the Sleafordian and Kimban orogenies) and may indicate that this block between the Tallacootra and Coorabie shear zones was exhumed as one (or a number) of 'blocks' during the Kararan-aged exhumation. Furthermore, the depth of granite emplacement may provide a potential measure of the amount of Kararan aged exhumation.

No Hiltaba-aged intrusions are interpreted west of the Coorabie Shear Zone. In contrast, the Wilgena Domain contains numerous intrusions are interpreted from the seismic section down to a depth of ~ 20 km (Fig. 2; Doublier et al., 2015). The available geochronology (Fanning et al., 2007) and cross cutting relationships (i.e., intrusion into the ~1650 Ma Tarcoola

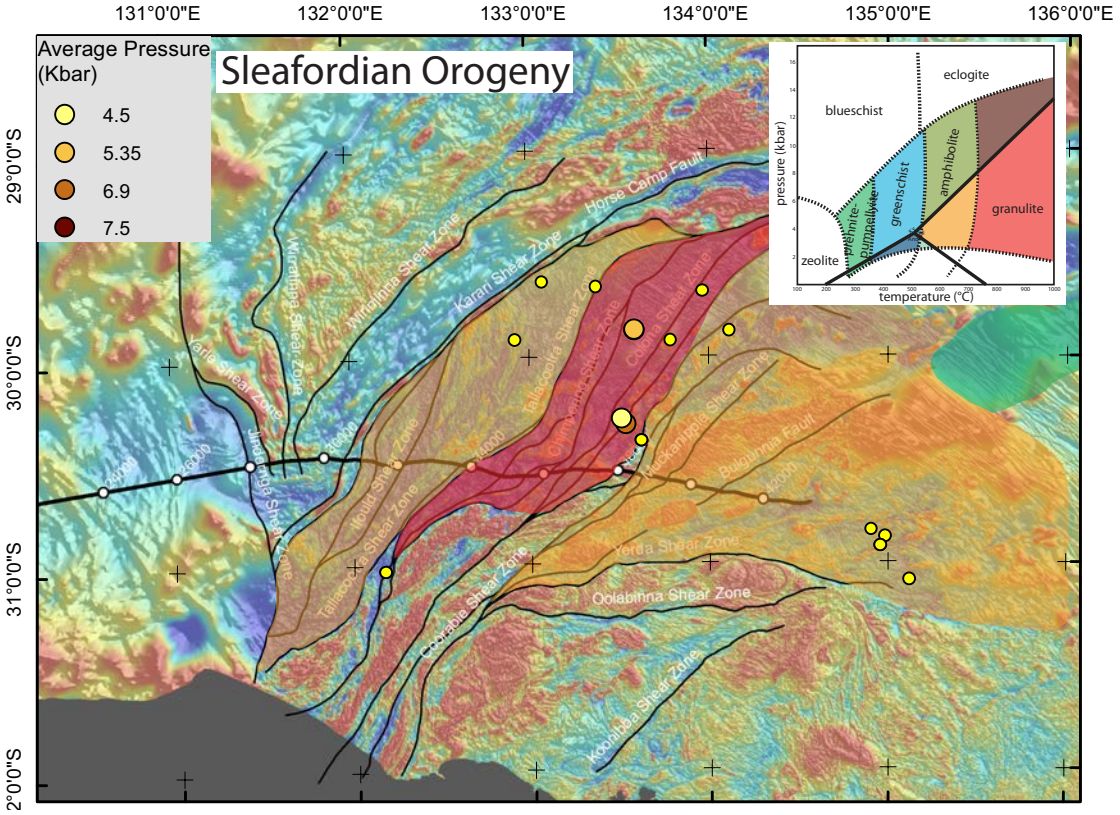

Figure 7 *See next page for caption*

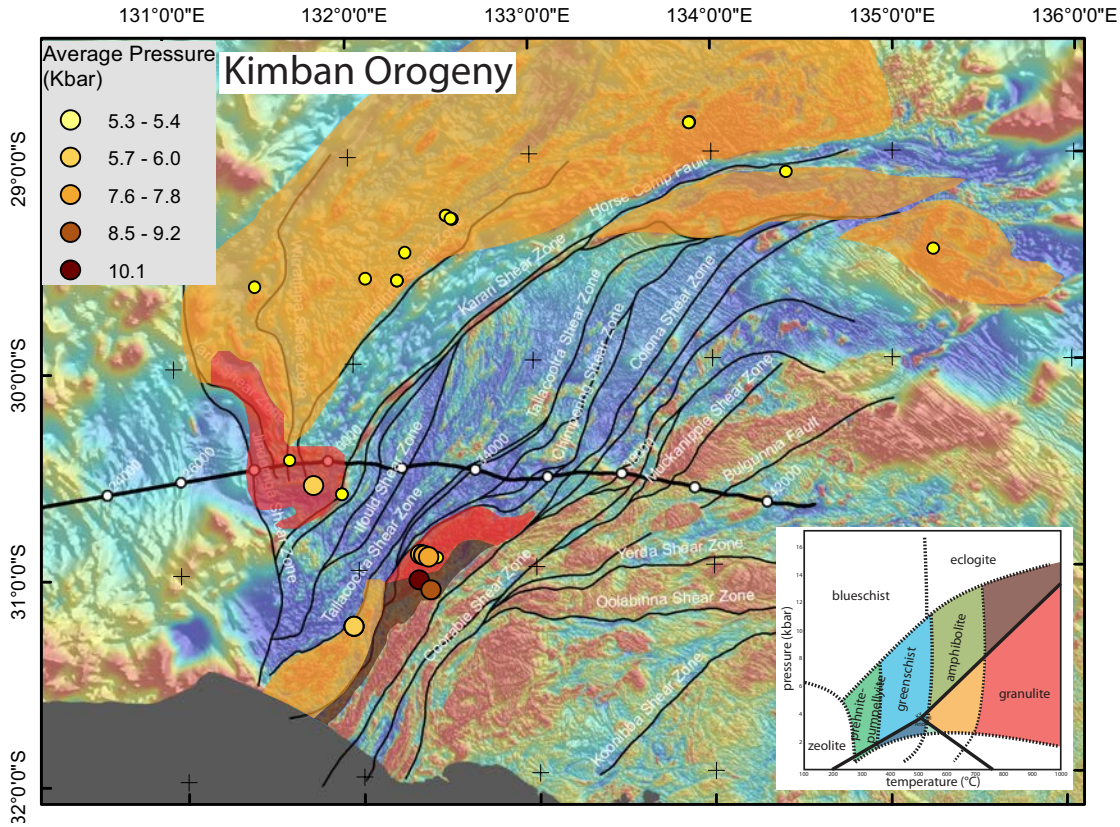

Figure 7 *See next page for caption*

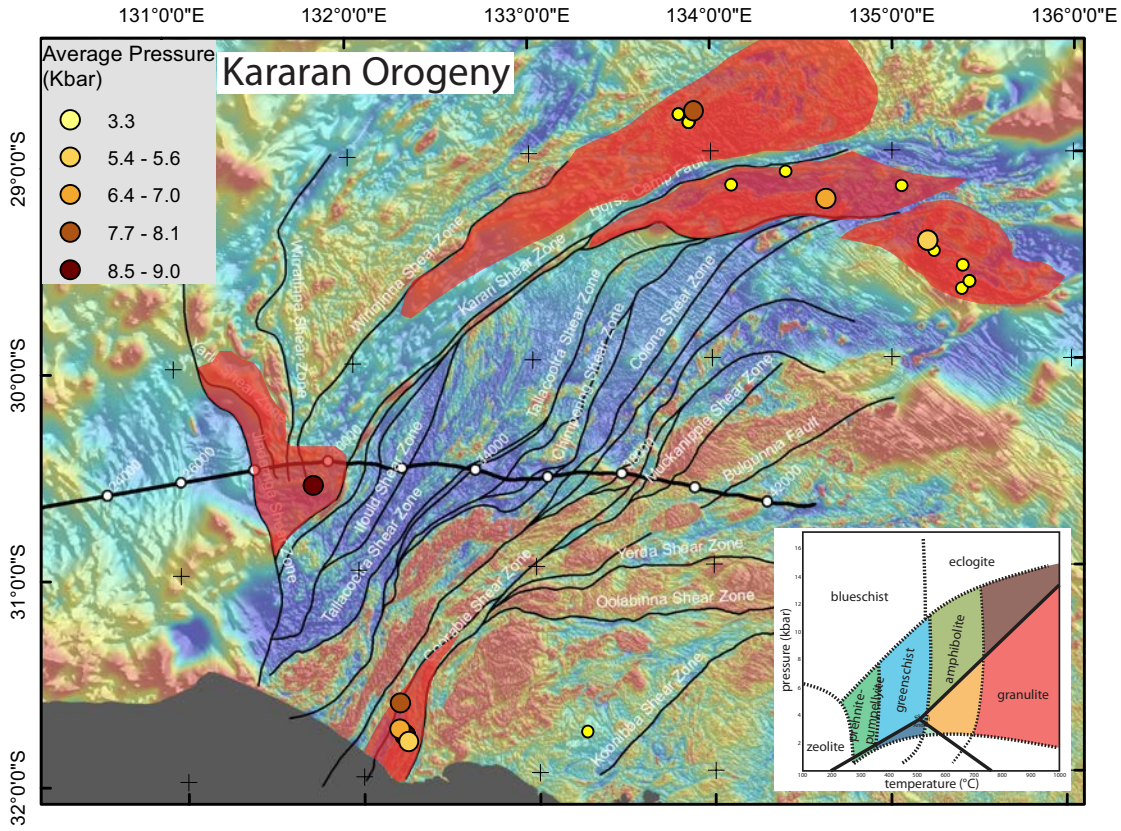

Figure 7 *Schematic metamorphic map of the western Gawler Craton. Maps are divided into Sleafordian, Kimban and Kararan orogenic time slices. Large circles denote locations with quantitative metamorphic P-T constraints, colour coded for average peak pressure. Smaller yellow circles show the locations of metamorphic zircon or monazite age constraints. The regional colour coding correlates with the shaded regions on the inset P-T diagram showing metamorphic facies and the kyanite-sillimanite-andalusite phase transition lines for reference. These diagrams are schematic only, and the locations of the transition between different metamorphic grades are interpreted. Data from Teasdale (1997); Tomkins (2002); Reid et al. (2008); Thomas et al. (2008); Cutts et al. (2011); Forbes et al. (2011); Cutts et al. (2013) and GSSA unpublished data.*

Formation) indicates these are intrusions of the *c.* 1595 – 1575 Ma Hiltaba Suite (Hand et al., 2007). These intrusions are broadly constrained to the hanging wall of the Muckanippie Shear Zone and are underlain by the seismically reflective lower crustal Central Gawler Seismic Province (CGSP; Figs 2 and 4), the significance of which is discussed below in section 3.1. The Bulgunnia Shear Zone, unlike the other major structures which tend to anastomose, appears as a largely straight structure in the potential field data (Fig. 3). It is also stitched by, and deflects around, interpreted Hiltaba-aged plutons. This suggests that the Bulgunnia Shear Zone can be structurally constrained as being active during the Kararan Orogeny, but may still represent the reactivation of an earlier structure.

Following the major reworking associated with the above mentioned orogenic and igneous events, the major structures underwent low temperature reworking, in a predominantly strike-slip regime during the *c.* 1470 – 1450 Ma Coorabie Orogeny (Fraser et al., 2002; Hand et al., 2007; Fraser et al., 2012). The predominantly strike-slip nature of many of the events affecting this region may account for some of the variable apparent offsets interpreted in the seismic section 13GA-EG1E.

2.2 Nawa Domain

The Nawa Domain forms a north-east trending region north of the Karari Shear Zone (Fig. 3). The geology of this region is poorly constrained due to the absence of outcrop, and the limited number of drill holes that penetrate through to crystalline basement. In the seismic section 13GA-EG1E, the Nawa Domain is imaged between the Karari Shear Zone to the east and the Jindarnga Shear Zone to the west (Fig. 2). In the seismic interpretation this domain has been separated into the upper-crustal Paleoproterozoic metasedimentary rocks which are underlain by two different seismic sub-domains which differ with respect to their seismic character (Doublier et al., 2015, this volume).

The Paleoproterozoic metasedimentary rocks have been sampled by a number of drill holes including the Ooldea DDH1, Ooldea DDH2 and Lake Maurice East 1 holes (Fig. 3; Daly et al., 1998; Payne et al., 2008). These holes intersected magnetite-rich metasedimentary rocks of the Moondrah Gneiss, which contain detrital zircon populations that provide a maximum depositional age of between *c.* 1740 – 1720 Ma (Payne et al., 2006). The maximum depositional ages in the Nawa Domain

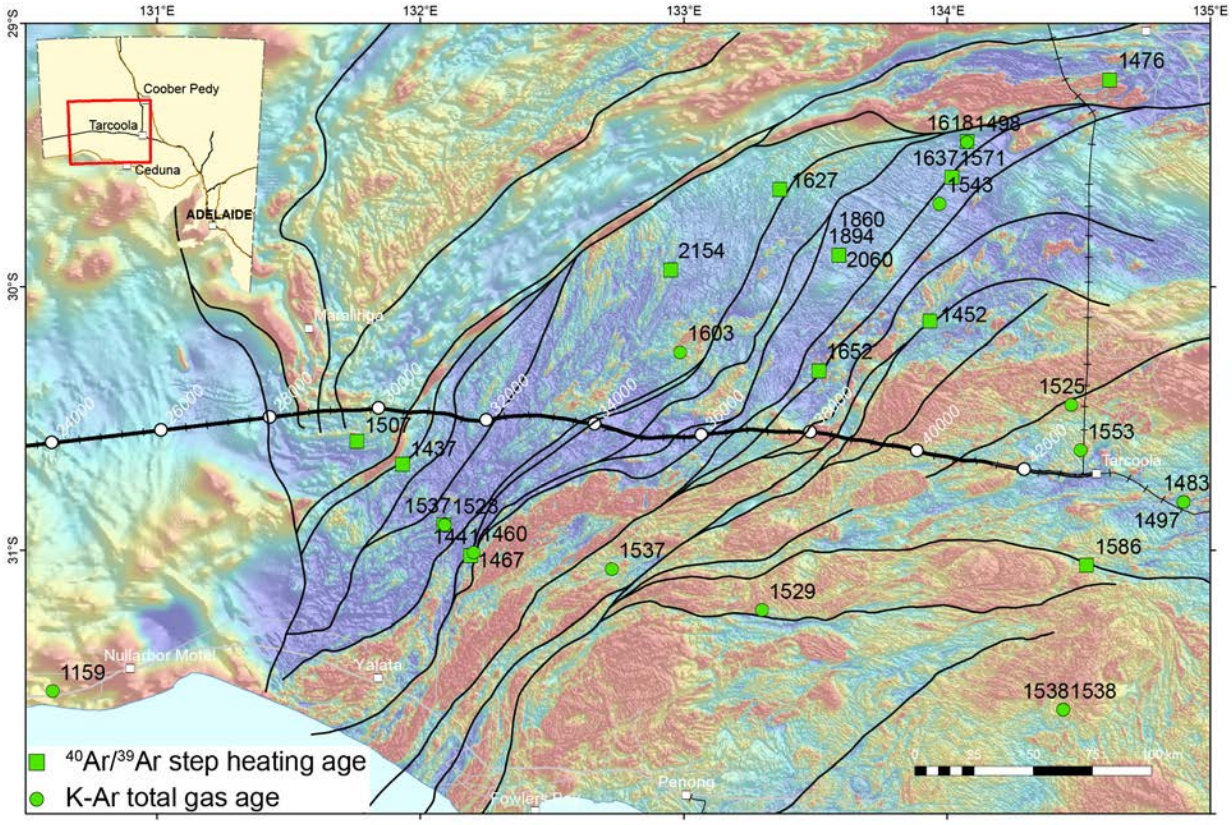

Figure 8 *Regional ^{40}Ar/^{39}Ar and K-Ar data collected on biotite from across the western Gawler Craton. See Figure 3 for shear zone labels. Data from Webb et al. (1982); Fraser et al. (2002); Tomkins et al. (2004); Fraser et al. (2012).*

are similar to those recorded from metasedimentary rocks in the Fowler Domain to the south of 13GA-EG1E (Fig. 3) ranging between 1760 – 1700 Ma (Howard et al., 2011a). In contrast, sedimentary rocks of this age are not widespread throughout the Christie or Wilgena domains. Consequently, it is proposed that deposition of these sediments was predominantly accommodated along the crustal scale structures imaged in the western part of 13GA-EG1E, including the Karari Shear Zone and the Wirinijinna Shear Zone, within an interpreted intra-continental setting (Payne et al., 2006).

The basement to the Moondrah Gneiss (i.e., the Paleoproterozoic metasedimentary rocks) within the Nawa Domain has been separated into two seismic subdomains based on different reflective character (Fig. 4). The Karari Seismic Subdomain to the east contains a reflective upper unit and a weakly reflective lower unit, whereas the Wirinijinna Seismic Subdomain to the west only consists of a weakly reflective unit (Fig. 2). This interpretation is consistent with the interpretation of the Nawa Domain from the GOMA seismic line by Korsch et al. (2010), who also distinguished a number of discrete seismic subdomains in the Nawa Domain, based on varying seismic character, and separated by north-dipping crustal-scale shear zones.

There are a number of possibilities for what these middle-crustal domains might represent, and consequently what the basement to the Moondrah Gneiss may be. Geochronological evidence from drill holes in the Nawa Domain indicate three possible ages for a pre-1750 Ma basement. Reid et al. (2014a) presented two possibilities from the GOMA 4 drill hole located just north of the Mabel Creek Ridge (Fig. 3); a *c.* 2526 Ma Neoarchean basement correlated with the Mulgathing Complex of the Christie Domain, and a previously unrecognised *c.* 1914 Ma age. Howard et al. (2011b) recognised younger ages of *c.* 1775 – 1750 Ma for granitic protoliths from the OBD drill holes located in the central western Nawa Domain (Fig. 3). Despite some uncertainty, based on the available geochronological data and the seismic character, it is proposed that the upper reflective package in the Karari Seismic Subdomain may be a correlative of the Mulgathing Complex, which is overlying weakly reflective middle crust of the Western Gawler Seismic Province (WGSP) similar to the configuration beneath the Christie and Wilgena domains. This reflective upper crust is missing from the Wirinijinna Seismic Subdomain, suggesting that the Wirinijinna Shear Zone marks the western extent of the Mulgathing Complex units and here the Moondrah Gneiss (or equivalents) were deposited directly on an older, weakly reflective basement that may correlate with the unreflective middle crust beneath

the Christie and Wilgena domains (i.e., the WGSP). Alternatively, the Wirinijinna Seismic Subdomain has experienced exhumation and erosion of the Mulgathing Complex prior to the deposition of the Moondrah Gneiss, and the Mulgathing Complex and equivalent units are no longer preserved.

The metamorphic evolution recorded in the aluminous sediments of the Moondrah Gneiss provides some constraints on the tectonic and exhumation history of the Nawa Domain in this area. The Moondrah Gneiss records an early HT-LP granulite facies event overprinted by a HT-MP granulite facies mylonitic fabric (Teasdale, 1997; Fraser et al., 2012; Cutts et al., 2013). Geochronological constraints suggest that these granulite facies metamorphic events occurred during the latter stages of the Kimban Orogeny at *c.* 1690 Ma with early, thinned, hot crust that was subsequently thickened (Cutts et al., 2013). We suggest that the Kimban Orogeny initiated during the late stages of Paleoproterozoic rifting and deposition, followed by minor basin inversion and thickening, probably in a transpressional setting (Vassallo and Wilson, 2002; Payne et al., 2008; Dutch et al., 2010; Cutts et al., 2013).

The gross architecture of the Nawa Domain imaged in 13GA-EG1E, including the apparent reverse offset interpreted on the shear zones (including the Yarle, Wirratinna, Wirinijinna and Karari shear zones; Fig. 2), and a significant increase in the depth of the Moho, suggests significant tectonic thickening in this area. While the metamorphic evidence above suggests that some thickening occurred during the latter stages of the Kimban Orogeny, there is little evidence from elsewhere across the Gawler Craton for significant thickening at this time. Farther north-east along the Karari Shear Zone, seismic imaging from the GOMA line suggests apparent south-directed thrust stacking, placing the Mabel Creek and Nawa domains over the Christie Domain (Korsch and Kositcin, 2010). Geochronological and metamorphic evidence from the Mabel Creek, Coober Pedy and Mt Woods domains indicate high grade metamorphism, exhumation and juxtaposition of lower crustal rocks over hot, upper crustal rocks during the Kararan Orogeny between *c.* 1620 – 1590 Ma (Cutts et al., 2011; Forbes et al., 2011; Fraser et al., 2012). We therefore suggest that the bulk of the exhumation of the granulite facies Moondrah Gneiss and thickening of the crust in the western Nawa Domain also occurred during the Kararan Orogeny at *c.* 1600 Ma. This assertion is supported by metamorphic rims on monazite from the Moondrah Gneiss with a *c.* 1600 Ma age (Cutts et al., 2013). $^{40}Ar/^{39}Ar$ ages from micas within the shear-fabric of the Karari Shear Zone yielded ages of *c.* 1450 Ma(Fraser et al., 2002; Fraser et al., 2012). This suggests that the Karari Shear Zone was also reactivated at *c.* 1450 Ma during the strike-slip dominated Coorabie Orogeny.

2.3 Coompana Domain

Very little is known about the lithostratigraphy or tectonic history of the Coompana Domain. In South Australia, the Mallabie 1 drill hole intersected a *c.* 1500 Ma isotopically juvenile granitic gneiss (Wade et al., 2007). Recent drilling and geochronology by the Geological Survey of Western Australia has recognised up to three tectono-magmatic events within the Forrest Zone in the western part of the Coompana Province; the *c.* 1610 Ma Toolgana Supersuite, the 1500 – 1490 Ma Undawidgi Supersuite and the 1192 – 1140 Ma Moodini Supersuite (Wingate et al., 2015), which affected a juvenile basement interpreted to have formed around 1950 Ma (Kirkland et al., 2013; Smithies et al., 2015). Based on age, geochemistry and isotopic constraints the *c.* 1610 Ma Toolgana Supersuite may be a correlative of the juvenile, arc-related St Peter Suite in the south-western Gawler Craton (Swain et al., 2008; Smithies et al., 2015). While only a small portion of the Coompana Province is imaged in 13GA-EG1E (Figs 2 and 4), the structural relationships suggest that this crust overlies or is tectonically overthrust (along the Jindarnga Shear Zone) onto the middle to lower-crustal WGSP. While it is possible that the WGSP basement extends westward beneath the Coompana Province, and that this contact represents an unconformity rather than a structural contact, the isotopic composition of the *c.* 1610 Ma and *c.* 1500 Ma supersuites indicate that this is unlikely as there is a distinct change in Nd model age between the western Gawler Craton (generally >2500 Ma; Swain et al., 2005; Reid et al., 2014b) and the Coompana Province (generally between 2000 – 1900 Ma; Wade et al., 2007; Smithies et al., 2015) suggesting the Gawler Craton must pinch out to the west. We suggest that this boundary is a structural contact, and the juvenile basement rocks of the Coompana Province have been thrust onto the Gawler Craton. The timing of this is unconstrained, but given the lack of evidence for *c.* 1500 Ma and 1200 – 1100 Ma deformation and metamorphism in the Gawler Craton, we suggest the thrusting occurred synchronous with the thrusting and exhumation recorded in the adjacent Nawa Domain during the Kararan Orogeny at *c.* 1600 Ma.

3 Middle to Lower Crust

The middle to lower crust in section 13GA-EG1E has been subdivided into two seismic provinces based on seismic character (Fig. 4; see Doublier et al., 2015, this volume). The main difference between the Central Gawler Seismic Province (CGSP) and the WGSP is that the former is seismically more reflective.

3.1 Central Gawler Seismic Province

The CGSP is a domain of reflective middle to lower-crust located at the eastern end of the line beneath the Wilgena Domain (Fig. 4). This region contains a number of west dipping anastomosing and sigmoidal shear zones that roughly parallel the Bulga Shear Zone, which represents the boundary between the CGSP and the WGSP.

There are a number of alternative hypotheses for the nature of the CGSP. One possibility is that this province represents the continuation of the reflective lower-crust in the WGSP, and

that the comparatively higher seismic reflectivity is caused by a different fabric inventory or fabric orientations related to structural thickening. The apparent extensional drag seen along the Bulga Shear Zone and the truncation of the shear zones within the CGSP by the Bulgunnia Shear Zone may indicate that this phase of structural thickening occurred prior to the deposition of the overlying Mulgathing Complex, although it is also likely that the truncations caused by the Bulgunnia Shear Zone occurred during later events.

A second, alternative explanation is that the different seismic character of the CGSP compared to the WGSP may indicate that the seismic provinces are indeed two different geological entities, with an entirely different composition, a different geological history, and potentially a different age. In this scenario, the Bulga SZ would represent a boundary between two Neoarchean (or older) crustal blocks: effectively an Archaean suture.

A third alternative is to suggest that the different seismic character of the CGSP is a result of younger tectonic processes that have modified the seismic character of the lower crust of the CGSP to make it distinct from the character of the WGSP. A prime candidate for a major intra-crustal process that could have resulted in wholesale modification of the entire middle to lower-crust is extensive crustal melting associated with the *c.* 1595 – 1575 Ma Gawler Range Volcanics and associated Hiltaba Suite intrusions. As discussed in section 2.1 above, Hiltaba Suite intrusions appear to be confined to the region above the CGSP and therefore, it is possible that the highly reflective nature of the CGSP is due to it being of a more residual composition caused by the extraction of large amounts of silicic melt during formation of the Gawler Range Volcanics and Hiltaba Suite (e.g. Daly et al., 1998; Pankhurst et al., 2011).

The MT data are consistent with the CGSP being a region of highly electrically resistive crust, which is typical of dry, residual Archaean crust (Thiel et al., 2015, this volume). For this type of crust we might expect a related gravity high in the potential field data. However, this is not the case, as this region displays a gravity low east of the Bulgunnia Shear Zone (Van der Wielen et al., 2015, this volume). This apparent contradiction is presumably related to the processing of the gravity data, more exactly the loss of the long wavelength data due to processing methodologies (see Van der Wielen et al., 2015 for a description). For that reason, the forward models presented by Van der Wielen et al. (2015, this volume) only effectively modelled the middle to upper crust. In this region the upper crust is dominated by lower density intrusions of the Hiltaba Suite and sedimentary rocks of the Tarcoola Formation, which likely resulted in the observed (apparent) gravity low. Consequently it is possible that the CGSP still represents relatively dense, refractive lower crust.

The interpreted refractory and seismically reflective nature of the CGSP crust, and the overall crustal architecture at the eastern end of the line is potentially consistent with some models for the formation of the magmatic event that produced the Gawler Range Volcanics and Hiltaba Suite. Most models for the formation of this predominantly felsic large igneous province invoke a mantle plume (Flint et al., 1993; Daly et al., 1998; Betts et al., 2007; Betts et al., 2009). These models propose that the large volume of A-type magmatism was the result of plume-derived mafic magmas ponding and fractionating in lower crustal magma chambers, where they also assimilated large amounts of crustal melt generated by the introduction of mantle heat. Such a process could account for the high seismic reflectivity. A consistent feature of both the GOMA and the present 13GA-EG1E seismic sections is the apparent thinning of the crust beneath the CGSP compared to the apparent Moho depths further to the north and west of this province. Conceivably, this thinning could have resulted from another major tectonic process: lithospheric delamination. Skirrow (2010) proposed that catastrophic lithospheric delamination from beneath the central Gawler Craton at *c.* 1590 Ma may have caused the A-type magmatism. Removal of a portion of the lower crust via delamination can also account for the high temperatures required to melt an already refractory Archaean lower crust, with the easterly shallowing level of the Moho in the CGSP potentially a signature of such an event.

3.2 Western Gawler Seismic Province

The Western Gawler Seismic Province is interpreted to occur beneath the western Wilgena, Christie, Nawa and Coompana domains, from the Bulga Shear Zone to the western extent of 13GA-EG1E (Doublier et al., 2015, this volume). Like the CGSP this seismic province is dominated by listric, west dipping structures, many of which continue through the upper-crustal Mulgathing Complex to the surface. As discussed above, the WGSP forms a Neoarchean or older basement to the Neoarchean and younger units of the upper-crustal domains. Unlike the CGSP however, this province contains two layers of different seismic character; a strongly reflective lower-crust, and domains of relatively unreflective middle-crust. The thickness of the seismic province varies along the line, including two 'bulges' of thickened crust beneath the eastern Christie Domain, and the Nawa Domain (Fig. 2). In at least two locations beneath the Christie and Wilgena domains, the reflective lower crust apparently migrates up into the middle-crust defining ramp- or duplex-like structures, one in the hanging wall of the Coorabie Shear Zone that terminates directly beneath the Chimpering Shear Zone, and an eastern one beneath the Muckanippie Shear Zone of the Wilgena Domain (Fig. 2). A number of alternative scenarios can be proposed to account for the timing and nature of these apparent structures.

One scenario is that these ramp-like geometries result from an early shortening event that pre-dates deposition of the Mulgathing Complex protoliths. This is supported by the

apparent truncation of these structures at the base of the Mulgathing Complex. This hypothesis would require these apparent reverse offsets to have been preserved, despite significant lithospheric extension during the deposition of the Mulgathing Complex, which is interpreted to have occurred in a back-arc or arc-rift setting (Swain et al., 2005; Reid et al., 2014b).

A second option is that these reflective zones represent unmodified lower-crust and the non-reflective zones between them are in fact an alteration or overprint which has destroyed the reflectivity in these regions. This hypothesis would suggest that the pre-modified WGSP looked much like the CGSP. In this scenario, the unreflective zones may represent melt-rich or metasomatised crust that has lost any fabric, or become homogeneous enough to provide no internal velocity contrast. However, these regions do not correlate well with modelled electrical conductors based on the MT data (Thiel et al., 2015, this volume), as may be expected if they did in fact represent 'alteration' or magma-rich zones.

A third scenario is that these apparent ramp structures resulted from lower- to mid-crustal thick-skinned shortening associated with the Kararan Orogeny. In the west, apparent thrust stacking in the upper-crustal Coompana and Nawa domains has been interpreted to coincide with the Kararan Orogeny (see section 2.2 above). The western-most Moho 'bulge' and coincident lower-crustal thickening is consistent with shortening and loading during this event. Within the Christie Domain, the evidence for significant Kararan deformation is less clear. However, as discussed in section 2.1, some of the exhumation of Sleafordian-aged granulites and the unroofing of late-Kimban and Tunkillia Suite intrusions likely occurred during the Kararan Orogeny. The majority of this movement was probably accommodated along the Coorabie Shear Zone, which is a crustal scale structure in the footwall of the western 'ramp' structure (Fig. 2). The apparent conflicting cross-cutting relationships at the base of the Mulgathing Complex may be accounted for if the upper-crust and lower-crustal blocks between the Chimpering and Coorabie shear zones were coupled and strain has become progressively localised into the Coorabie Shear Zone. East vergent exhumation of this block between the Tallacootra and Coorabie shear zones, together with the 'out of plane loading' due to shortening of the Fowler Domain (which is not crossed by the seismic line but intersects with the Christie Domain between the Tallacootra and Coorabie shear zones; Fig. 3) can account for the observed crustal thickening beneath the eastern Christie Domain. The eastern 'ramp' structure may terminate at the base of the Mulgathing Complex beneath the Wilgena Domain, or alternatively may form an apparent duplex truncated against the Bulga Shear Zone (the two interpretations are shown on Fig. 2; also see figure 9 in Doublier et al., 2015, this volume) . It may be that the predominantly east dipping structural orientation in the Wilgena Domain prevented this 'ramp' from propagating through to the surface, and instead the base of the Mulgathing Complex has acted as a décollement surface and shortening has been accommodated by middle to lower-crustal lateral flow (e.g., Chardon et al., 2009; Chardon et al., 2011). In this scenario the description of these structures as 'ramps' and 'duplexes' may be misleading. At these crustal levels, and the inferred high geothermal gradients during the orogenic events (Teasdale, 1997; Tomkins, 2002; Thomas et al., 2008; Cutts et al., 2011; Forbes et al., 2011; Cutts et al., 2013), the middle to lower-crust is likely to have undergone significant orogen parallel horizontal and lateral flow, limiting the ability for wholesale tectonic stacking in the middle and lower-crust (e.g., Chardon et al., 2009 and references therein).

In any discussion of the crustal architecture of the middle to lower crust it must also be remembered that the current crustal architecture cannot be attributed to a single event or scenario, but rather is a composite. For example, it is quite possible that an early, pre-Mulgathing Complex architecture is overprinted and reactivated during both extension related to the Mulgathing Complex deposition, and renewed shortening during the multiple orogenic events that have affected these seismic provinces. The composite character of the architecture, as well as significant out-of-plane movement due to the orientation of the seismic section with respect to the structures (Fig. 3) and the interpreted transpressional nature of the orogenic events (Reid and Dutch, 2015, this volume), accounts for some of the apparent contradicting and/or inconsistent offsets along some of the fault structures.

4 Economic implications

Major crustal boundaries and crustal-scale structures can act as conduits for the passage of magma and associated fluids from the deep crust or mantle into the upper crust (e.g., Begg et al., 2009). Fluid pathways are also very pronounced at edges of cratonic blocks, which are sites of major discontinuity within the lithosphere. The deep seismic reflection section 13GA-EG1E provides evidence for a number of major crustal discontinuities and structures, with several of these structures, including the Tallacootra, Karari and Coorabie shear zones, also being imaged in the MT data. These shear zones, and their overlying hanging walls are therefore suggested to be sites of increased mineral potential, as lower crustal or mantle-derived fluids or magmas may have transported metals such as Au, Ni, Cu, PGE and potentially other base metals during their ascent. The presence of sulphide-bearing mafic rocks within the western Gawler Craton and Fowler Domain attest that such processes have indeed occurred (Daly and Martin, 1989; Morris et al., 1994; Daly et al., 1998).

The Mulgathing Complex contains mafic rocks with Ni-Cu sulphides, albeit to date no economically significant accumulations of sulphides have been found (Daly and Martin, 1989; Reid and Daly, 2009). The Archaean lithosphere from which those sulphide-bearing mafic rocks were generated was itself subject to a number of cycles of re-melting as a

result of the complex tectonics of the western Gawler Craton. For example, re-melting is interpreted to have occurred (i) during initial rifting associated with deposition of the volcano-sedimentary sequences of the Nawa and Fowler domains, (ii) during the Kimban Orogeny and, (iii) in some regions again during the Kararan Orogeny and associated Hiltaba Suite-Gawler Range Volcanics magmatic event. Since the Mulgathing Complex has both sulphide-bearing mafic rocks and a known gold endowment, the re-melting and reworking of such a crust during Paleoproterozoic tectonic events may have facilitated the concentration of these elements of economic interest into Paleoproterozoic magmas and their associated fluids.

The recognition of significant volumes of Hiltaba-aged magmatism in the eastern Wilgena Domain confirms this region as highly prospective for potential IOCG, or Au only type mineralisation (Skirrow et al., 2002; Drown, 2003; Ferris and Schwarz, 2003; Budd and Fraser, 2004; Budd and Skirrow, 2007; Fraser et al., 2007; Skirrow et al., 2007). This region already contains a number of gold prospects (see Reid and Dutch, 2015, this volume) and the recognition of middle-crustal scale east dipping shear zones, which acted as conduits for Hiltaba-aged magmatism, further enhances the potential for lode-gold mineralisation. The proximity of the low-metamorphic grade Tarcoola Formation to these structures and associated Hiltaba Suite intrusions has potential for skarn related mineralisation.

An important factor to consider in evaluating the mineral potential of the region is the regional metamorphic grade, and how it developed through time (Reid and Fabris, 2015). Although the majority of the region preserves at least amphibolite facies metamorphic mineral assemblages, wide areas, such as parts of the Mulgathing Complex, have been in the upper crust since the Paleoproterozoic, and hence are prospective for mineral deposits forming at this crustal level. Where magmas of suitable chemistry have been emplaced into the Mulgathing Complex, there exists the potential that magmatically-derived hydrothermal fluids could have resulted in mineralisation, such as intrusion-related gold systems, with those systems being preserved in the current upper crust.

The mineral potential of the Nawa Domain is more difficult to assess due to the limited available drill hole intersections. The similarity in the provenance and interpreted tectonic setting of the sequences in the Nawa and Fowler domains during their deposition suggests we can potentially infer the presence of mafic and ultramafic intrusions in the Nawa Domain as found in the Fowler Domain (Constable et al., 2005), and this raises the possibility of Ni-Cu-PGE prospectivity. Additionally, the abundance of fold structures, shear zones and other structural culminations within the Nawa Domain that are evident within the seismic section should provide encouragement that, mineralised fluids would have found a suitable pathway architecture, and may have been channeled into zones of low pressure such as regional antiformal structures and/or releasing bends. The presence of highly electrically conductive regions within the Nawa Domain evident in MT data may also indicate that regional-scale fluid flow has occurred.

Mineral exploration targeting in the Nawa Domain, which is mostly buried, will require close attention to the interpretation of potential field data, combined with extracting as much information as possible from any available drill cores from the region. Ideally, future drilling for regional stratigraphic purposes and associated geochemical characterisation would provide a framework for exploration discovery in this part of South Australia.

The Neoproterozoic and younger units imaged in the central and western part of 13GA-EG1E are also prospective. Within the Officer Basin, mafic volcanics and salt horizons are present and provide prospectivity for Zambian-style copper mineralisation (e.g., Hitzman et al., 2005; Selley et al., 2005). The seismic line has imaged Officer Basin structures as well as reactivated basement structures that propagate through the overlying basins, which may have focused mineralising fluids.

5 Summary

A number of potential scenarios have been presented above that may be able to explain the interpreted features of the 13GA-EG1E seismic line. Below is a summary of the preferred interpretation for the geological evolution of this region. In the following discussion we use the notation 'E' to designate the different 'events' that may have affected the region.

(E1) The earliest potential structural and tectonic events recorded in 13GA-EG1E is a pre-Mulgathing shortening event, reflected in (i) a possible 'suture' at the Bulga Shear Zone between the Neoarchean or older middle- to lower-crustal seismic provinces, the CGSP and WGSP; and (ii) an early shortening event within the WGSP producing the apparent lower crustal ramp structures. The timing of this event, and even its existence, is speculative.

(E2) The oldest event that can be confidently recognised is extension associated with the deposition of the Mulgathing Complex protoliths. Extension was accommodated along a series of east and west dipping crustal scale faults and shear zones that penetrate through the WGSP and likely represent reactivation of earlier structures in this Neoarchean or older basement.

(E3) Mafic and felsic magmatism in the Mulgathing 'rift basin' was accompanied by HT-LP high geothermal gradient metamorphism during the *c.* 2465 – 2410 Ma Sleafordian Orogeny. This apparently long lived, hot metamorphic event was likely associated with ongoing extension punctuated by compressive deformation producing large wavelength regional

folding within the upper-crust. The upper crust was largely decoupled from a hot and highly ductile middle to lower-crust represented by the CGSP and WGSP, which potentially responded by lateral flow to these punctuated shortening events. This event was followed by slow cooling and slow exhumation.

(E4) Extension along the margins of the proto-Gawler Craton (Mulgathing Complex) led to the deposition of the Paleoproterozoic metasediments of the Nawa and Fowler domains between *c.* 1750 and 1720 Ma.

(E5) Sedimentary deposition in the Nawa and Fowler domains was terminated by deformation associated with the craton-wide 1730 – 1690 Ma Kimban Orogeny. In the Nawa Domain, early HT-LP granulite facies metamorphism was followed by an increase in pressure to produce an apparent anti-clockwise P-T path. The onset of Kimban-aged metamorphism during deposition of the Nawa Domain sediments and the interpreted metamorphic P-T path suggests that, in the northern and western Gawler Craton at least, orogenesis occurred in a predominantly extensional setting, followed by compression in a probable transpressional setting with minimal exhumation. In the Christie Domain, there is no evidence of pervasive Kimban metamorphism, and deformation is constrained to reactivation along major structures. In the Wilgena Domain the effects were even less pronounced, with ongoing sedimentation occurring within the Wilgena Domain and along the current eastern margin of the Gawler Craton. Significant syn- to post Kimban Orogeny magmatism is also recognized from across the province. In 13GA-EG1E this is recorded in the eastern Christie Domain by magnetic and non-magnetic intrusions of the syn- to post-Kimban granitoids and Tunkillia Suite.

(E6) Between *c.* 1640 – 1607 Ma significant calc-alkaline magmatism occurred in the south western Gawler Craton (St Peter Suite) and within the Coompana Province (Toolgana Supersuite). The Tarcoola Formation was deposited into localised basins within the Wilgena Domain between *c.* 1650 – 1600 Ma.

(E7) Between *c.* 1600 – 1580 Ma the western Gawler Craton underwent a major phase of deformation (Kararan Orogeny) and significant magmatism associated with the Gawler Range Volcanics and Hiltaba Suite granites. At this time apparently east-vergent thick-skinned thrusting led to the juxtaposition of the Coompana Domain on top of the western Nawa Domain at the western edge of 13GA-EG1E. Tectonic stacking produced a significantly thickened crust beneath the Nawa Domain and exhumed the HT-MP Kimban-aged granulites of the Moondrah Gneiss. Reactivation of major west-dipping structures in the Christie Domain led to crustal thickening and further exhumation of Sleafordian-aged granulites in the eastern Christie Domain. Significant Hiltaba-aged magmatism is confined to the eastern part of the Wilgena Domain overlying the CGSP. The apparent easterly rise of the Moho and highly reflective character of the CGSP may be a result of a mantle plume or lithospheric delamination generating the significant felsic crustal melts that produced the Hiltaba Suite and Gawler Range Volcanics. The youngest feature clearly observed on the seismic line is the reactivation of the Bulgunnia Shear Zone, which offsets Hiltaba-aged plutons and cross-cuts the earlier developed shear zones in the CGSP, and may have occurred during E7 and/or E8.

(E8) At *c.* 1450 Ma, the major structures in the western Gawler Craton underwent low-temperature reactivation during the Coorabie Orogeny, in a predominantly strike-slip regime.

(E9) Renewed extension during the Neoproterozoic to Cambrian associated with the development of the Centralian Superbasin and the Adelaide Geosyncline reactivated existing basement structures in the Nawa and Coompana domains to accommodate the deposition of sediments of the Officer Basin.

(E10) Regional down warping and marine transgression during the Cenozoic led to the deposition of the sediments of the Eucla Basin and the paleostrandlines of the Ooldea and Barton ranges.

Acknowledgements

Tristan Kemp and the Geoscience Australia Seismic and MT Acquisition and Processing group are thanked for all aspects of managing the acquisition of this data set. Catherine Spaggiari, Ian Tyler and the Geological Survey of Western Australia are thanked for their collaborative spirit and welcome input into the process of interpreting such a dataset. AuScope are acknowledged for their additional funding that got the 13GA-EG1 line all the way to Tarcoola. Jessica Bonsell (ERD), Rachel Froud and Zoe French (RI) are thanked for figure compilation and publishing. Wolfgang Preiss and Wayne Cowley (GSSA) are thanked for constructive reviews of this abstract.

References

Begg, G., Griffin, W., Natapov, L., O'Reilly, S. Y., Grand, S., O'Neill, C., Hronsky, J., Djomani, Y. P., Swain, C., and Deen, T., 2009, The lithospheric architecture of Africa: seismic tomography, mantle petrology, and tectonic evolution: Geosphere, v. 5, no. 1, p. 23-50.

Betts, P. G., Giles, D., Foden, J., Schaefer, B. F., Mark, G., Pankhurst, M. J., Forbes, C. J., Williams, H. A., Chalmers, N. C., and Hills, Q., 2009, Mesoproterozoic plume-modified orogenesis in eastern Precambrian Australia: Tectonics, v. 28, no. 3.

Betts, P. G., Giles, D., Schaefer, B. F., and Mark, G., 2007, 1600–1500 Ma hotspot track in eastern Australia: implications for Mesoproterozoic continental reconstructions: Terra Nova, v. 19, no. 6, p. 496-501.

Budd, A., and Fraser, G. L., 2004, Geological relationships and $^{40}Ar/^{39}Ar$ age constraints on gold mineralisation at Tarcoola, Central Gawler Gold Province, South Australia: Australian Journal of Earth Sciences, v. 51, p. 685-700.

Budd, A. R., and Skirrow, R. G., 2007, The nature and origin of gold deposits of the Tarcoola goldfield and implications for the central Gawler gold province, South Australia: Economic Geology, v. 102, no. 8, p. 1541-1563.

Chardon, D., Gapais, D., and Cagnard, F., 2009, Flow of ultra-hot orogens: A view from the Precambrian, clues for the Phanerozoic: Tectonophysics, v. 477, no. 3–4, p. 105-118.

Chardon, D., Jayananda, M., and Peucat, J.-J., 2011, Lateral constrictional flow of hot orogenic crust: Insights from the Neoarchean of south India, geological and geophysical implications for orogenic plateaux: Geochemistry, Geophysics, Geosystems, v. 12, no. 2.

Constable, S., Fairclough, M. C., and Gum, J., 2005, Nickel mineralisation models in the Fowler Domain and Musgrave Province — applying the Thompson Nickel Belt as an analogue: MESA Journal, v. 39, p. 14-21.

Cowley, W. M., 2001, Geological Map of South Australia 1:2,000,000 scale: Department of Primary Industries and Resources. South Australia.

Cowley, W. M., 2006, Solid geology of South Australia: Department of Primary Industries and Resources, South Australia. Mineral Exploration Data Package, 15 (version 1.1).

Cutts, K., Hand, M., and Kelsey, D., 2011, Evidence for early Mesoproterozoic (ca. 1590 Ma) ultrahigh-temperature metamorphism in southern Australia: Lithos, v. 124, no. 1, p. 1-16.

Cutts, K., Kelsey, D., and Hand, M., 2013, Evidence for late Paleoproterozoic (ca 1690–1665 Ma) high-to ultrahigh-temperature metamorphism in southern Australia: Implications for Proterozoic supercontinent models: Gondwana Research, v. 23, no. 2, p. 617-640.

Daly, S. J., Fanning, C. M., and Fairclough, M. C., 1998, Tectonic evolution and exploration potential of the Gawler Craton, South Australia: AGSO Journal of Australian Geology and Geophysics, v. 17, no. 3, p. 145-168.

Daly, S. J., and Martin, A. R., 1989, Nundroo 1, 2 and 3 - well completion report: South Australia. Department of Mines and Energy. Report Book 1989/00039.

Doublier, M. P., Dutch, R. A., Clark, D., Pawley, M. J., Fraser, G. L., Wise, T. W., Kennett, B. L. N., Reid, A. J., Spaggiari, C. V., Calvert, A. J., van der Wielen, S., Dulfer, H., Bendall, B., Thiel, S., and Holzschuh, J., 2015, Interpretation of the western Gawler Craton section of Seismic line 13GA–EG1, in Dutch, R. A., Pawley, M. J., and Wise, T. W., eds., What lies beneath the western Gawler Craton? 13GA-EG1E Seismic and Magnetotelluric Workshop 2015, Report Book 2015/00029. Department of State Development, South Australia, Adelaide.

Drown, C., 2003, The Barns Gold Prospect - discovery in an emerging district: MESA Journal, v. 28: 4-9.

Dutch, R. A., Hand, M., and Kelsey, D. E., 2010, Unravelling the tectonothermal evolution of reworked Archean granulite facies metapelites using in situ geochronology: An example from the Gawler Craton, Australia: Journal of Metamorphic Geology, v. 28, no. 3, p. 293-316.

Fanning, C. M., Reid, A. J., and Teale, G. S., 2007, A geochronological framework for the Gawler Craton, South Australia: South Australia Geological Survey, Bulletin, v. 55.

Ferris, G., Schwarz, M., and Heithersay, P., 2002, The Geological Framework, Distribution and Controls of Fe-Oxide and Related Alteration, and Cu-Au Mineralisation in the Gawler Craton, South Australia: Part 1: Geological and Tectonic Framework, in Porter, T., ed., Hydrothermal Iron Oxide Copper-Gold & Related Deposits: A Global Perspective, Volume 2, PGC Publishing, Adelaide.

Ferris, G. M., and Schwarz, M. P., 2003, Proterozoic gold province of the Central Gawler Craton: MESA Journal, v. 30, p. 4-12.

Flint, R. B., Blissett, A. H., Conor, C. H. H., Cowley, W. M., Cross, K. C., Creaser, R. A., Daly, S. J., Krieg, G. W., Major, R. B., Teale, G. S., and Parker, A. J., 1993, Mesoproterozoic, in Drexel, J. F., Preiss, W. V., and Parker, A. J., eds., The geology of South Australia; Volume 1, The Precambrian., p. 106-169.

Forbes, C. J., Giles, D., Hand, M., Betts, P. G., Suzuki, K., Chalmers, N., and Dutch, R., 2011, Using P-T paths to interpret the tectonothermal setting of prograde metamorphism: An example from the northeastern Gawler Craton, South Australia: Precambrian Research, v. 185, no. 1-2, p. 65-85.

Fraser, G., Lyons, P., and Direen, N. G., 2002, Mesoproterozoic tectonism in the Northwest Gawler Craton; (^{40}) Ar/ (^{39}) Ar geochronology, geophysical interpretations and extrapolations, in Preiss, V. P., ed., Geoscience 2002; expanding horizons; abstracts of the 16th Australian geological convention., Geological Society of Australia. Sydney, N.S.W., Australia. 2002.

Fraser, G., Reid, A., and Stern, R., 2012, Timing of deformation and exhumation across the Karari Shear Zone, north-western Gawler Craton, South Australia: Australian Journal of Earth Sciences, v. 59, no. 4, p. 547-570.

Fraser, G. L., Skirrow, R. G., Schmidt-Mumm, A., and Holm, O., 2007, Mesoproterozoic gold in the central Gawler craton, South Australia: geology, alteration, fluids, and timing: Economic Geology, v. 102, no. 8, p. 1511-1539.

Hand, M., Reid, A., and Jagodzinski, L., 2007, Tectonic Framework and Evolution of the Gawler Craton, South Australia: Economic Geology, v. 102, p. 1377-1395.

Hitzman, M. W., Kirkham, R., Broughton, D., Thorson, J., and Selley, D., 2005, The sediment-hosted stratiform copper ore system, in Hedenquist, J. W., Thompson, J. F. H., Goldfarb, R. J., and Richards, J. P., eds., Economic Geology - 100th Anniversary Volume, p. 609-642.

Holzschuh, J., 2015, 13GA–EG1 Eucla-Gawler Seismic Survey – Acquisition and Processing of the western Gawler Craton section, in Dutch, R. A., Pawley, M. J., and Wise, T. W., eds., What lies beneath the western Gawler Craton? 13GA-EG1E Seismic and Magnetotelluric Workshop 2015, Report Book 2015/00029. Department of State Development, South Australia, Adelaide.

Hou, B., Keeling, J., Reid, A. J., Warland, I., Belousova, E., Frakes, L., Hocking, R., and Fairclough, M., 2011, Heavy mineral sands in the Eucla Basin, Southern Australia: deposition and province-scale prospectivity: Economic Geology, v. 106, p. 687-712.

Howard, K. E., Hand, M., Barovich, K. M., Payne, J. L., and Belousova, E. A., 2011a, U-Pb, Lu-Hf and Sm-Nd isotopic constraints on provenance and depositional timing of metasedimentary rocks in the western Gawler Craton: Implications for Proterozoic reconstruction models: Precambrian Research, v. 184, no. 1-4, p. 43-62.

Howard, K. E., Hand, M., Barovich, K. M., Payne, J. L., Cutts, K. A., and Belousova, E. A., 2011b, U-Pb zircon, zircon Hf and whole-rock Sm-Nd isotopic constraints on the evolution of Paleoproterozoic rocks in the northern Gawler Craton: Australian Journal of Earth Sciences, v. 58, no. 6, p. 615-638.

Kirkland, C. L., Smithies, R. H., Woodhouse, A. J., Howard, H. M., Wingate, M. T. D., Belousova, E. A., Cliff, J. B., Murphy, R. C., and Spaggiari, C. V., 2013, Constraints and deception in the isotopic record; the crustal evolution of the west Musgrave Province, central Australia: Gondwana Research, v. 23, no. 2, p. 759-781.

Korsch, R. J., and Kositcin, N., 2010, GOMA (Gawler Craton–Officer Basin–Musgrave Province–Amadeus Basin) Seismic and MT Workshop 2010, Geoscience Australia, Record 2010/39, p. 162.

Korsch, R. J., Kositcin, N., Blewett, R. S., Fraser, G. L., Baines, G., Kennet, B. L. N., Neumann, N. L., Reid, A. J., Preiss, W. V., Giles, D., Armit, R., and Betts, P. G., 2010, Geodynamic implications of the deep seismic reflection line 08GA-OM1: Gawler Craton-Officer Basin-Musgrave Province-Amadeus Basin (GOMA), South Australia and Northern Territory, in Korsch, R. J., and Kositcin, N., eds., GOMA (Gawler Craton–Officer Basin–Musgrave Province–Amadeus Basin) Seismic and MT Workshop 2010, Geoscience Australia, Record 2010/39, p. 162.

McFarlane, C. R. M., 2005, Palaeoproterozoic evolution of the Challenger Au deposit, South Australia, from monazite geochronology: Journal of Metamorphic Geology, v. 24, no. 1, p. 75-87.

Morris, B. J., Hill, P. W., and Ferris, G. M., 1994, Barton bedrock drilling project: South Australia. Department of Primary Industries and Resources. Report Book, 1994/00019.

Pankhurst, M., Schaefer, B., Betts, P., Phillips, N., and Hand, M., 2011, A Mesoproterozoic continental flood rhyolite province, the Gawler Ranges, Australia: the end member example of the Large Igneous Province clan: Solid Earth, v. 2, no. 1, p. 25-33.

Parker, A. J., 1990, Gawler Craton and Stuart Shelf; regional geology and mineralisation, in Hughes, F. E., ed., Geology of the mineral deposits of Australia and Papua New Guinea, Volume 14, p. 999-1008.

Payne, J. L., Barovich, K. M., and hand, M., 2006, Provenance of metasedimentary rocks in the northern Gawler Craton, Australia: Implications for Palaeoproterozoic reconstructions: Precambrian Research, v. 148, no. 3-4, p. 275-291.

Payne, J. L., Hand, M., Barovich, K. M., and Wade, B. P., 2008, Temporal constraints on the timing of high-grade metamorphism in the northern Gawler Craton: implications for the assembly of the Australian Proterozoic: Australian Journal of Earth Sciences, v. 55, no. 5, p. 623-640.

Reid, A., Hand, M., Jagodzinski, E., Kelsey, D. E., and Pearson, N., 2008, Palaeoproterozoic orogenesis in the southeastern Gawler Craton, South Australia: Australian Journal of Earth Sciences, v. 55, p. 449-471.

Reid, A., Jagodzinski, E. A., Armit, R., Dutch, R. A., Kirkland, C. L., Betts, P. G., and Schaefer, B. F., 2014a, U-Pb and Hf isotopic evidence for a Neoarchean and Paleoproterozoic basement to the buried northern Gawler Craton, South Australia: Precambrian Research, v. 250, p. 127-142.

Reid, A. J., and Daly, S. J., 2009, The Mulgathing and Sleaford complexes of the Gawler Craton: a historical perspective of the geology and mineral potential: MESA Journal, v. 52, p. 4-12.

Reid, A. J., and Dutch, R. A., 2015, Lithostratigraphy, structure and metamorphic architecture of a reworked Paleoproterozoic continental rift in the western Gawler Craton in Dutch, R. A., Pawley, M. J., and Wise, T. W., eds., What lies beneath the western Gawler Craton? 13GA-EG1E Seismic and Magnetotelluric Workshop 2015, Report Book 2015/00029. Department of State Development, South Australia, Adelaide.

Reid, A. J., and Fabris, A., 2015, Influence of Preexisting Low Metamorphic Grade Sedimentary Successions on the Distribution of Iron Oxide Copper-Gold Mineralization in the Olympic Cu-Au Province, Gawler Craton: Economic Geology, v. 110, no. 8, p. 2147-2157.

Reid, A. J., Jagodzinski, E. A., Fraser, G. L., and Pawley, M. J., 2014b, SHRIMP U-Pb zircon age constraints on the tectonics of the Neoarchean to early Paleoproterozoic transition within the Mulgathing Comlpex, Gawler Craton, South Australia: Precambrian Research, v. 250, p. 27-49.

Selley, D., Broughton, D., Scott, R., Hitzman, M. W., Bull, S., Large, R., McGoldrick, P., Croaker, M., Pollington, N., and Barra, F., 2005, A new look at the geology of the Zambian Copperbelt, in Hedenquist, J. W., Thompson, J. F. H., Goldfarb, R. J., and Richards, J. P., eds., Economic Geology - 100th Anniversary Volume, p. 965-1000.

Skirrow, R. G., 2010, 'Hematite-group' IOCG±U ore systems: Tectonic settings, hydrothermal characteristics, and Cu-Au and U mineralizing processes. , in Corriveau, L., and Mumin, H., eds., Exploring for Iron Oxide Copper-Gold Deposits: Canada and Global Analogues. Shortcourse Notes, GAC-MAC-SEG-SGA 2008, Quebec City, 29-30th May 2008, Geological Association of Canada, p. 39-58.

Skirrow, R. G., Bastrakov, E., Davidson, G. J., Raymond, O. L., and Heithersay, P., 2002, The geological framework, distribution and controls of Fe-oxide Cu-Au mineralisation in the Gawler Craton, South Australia; Part II, Alteration and mineralisation, in Porter, T. M., ed., Hydrothermal iron oxide copper-gold and related deposits; a global perspective; Vol. 2: Adelaide, AMF, p. 33-47.

Skirrow, R. G., Bastrakov, E. N., Barovich, K., Fraser, G. L., Creaser, R. A., Fanning, C. M., Raymond, O. L., and Davidson, G. J., 2007, Timing of iron oxide Cu-Au-(U) hydrothermal activity and Nd isotope constraints on metal sources in the Gawler Craton, South Australia: Economic Geology, v. 102, no. 8, p. 1441-1470.

Smithies, R. H., Spaggiari, C. V., Kirkland, C. L., Wingate, M. T. D., and England, R. N., 2015, Forrest Zone: geochemistry and petrogenesis, in Spaggiari, C. V., and Smithies, R. H., eds., Eucla basement stratigraphic drilling results release workshop: extended abstracts, Geological Survey of Western Australia, Record 2015/10, p. 41-51.

Spaggiari, C. V., Occhipinti, S. A., Korsch, R. J., Doublier, M. P., Clark, D. J., Dentith, M. C., Gessner, K., Doyle, M. G., Tyler, I. M., Kennet, B. L. N., Costelloe, R. D., Fomin, T., and Holzschuh, J., 2014, Interpretation of Albany-Fraser seismic lines 12GA-AF1, 12GA-AF2 and 12GA-AF3: implications for crustal architecture, in Spaggiari, C. V., and Tyler, I. M., eds., Albany-Fraser orogen seismic and magnetotelluric (MT) workshop 2014: Extended abstracts, Geological Survey of Western Australia, Record 2014/6, p. 165.

Swain, G., Barovich, K. M., Hand, M., Ferris, G. M., and Schwarz, M., 2008, Petrogenesis of the St Peter Suite, southern Australia: arc magmatism and Proterozoic crustal growth of the South Australian Craton: Precambrian Research, v. 166, p. 283-296.

Swain, G., Woodhouse, A., Hand, M., Barovich, K. M., and Schwarz, M., 2005, Provenance and tectonic development of the late Archaean Gawler Craton, Australia; U-Pb zircon, geochemical and Sm-Nd isotopic implications: Precambrian Research, v. 141, p. 106-136.

Teasdale, J., 1997, Methods for understanding poorly exposed terrains: The interpretive geology and tectonothermal evolution of the western Gawler craton PhD.: University of Adelaide, 182 p.

Thiel, S., Duan, J., and Wise, T. W., 2015, Crustal resistivity structure of the western Gawler Craton and margins derived from the 13GA-EG1E magnetotelluric profile, in Dutch, R. A., Pawley, M. J., and Wise, T. W., eds., What lies beneath the western Gawler Craton? 13GA-EG1E Seismic and Magnetotelluric Workshop 2015, Report Book 2015/00029. Department of State Development, South Australia, Adelaide.

Thomas, J. L., Direen, N. G., and Hand, M., 2008, Blind orogen: Integrated appraisal of multiple episodes of Mesoproterozoic deformation and reworking in the Fowler Domain, western Gawler Craton, Australia: Precambrian Research, v. 166, no. 1, p. 263-282.

Tomkins, A. G., 2002, Evolution of the granulite-hosted Challenger Gold Deposit, South Australia: implications for ore genesis PhD: Australian National University, 222 p.

Tomkins, A. G., Dunlap, W. J., and Mavrogenes, J. A., 2004, Geochronological constraintson the polymetamorphic evolution of the granulite-hosted Challenger gold deposit: implications for the assembly of the northwest Gawler Craton. Australia: Australian Journal of Earth Sciences, v. 51, no. 1, p. 1-14.

Tomkins, A. G., and Mavrogenes, J. A., 2002, Mobilisation of gold as a polymetalic melt during pelite anatexis at the Challenger deposit, South Australia; a metamorphosed Archean gold deposit: Economic Geology, v. 97, p. 1249-1271.

Van der Wielen, S., Goodwin, J., Nicoll, M., and Keeping, T., 2015, Potential Field Investigation of the western Gawler Craton Section of Seismic Reflection Line 13GA-EG1E, in Dutch, R. A., Pawley, M. J., and Wise, T. W., eds., What lies beneath the western Gawler Craton? 13GA-EG1E Seismic and Magnetotelluric Workshop 2015, Report Book 2015/00029. Department of State Development, South Australia, Adelaide.

Vassallo, J. J., and Wilson, C. J. L., 2002, Palaeoproterozoic regional-scale non-coaxial deformation; an example from eastern Eyre Peninsula, South Australia: Journal of Structural Geology, v. 24, no. 1, p. 1-24.

Wade, B. P., Payne, J. L., Hand, M., and Barovich, K. M., 2007, Petrogenesis of ca 1.50 Ga granitic gneiss of the Coompana Block: filling the 'magmatic gap' of Mesoproterozoic Australia: Australian Journal of Earth Sciences, v. 54, no. 8, p. 1089-1102.

Webb, A. W., Thompson, B. P., Blissett, A. H., Daly, S. J., Flint, R. B., and Parker, A. J., 1982, Geochronology of the Gawler Craton, South Australia: South Australia. Department of Primary Industries and Resources. Report Book, 1982/00086.

Wingate, M. T. D., Kirkland, C. L., Spaggiari, C. V., and Smithies, H. R., 2015, U-Pb geochronology of the Forrest Zone of the Coompana Province, in Spaggiari, C. V., and Smithies, H. R., eds., Eucla basement stratigraphic drilling results release workshop: extended abstracts, Geological Survey of Western Australia, Record 2015/10, p. 37-40.

FURTHER INFORMATION

R.A. Dutch
rian.dutch@sa.gov.au
Geological Survey of South Australia,
Department of State Development,
GPO Box 320, Adelaide, South Australia, 5001

The nature of the lithosphere in the vicinity of the Eucla-Gawler reflection seismic line

B. L. N. Kennett[1] and R. Chopping[1,2]
1 Research School of Earth Sciences, The Australian National University
2 Resources Division, Geoscience Australia

1 Introduction

The recent and ongoing program of reflection profiling in western and central Australia has provided considerable insight into the nature of crustal architecture. Complementary information on the nature of the whole lithosphere comes from a broad range of seismological studies using both man-made and natural sources. The Eucla-Gawler line crosses a region for which there was little prior information. The reflection line provides important information about the crust-mantle boundary, but for the wavespeeds in the crust we are dependent on extrapolation of isolated refraction experiments from before 1980 and a few receiver functions at broad-band stations linked with ambient noise tomography.

For the mantle component of the lithosphere the primary information comes from surface wave tomography. These results provide indications of distinct lithospheric units.

2 Lithospheric analysis

The Australian National University has carried out an extensive set of deployments of portable high-fidelity broad-band stations across the continent with more than 220 sites occupied. In addition Geoscience Australia has significantly augmented the national network to provide better tsunami warning. The seismograms from the portable and permanent seismic stations across the continent have been analysed to extract information on lithospheric structure beneath the Australian region, both in the crust and uppermost mantle. A wide variety of methods have been employed to study the lithosphere (e.g. Kennett, 2003; Kennett and Blewett, 2012).

The principal information from regional earthquakes comes from the analysis of the large amplitude surface waves late in the seismograms. These surface waves travel almost horizontally through the lithosphere and with a sufficient density of crossing paths can be used in a tomographic inversion to determine 3D structure in the lithospheric mantle. Receiver based studies at individual stations exploit the conversions and reverberations following the onset of the P wave energy. From distant earthquakes information can be extracted about the structure in the crust and uppermost mantle, since the paths arriving at the stations are near vertical.

Additional information has begun to be extracted from the seismic noise field, through the stacked cross-correlation of signals at pairs of stations that provide an approximation to the signal expected for a source at one station recorded at the other location. This ambient noise tomography approach was pioneered in Australia by Saygin (2007) using the continuous data recordings at the portable stations in association with permanent seismic stations to link different experiments. The main signal comes from high frequency surface waves, which provide imaging of upper to middle crustal structure, and are particularly sensitive to the presence of sediments (Saygin and Kennett, 2010; 2012).

Recently a major synthesis of the available seismological constraints on lithospheric structure has been carried out to produce the Australian Seismological Reference Model (AuSREM). An overview of the AuSREM model is given in Kennett and Salmon (2012). A detailed description of the crustal component and its construction is presented in Salmon et al. (2013a), with a comparable treatment for the mantle component in Kennett et al. (2013). The crustal and mantle components are linked through the Moho model constructed using all available information, including reflection picks (Kennett et al., 2011; Salmon et al., 2013a,b). We have further augmented the Moho model with picks from all the reflection surveys carried out in 2013-2015.

We build on the results from the AuSREM model in this summary of lithospheric properties in the neighbourhood of the Eucla-Gawler reflection line. There have been only a limited number of refraction and receiver function studies in the region and so the information on crustal structure depends heavily on the ambient noise studies.

3 Crustal Structure

The primary crustal results for the region around the Eucla-Gawler reflection line come from the AuSREM crustal model (Salmon et al., 2013a). The results from receiver functions provide S wavespeed profiles in the immediate neighbourhood of the seismic stations, together with an estimate of the ratio between P and S wavespeeds. Refraction experiments provide P wavespeed along the line of stations with full crustal penetration only near the midpoints. From the P/S wavespeed ratio derived from more than 150 receiver functions across the continent smooth interpolation of the ratio between P

and S wavespeeds was produced and used to convert the S wavespeed distribution of Saygin and Kennett (2012) derived from ambient noise tomography to an equivalent P wavespeed model. Finally the estimates of the P wavespeed from refraction and receiver function studies are combined with the tomographic results to produce a P wavespeed model for the continent, and offshore where there are refraction experiments.

The resulting model is illustrated in Figure 1 with depth slices at 10 km intervals starting at 5 km depth. The constraints from the ambient noise tomography are rather weak below 25 km, and so there are portions of the model without direct control. We have blanked out those regions that lie further than 200 km from a refraction or receiver function control point in Figure 1, notably just north of the AF3 reflection line. This hole will be filled in when full results are available from the current passive seismic deployment in the Albany-Fraser region.

At 5 km depth we see the influence of the deep sediments in the Canning Basin, contrasting with the Proterozoic metasediments in the Capricorn Orogen. Shallow control is relatively weak for the Eucla-Gawler line itself. The thinner crust in the Pilbara is reflected in the presence of mantle wavespeeds at 35 km depth, and rather high P wavespeeds are encountered in the southern Yilgarn, adjacent to the Albany-Fraser belt. The eastern end of the Eucla-Gawler line crosses rather thick crust and this leads to only moderate P wavespeeds at 35 km depth.

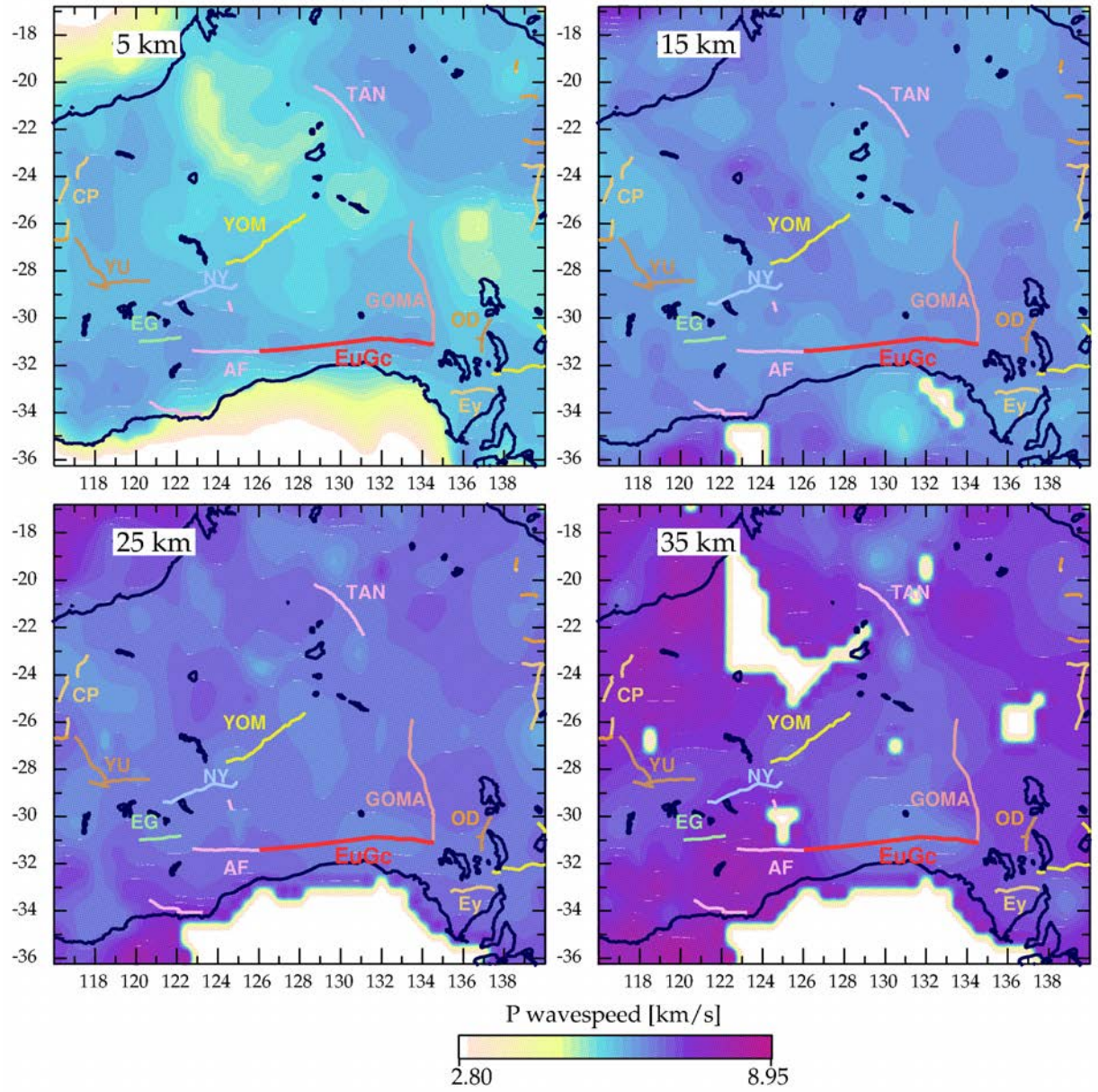

Figure 1 *Depth slices through the AuSREM crustal model for P wavespeed for the region around the Eucla-Gawler reflection line. The same wavespeed scale is used for all depths, since mantle speeds are encountered at 15 km off shore. Regions without direct control on wavespeed are blanked out at depth. In each panel distinctively coloured lines indicate the locations of the recent seismic reflection profiles.*

4 Lithospheric mantle

The earthquake belts to the north of Australia along the Indonesian arc into New Guinea and to the east in the Tonga-Fiji zone provide frequent seismic events of suitable magnitude to be recorded well in Australia. There are less common events to the south along the mid-oceanic ridge between Australia and Antarctica, but these are important in providing additional directional control. All of the events have been exploited in a number of different ways to extract S wavespeed structure, and the longer wavelength components are in good agreement between different studies.

We can now have considerable confidence in the main structures in the lithosphere at a horizontal scale of about 200 km and a vertical resolution around 30 km. Figure 2 illustrates the shear wave structure in western and central Australia using the AuSREM mantle model developed by collaboration between the authors of a number of different studies (Yoshizawa and Kennett, 2004, Fishwick and Rawlinson, 2012; Fichtner et al., 2010). This new model benefits from the incorporation of more paths than in any individual study and includes the use of techniques that provide improved resolution at depth. The variations in seismic S wave velocity are displayed in terms of the absolute shear wavespeed at each depth, with the neutral colour chosen to represent typical continental values.

Regions with faster S wavespeed than the continental reference are indicated by bluish tones, and zones with slower S wavespeed are shown in tones of brown in Figure 2. Reductions in seismic wavespeed are expected from the influence of temperature or the presence of volatiles. Cooler temperatures will produce faster shear wavespeeds, but the very fast wavespeeds seen in Figure 2 are very difficult to produce by temperature alone and suggest the presence of chemical heterogeneity.

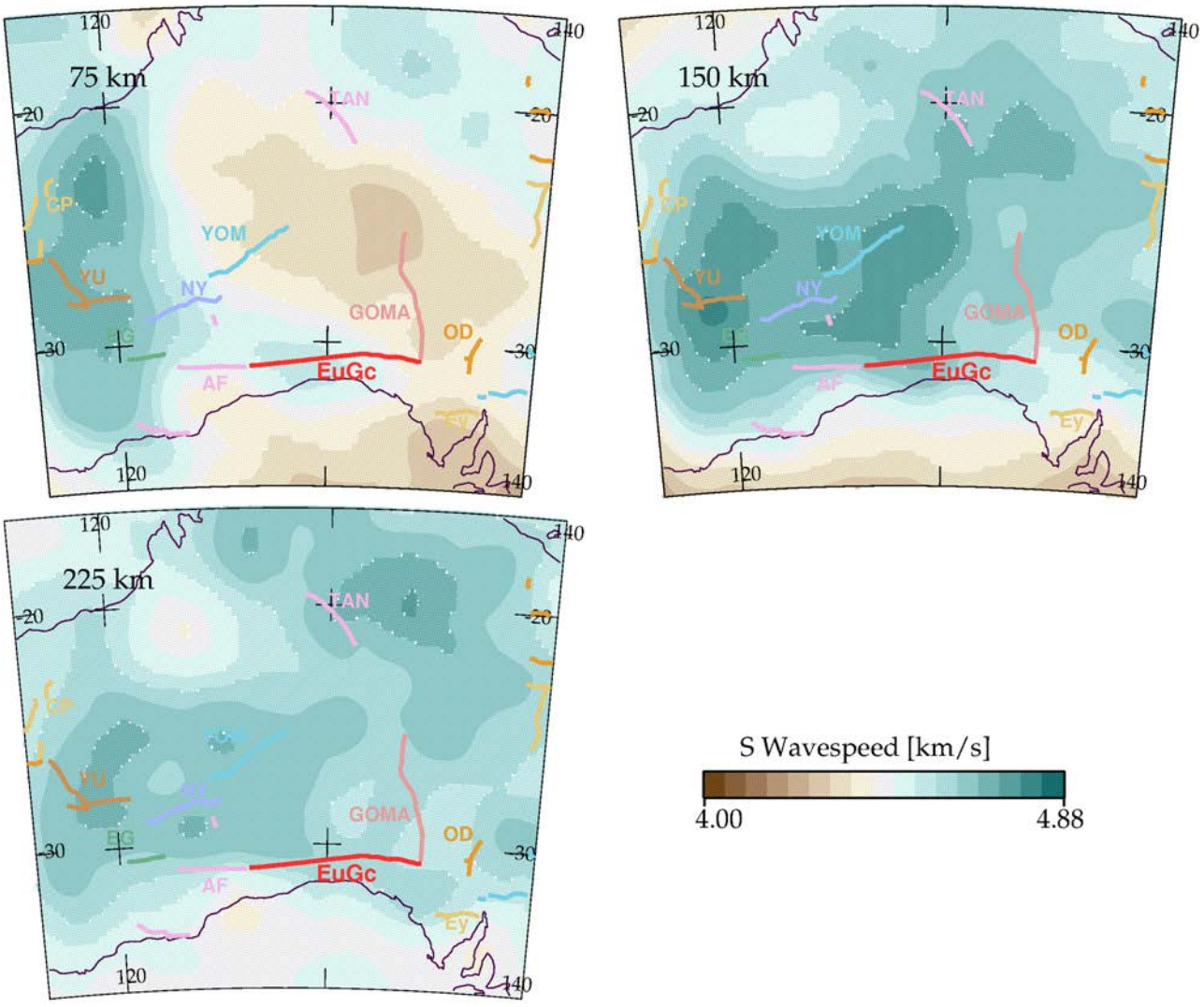

Figure 2 *Seismic shear-wavespeed structure in western to central Australia from the AuSREM mantle model, largely controlled by surface wave tomography. The panels show estimates of seismic wavespeed variation at 75, 150, and 225 km depth. In each panel distinctively coloured lines indicate the locations of the recent seismic reflection profiles.*

The mantle lithosphere below 100 km is marked by distinct fast seismic wavespeeds, but at about 75 km there is an indication of somewhat reduced wavespeeds in the centre of Australia (Fig. 2), that may be linked in part to the presence of thickened crust. The YOM reflection profile crosses into this lower wavespeed zone, yet at greater depth shear wavespeeds are very fast. The area of lower S wavespeed is not associated with enhanced seismic attenuation as might be expected if the cause was a concentration of radioactivity in the uppermost mantle, and its origin remains somewhat enigmatic. The zone of very fast shear wavespeeds beneath the Yilgarn extends towards central Australia and remains quite fast even at 225 km depth. This zone of elevated wavespeeds is among the thickest seismic lithosphere on the Australian continent.

The area beneath the Eucla-Gawler reflection line lies just to at the edge of the zone of good resolution, the patterns of wavespeed variation should be reliable but the apparent reduction in seismic wavespeeds to the east may arise in part from a loss in resolution in the surface wave tomography.

Preliminary results for seismic tomography exploiting the Pn seismic phase from both earthquake and explosive sources provide new information on the uppermost mantle.

These results suggest that the variations in seismic wavespeed can be linked to blocks of lithosphere with distinctive properties.

5 Other lithospheric constraints

A very different view of lithospheric structure is provided by the analysis of magnetic results.

Chopping and Kennett (2015) use a stabilised version of the magnetic anomalies with a spatial resolution of 1.2 km to extract information on the base of magnetisation and the character of magnetic heterogeneity, using a laterally varying fractal model for magnetic character. The results, as shown in Figure 3, support the presence of distinct lithospheric domains, not just confined to the crust, whose location ties well with the seismic results.

Thus the pattern of very distinctive crustal reflectivity for different parts of the Eucla-Gawler reflection line appears to have its origin in the fusion of a suite of lithospheric domains, probably in the process of amalgamation of the West Australian craton with the South Australian/Mawson craton.

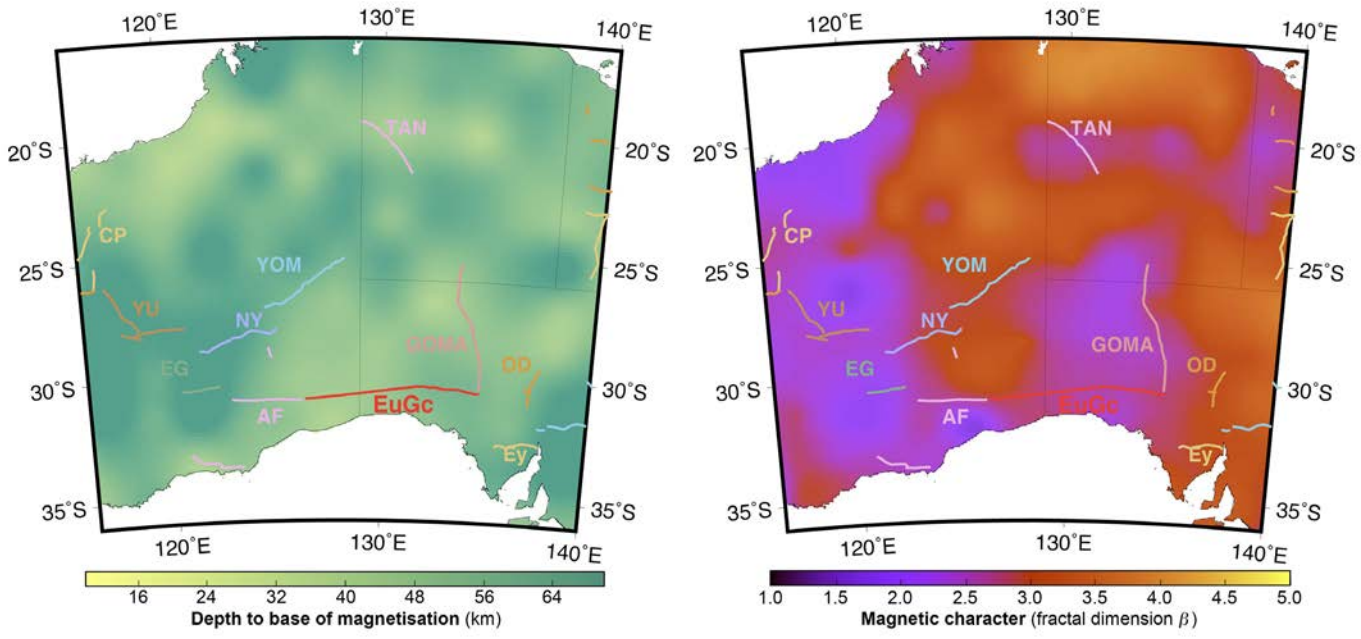

Figure 3 *Depth to base of magnetisation and fractal dimension of magnetic character, from analysis of the full continental magnetic anomalies. In each panel distinctively coloured lines indicate the locations of recent seismic reflection profiles.*

Acknowledgements

The deployments of portable broad-band stations across Australia have depended on the efforts of many people often working in trying circumstances. Particular thanks are due to John Grant, Steve Sirotjuk and Qi Li for their major role in maintaining equipment and logistics and to Armando Arciadiaco for field support and a critical role in data handling and organization. Receiver function results draw on the work of Drs Geoff Clitheroe, Anya Reading, Steve Revets, Erdinc Saygin, Michelle Salmon, and Elizabeth Vanacore. Particular thanks go to Anya Reading for her systematic studies of seismic structure in Western Australia, which have been very significant in the construction of the crustal wavespeed distribution. Weijia Sun has carried out the Pn tomography for the Australian continent.

References

Chopping R. and Kennett B.L.N., 2015. The depth to magnetisation in Australia and its uncertainty: GeoResJ, v. 7, p. 70-77. doi: 10.1016/j.grj.2015.06.003.

Fichtner A., Kennett B.L.N., Igel H. and Bunge H.-P., 2010. Full seismic waveform tomography for radially anisotropic structure: New insights into the past and present states of the Australasian upper mantle: Earth and Planetary Science Letters, v. 290, p. 270-280.

Fishwick S. and Rawlinson N., 2012. 3-D structure of the Australian lithosphere from evolving seismic datasets, Australian Journal of Earth Sciences, v. 59, p. 809--826.

Gorbatov A., Kennett B.L.N. and Saygin E., 2013. Crustal properties from seismic station autocorrelograms, Geophysical Journal International, v. 192,p. 861-870.

Kennett B.L.N., 2003. Seismic Structure in the mantle beneath Australia, 7-23, in The Evolution and Dynamics of the Australian Plate, Geological Society of Australia Special Publication 22 (Ed. D. Müller & R. Hillis).

Kennett B.L.N. and Blewett R., 2012. Lithospheric Framework of Australia, Episodes, v. 35, p. 9-22.

Kennett B.L.N. and Salmon M., 2012. AuSREM: Australian seismological reference model, Australian Journal of Earth Science, v. 59, p. 1091-1103.

Kennett B.L.N., Salmon M. and Saygin E., AusMoho working group, 2011, AusMoho: the variation in Moho depth across Australia, Geophysical Journal International, v. 187, p. 946-958

Kennett B.L.N., Fichtner A., Fishwick S. and Yoshizawa K., 2013. Australian Seismological Reference Model (AuSREM): mantle component, Geophysical Journal International., v. 192, p. 871- 887

Salmon M., Kennett B.L.N. and Saygin E., 2013a. Australian Seismological Reference Model (AuSREM): crustal component, Geophysical Journal International., v. 192, p. 190-206.

Salmon M., Kennett B.L.N., Stern T. and Aitken A.R.A., 2013b. The Moho in Australia and New Zealand, Tectonophysics, v. 609, p. 288-298.

Saygin E., 2007, *Seismic receiver and noise correlation based studies in Australia*, PhD. Thesis, Australian National University

Saygin E. and Kennett B.L.N., 2010. Ambient noise tomography for the Australian Continent, Tectonophysics, v. 481, p. 116-125, doi:10.106/j.tecto.2008.11.013.

Saygin, E. and Kennett B.L.N., 2012. Crustal structure of Australia from ambient seismic noise tomography, Journal of Geophysical Research, v. 117, B01304; doi: 10.1029/2011JB008403.

Yoshizawa K. and Kennett B.L.N., 2004. Multi-mode surface wave tomography for the Australian region using a 3-stage approach incorporating finite frequency effects, Journal of Geophysical Research, v. 109, B02310; doi: 10.129/2002JB002254.

FURTHER INFORMATION

B. L. N. Kennett
Brian.Kennett@anu.edu.au
Research School of Earth Sciences,
Australian National University, Canberra, ACT, 0200

DEPARTMENT OF STATE DEVELOPMENT

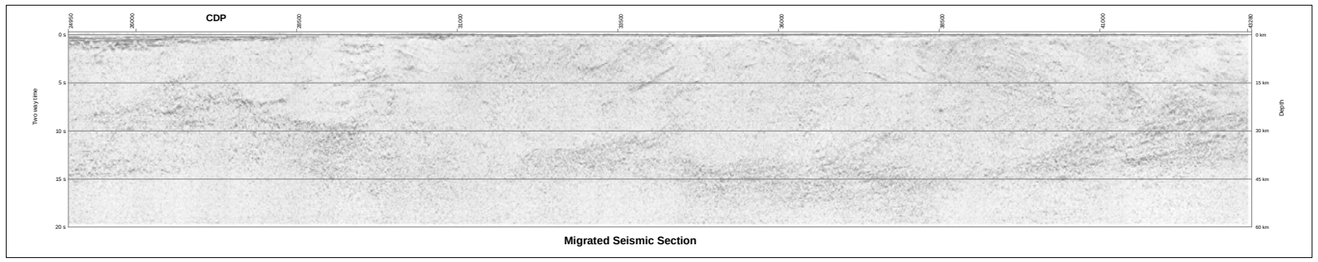

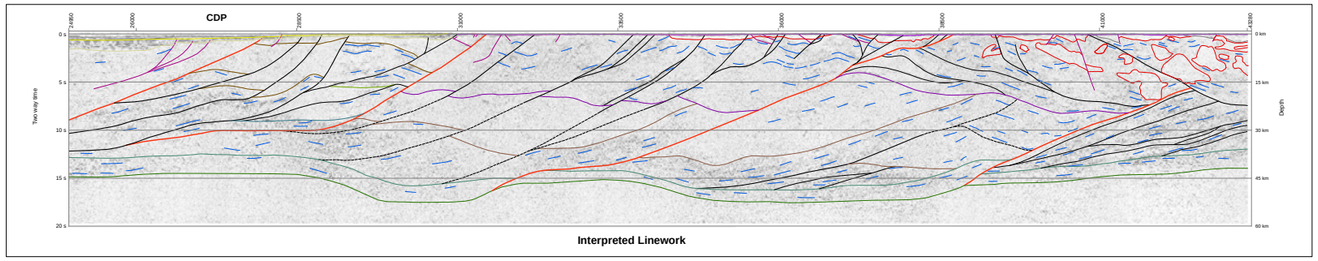

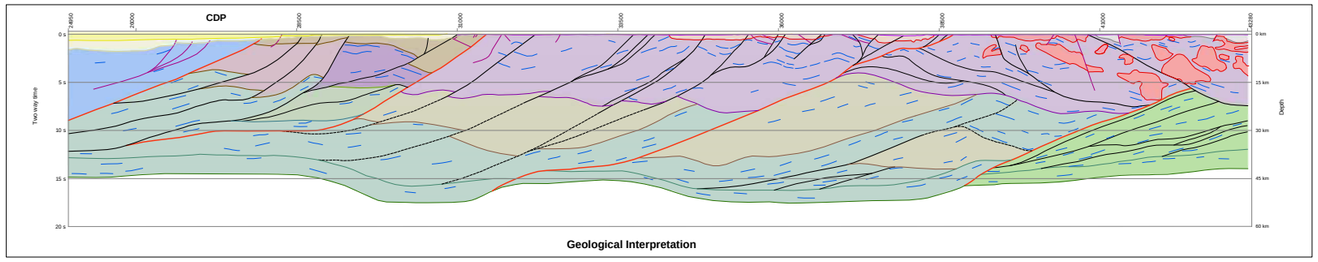

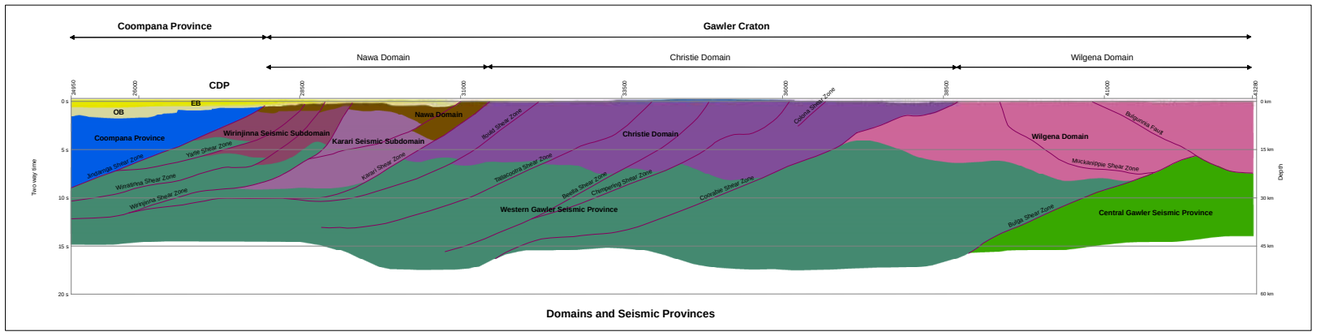

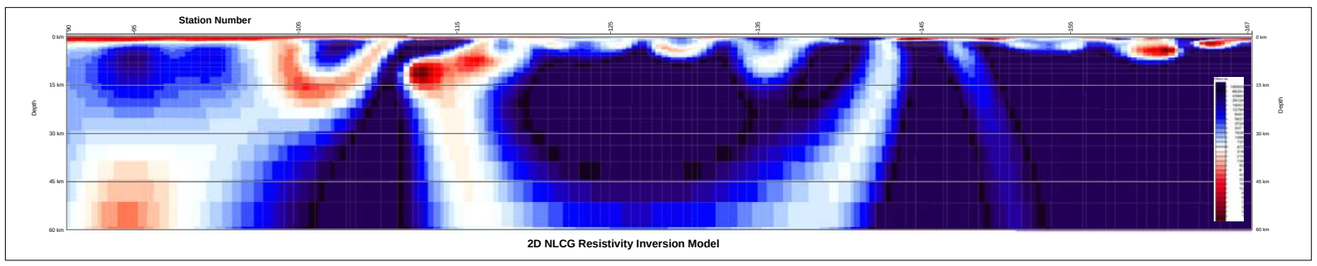

Seismic Interpretation Legend

Tertiary-Recent
- Eucla Basin
- Barton Range
- Ooldea Range
- Weathered rock and Cenozoic cover

Neoproterozoic-Cambrian
- Officer Basin

Mesoproterozoic
- Hiltaba Suite

Palaeoproterozoic
- Coompana Province
- Tarcoola Formation
- Kimban Granites
- Nawa Domain metasedimentary rocks

Archaean-Palaeoproterozoic
- Karari Seismic Subdomain upper reflective crust
- Mulgathing Complex
- Karari Seismic Subdomain weakly reflective middle crust
- Weakly reflective Wirriinjna Seismic Subdomain
- Western Gawler Seismic Province Weakly reflective middle crust
- Western Gawler Seismic Province reflective lower crust
- Central Gawler Seismic Province

Structure
- Form line
- Fault
- Shear zone
- Shear zone, splay
- Shear zone, major
- Shear zone, major, inferred
- Shear zone, major, domain boundary

Contact
- Base of Barton Range
- Base of Eucla Basin
- Base of Ooldea Range
- Base of Tallaringa Trough
- Base of Officer Basin
- Top of basement
- Granite
- Base of Tarcoola Formation
- Base of Palaeoproterozoic Nawa Domain
- Base of reflective upper Karari Seismic Subdomain
- Base of Karari Seismic Subdomain
- Base of Mulgathing Complex
- Base of Wirriinjna Seismic Subdomain
- Base of weakly reflective Western Gawler Seismic Province middle crust
- Top of lowest crust
- Moho

Geological Interpretation of the Gawler Craton section of the Eucla-Gawler Seismic Line (13GA-EG1E)

Geological Interpretation of the Gawler Craton section of the Eucla-Gawler Seismic Line (13GA-EG1E) was compiled by TW Wise
(Geological Survey of South Australia) based on interpretations by
MP Doublier, RA Duitch, D Clark, MJ Pawley, GL Fraser, TW Wise, BLN Kennett, A Reid, CV Spaggiari, AJ Calvert, S van der Wielen, H. Duffet, B Bentzli, S Thiel, J Holzschuh
Contributions also by many individuals and researchers from the Geological Survey of South Australia,
Cartography by Geological Survey of South Australia,
Department of State Development.
Topographic detail based on GEODATATOPO 250K Series 3, supplied by Geoscience Australia, ACT.
The relationship between these data and DSD data is not guaranteed.
Published 17th November 2015
Dr Don Russell, Chief Executive, Department of State Development,
Dr Steve Hill, Director, Geological Survey of South Australia,
The Honorable Tom Koutsantonis, M.P., Treasurer, Minister for Finance, State Development, Mineral Resources and Energy,
Automotive Transformation and Small Business.

TW Wise, MP Doublier, RA Duitch, D Clark, MJ Pawley, GL Fraser, BLN Kennett, A Reid, CV Spaggiari, AJ Calvert, S van der Wielen, H. Duffet, B Bentzli, S Thiel, J Holzschuh, 2015. Geological Interpretation of the Gawler Craton section of the Eucla-Gawler Seismic Line (13GA-EG1E) Plate 1 in Dutch, R. A., Pawley, M. J., and Wise, T. W., eds., What lies beneath the western Gawler Craton? 13GA-EG1E Seismic and Magnetotelluric Workshop 2015, Report Book 2015/00029. Department of State Development, South Australia, Adelaide. Geological Survey of South Australia, Adelaide.

Solid Geology Legend

MESOPROTEROZOIC
- ?Mp *PITJANTJATJARA SUPERSUITE*

MESOPROTEROZOIC
- Mj *MUNJEELA SUITE*
- Mh *HILTABA SUITE*
- Mh6 *Mafic to felsic plugs*
- Ma *GAWLER RANGE VOLCANICS*
- Ma10 *Upper Gawler Range Volcanics*
- Ma8 *Lower Gawler Range Volcanics*
- M40 *Basement rocks of Coompana Block*

PALAEO-MESOPROTEROZOIC
- LM14 *Deformed gabbro to granite and metamorphic rocks*

PALAEOPROTEROZOIC
- L44 *St Peter Suite, St Francis Suite*
- L32 *Tarcoola Formation, Labyrinth Formation and Eba Formation*
- Ln *TUNKILLIA SUITE*
- L36 *Syn-Kimban Orogeny granitoids*
- Lu *MUCKANIPPIE SUITE*
- L-d *MOONDRAH GNEISS*
- L38 *Undifferentiated metasediments of Nawa Domain*
- L40 *Schist, granitic gneiss and granite of Nawa Domain*
- L39 *Iron formations of Nawa Domain*
- L37 *Iron formation in Mount Woods, Coober Pedy and Olympic Domains*
- L-i *WILGENA HILL JASPILITE*
- Lq *MOUNT WOODS COMPLEX*

ARCHAEAN-MESOPROTEROZOIC
- AM1 *Undifferentiated Archaean to Mesoproterozoic rocks of Nawa Domain*

ARCHAEAN-PALAEOPROTEROZOIC
- ALm *MULGATHING COMPLEX*
- ALm7 *Lake Harris Komatiite, acid volcanics, metasediments*
- ALmg *GLENLOTH GRANITE*

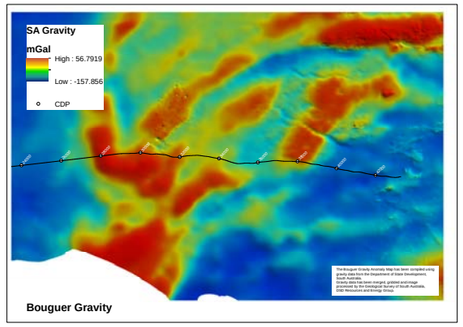

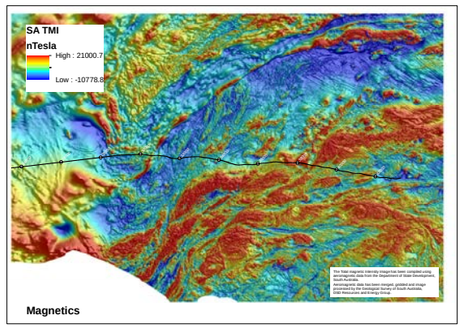

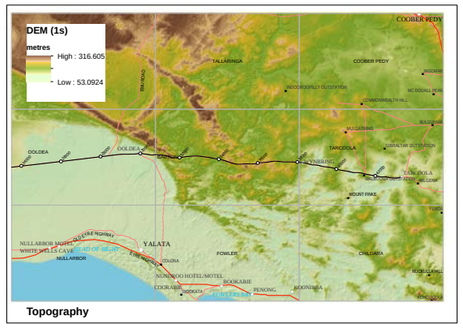

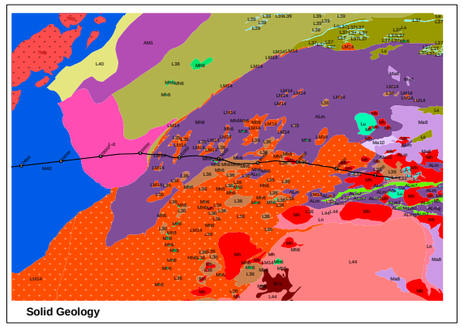

Plate 1 *Geological interpretation of the Gawler Craton section of the Eucla-Gawler Seismic Line (13GA-EG1E).*

NOTES

Contact

Resources and Energy

Department of State Development
Level 7, 101 Grenfell Street, Adelaide
GPO Box 320, Adelaide SA 5001
Phone +61 8 8463 3000
Email Resources.CustomerServices@sa.gov.au
www.minerals.statedevelopment.sa.gov.au

South Australian Resources Information Geoserver (SARIG)
www.statedevelopment.sa.gov.au/sarig

SOUTH AUSTRALIA

Government of South Australia
Department of State Development